

APPLICATION OF BEAU METHODS FOR CANDU CHANNEL POWER

APPLICATION OF BEST ESTIMATE AND ANALYSIS OF UNCERTAINTY  
METHODS TO CANDU CHANNEL POWER

By

IAN HILL, B.Eng.

A Thesis

Submitted to the School of Graduate Studies

In Partial Fulfillment of the Requirements

For the Degree

Master of Applied Science

McMaster University

©Copyright by Ian Hill, September 2006

MASTER OF APPLIED SCIENCE(2006)  
(Engineering Physics)

MCMASTER UNIVERSITY  
HAMILTON, ONTARIO

TITLE: APPLICATION OF BEST ESTIMATE METHODS AND  
ANALYSIS OF UNCERTAINTY METHODS TO CANDU  
CHANNEL POWER

AUTHOR: Ian Hill  
B.Eng (Engineering Physics)  
McMaster University

SUPERVISOR: Dr. J.C. Luxat, Professor  
Department of Engineering Physics  
McMaster University

NUMBER OF PAGES: x, 116

Abstract:

Best estimate and analysis of uncertainty methods are used to examine the variability of the H factor, which converts the global flux in a lattice cell to power. The assumption of a constant H factor is tested, by examining the sensitivity of the components of the H factor to perturbations in reactor conditions, such as, moderator temperature, boron content in the moderator, moderator purity, RIH temperature, ROH pressure, and exit burnup. The local flux profile, which is a component of the H factor, is calculated for a typical CANDU reactor lattice cell using WIMS 2.5d. Another component of the H factor, the distribution of fission energy in a lattice cell, is found by exploring the location of each source of energy released from a fission event. To examine the location of the gamma ray energy deposition a two dimensional Monte Carlo code was created and subsequently benchmarked against an analysis done by C.R.Boss. Using the Monte Carlo code, the best estimate of the percentage of gamma ray energy deposited in the heat transport system was found to be 83.7%. The moderator temperature and the exit channel burnup are shown to have the largest influence on the H factor, which was found to vary between 99.6% and 100.4% of the best estimate value.

### **Acknowledgements:**

Every person is in part a product of their environment. As a result, any of the accomplishments of this work or any other that I produce was through the aid of countless people.

The technical component of this work was aided greatly by the author's supervisor Dr. John Luxat. John always had an open door, and acted as an encyclopedia of nuclear information that readily dispensed answers to any questions, a reference that I was lucky to have. On a daily basis, my colleague Omar Shaikh was always quick to provide excellent technical feedback, and I have no doubt that without his presence the author would be a far lesser man, still unable to cut and paste objects on his own. Without Mr. Shaikh, the days in JHE 327 would have passed far more slowly.

As a second order effect in my younger undergraduate days, Dr. Bill Garland was a shining beacon to myself and others enrolled in his thermodynamics and reactor physics courses. There is no doubt that without Bill's tireless dedication, McMaster's nuclear engineering program would have ceased to exist.

Of course a man's technical knowledge ultimately means very little in one's life. The support from my mother Irene Ann Hill was no doubt the largest influence of my life, she was there in the beginning and I cannot picture the world without her presence.

Finally, the love of my life Melissa Louise Nock. Her contributions to my existence are both quantitative and qualitative. She gives my life meaning, which is the most important gift that anyone could ask for.

# Table of Contents

<b>ABSTRACT:</b> .....	<b>III</b>
<b>ACKNOWLEDGEMENTS:</b> .....	<b>IV</b>
<b>LIST OF FIGURES</b> .....	<b>VII</b>
<b>LIST OF TABLES:</b> .....	<b>VIII</b>
<b>NOMENCLATURE</b> .....	<b>IX</b>
<b>CHAPTER ONE</b> .....	<b>1</b>
<b>1.0 Introduction</b> .....	<b>1</b>
<b>1.1 Literature Review</b> .....	<b>3</b>
<b>CHAPTER TWO</b> .....	<b>5</b>
<b>2.0 Outline of Best Estimate and Analysis of Uncertainty Methodology</b> .....	<b>5</b>
<b>2.1 Phenomena and Key Parameter Identification and Ranking</b> .....	<b>7</b>
<b>2.3 Sensitivity Study of Parameters</b> .....	<b>10</b>
<b>2.4 Physical Interdependency Functional Relationships</b> .....	<b>12</b>
<b>2.5 Integrated Uncertainty Analysis</b> .....	<b>13</b>
<b>CHAPTER THREE</b> .....	<b>14</b>
<b>3.0 Model for the Calculation of Power in a CANDU Reactor</b> .....	<b>14</b>
<b>3.1 Equations Relating Nuclear Fission and Power</b> .....	<b>14</b>
<b>3.2 Equations for Neutron Flux</b> .....	<b>19</b>
3.2.1 Transport Equation .....	19
3.2.2 CANDU Lattice Cell Approximation .....	23
3.2.3 Two Group Diffusion Equation .....	26
<b>3.3 Estimating CANDU Channel Power</b> .....	<b>28</b>
<b>CHAPTER FOUR</b> .....	<b>35</b>

<b>4.0 Examination of The Energy Released From Fission.....</b>	<b>35</b>
<b>4.1 Exploring the Energy Emitted from Fission .....</b>	<b>35</b>
<b>4.2 Kinetic Energy of Fission Fragments .....</b>	<b>37</b>
<b>4.2 Energy from Beta Particles.....</b>	<b>40</b>
<b>4.3 Energy from Neutrons.....</b>	<b>41</b>
4.3.1 Elastic Scattering.....	41
4.3.2 Inelastic Scattering.....	42
4.3.3 Neutron Capture.....	43
<b>4.4 Energy Emitted from Gamma's .....</b>	<b>44</b>
4.4.1 Prompt Gamma Rays .....	44
4.4.2 Delayed Gamma Rays .....	46
4.4.3 Gamma rays from Neutron Capture .....	48
<b>4.5 Gamma ray Interactions with matter .....</b>	<b>51</b>
4.5.1 Photoelectric Effect.....	51
4.5.2 Compton Scattering .....	53
4.5.3 Pair Production .....	55
<b>4.6 Monte Carlo Simulation of Gamma Ray Energy Deposition in A CANDU Lattice Cell....</b>	<b>55</b>
 <b>CHAPTER FIVE.....</b>	 <b>71</b>
<b>5.0 Applying BEUA Methods to the Reactor Physics System .....</b>	<b>71</b>
<b>5.1 Parameter Interaction Table for Reactor Power System .....</b>	<b>71</b>
<b>5.2 Parameter Interaction Diagram for the Reactor Channel Power .....</b>	<b>73</b>
5.2.1 Exit Burnup.....	75
5.2.2 Thermalhydraulic Model.....	84
5.2.3 Fuel Temperature.....	88
5.2.4 Coolant Temperature.....	90
5.2.4 Void Fraction .....	91
5.2.5 Cladding Temperature.....	94
5.2.6 ROH Pressure .....	94
5.2.7 RIH Temperature.....	95
5.2.8 Moderator Temperature .....	96
5.2.9 Moderator Isotropic Purity.....	99
5.2.10 Moderator Boron Content .....	100
5.2.11 Survey Work Examining the Effects of Region Power on SORO Error .....	104
<b>5.3 Summary of Sensitivity Results .....</b>	<b>107</b>
<b>5.4 Uncertainty Analysis .....</b>	<b>109</b>
 <b>CHAPTER SIX.....</b>	 <b>112</b>

**6.0 Conclusion and Recommendations ..... 112**

## LIST OF FIGURES

**FIGURE 2.1: EXAMPLE OF A PARAMETER INTERACTION DIAGRAM FOR THE REACTOR PHYSICS SYSTEM. 8**

**FIGURE 3.1: DEPICTION OF THE PARTICLES INVOLVED IN A FISSION EVENT. .... 15**

**FIGURE 3.2: DEPICTION OF THE NEUTRON DENSITY ..... 16**

**FIGURE 3.3: DEPICTION OF A CANDU REACTOR CORE ..... 22**

**FIGURE 3.4: CANDU FUEL BUNDLE ..... 23**

**FIGURE 3.5: CANDU LATTICE CELL ..... 24**

**FIGURE 3.6: DEPICTION OF THE MEASUREMENT AND COMPUTATIONAL SCHEME TO CALCULATE CHANNEL AND BUNDLE POWER..... 30**

**FIGURE 4.1: DEPICTION OF ELASTIC SCATTERING OF NEUTRONS ..... 41**

**FIGURE 4.2: DEPICTION OF INELASTIC SCATTERING OF NEUTRONS..... 43**

**FIGURE 4.3: EXAMPLE OF NEUTRON CAPTURE IN A HYDROGEN ATOM ..... 44**

**FIGURE 4.4: ENERGY SPECTRUM FOR PROMPT GAMMA RAYS FROM U235 ..... 45**

**FIGURE 4.5: THE DELAYED GAMMA RAY YIELD FOR MAJOR FISSIONABLE ISOTOPES ..... 47**

**FIGURE 4.6: DEPICTION OF ATOMIC SHELLS ..... 52**

**FIGURE 4.7: DEPICTION OF PHOTOELECTRIC EFFECT ..... 53**

**FIGURE 4.8: DEPICTION OF COMPTON SCATTERING ..... 53**

**FIGURE 4.9: DEPICTION OF PAIR PRODUCTION..... 55**

**FIGURE 4.10: DEPICTION OF THE SHIELDING EFFECT OF THE OUTER ELEMENTS ..... 58**

**FIGURE 4.11: DEPICTION OF FUEL ELEMENT SAMPLING ..... 60**

**FIGURE 4.12: PREPRO PLOT OF PHOTON INTERACTION CROSS SECTIONS FOR URANIUM USING THE PREPRO ROUTINE EVALPLOT ..... 62**

**FIGURE 4.13: FLOW CHART OF GAMMA RAY CODE..... 68**

**FIGURE 4.14: MONTE CARLO GAMMA RAY ENERGY DEPOSITION SIMULATION, FOR A CANDU LATTICE, FOR A BE CASE ..... 69**

**FIGURE 5.1: PARAMETER INTERACTION DIAGRAM FOR THE CALCULATION OF CHANNEL POWER. THE PARAMETERS IN BLUE ARE EXAMINED IN THIS WORK. .... 75**

**FIGURE 5.2: VARIATION OF MAJOR FISSIONABLE ISOTOPES IN THE FUEL VS BURNUP ..... 78**

**FIGURE 5.3: TOTAL ADJUSTED FISSION CROSS SECTION VS BURNUP..... 79**

**FIGURE 5.4: CLOSE UP VIEW OF THE VARIATION OF THE ADJUSTED FISSION CROSS SECTION OVER A SMALL RANGE OF BURNUP ..... 80**

**FIGURE 5.5: GAMMA RAY ENERGY RELEASED PER FISSION EVENT VS BURNUP ..... 81**

**FIGURE 5.6: VARIATION OF RECOVERABLE ENERGY VS BURNUP..... 81**

**FIGURE 5.7: ILLUSTRATION OF THE INTERACTION OF H FACTOR WITH RIH TEMPERATURE AND ROH PRESSURE ..... 88**

**FIGURE 5.8: FISSION CROSS SECTION VS FUEL TEMPERATURE ..... 90**

**FIGURE 5.9: FISSION CROSS SECTION VS COOLANT TEMPERATURE ..... 91**

**FIGURE 5.10: FISSION VS COOLANT DENSITY ..... 93**

**FIGURE 5.11: PERCENTAGE OF GAMMA RAY ENERGY RECOVERABLE VS COOLANT DENSITY..... 93**

**FIGURE 5.12: RECOVERABLE ENERGY VS THE CHANGE IN THE MODERATOR DENSITY ..... 97**

**FIGURE 5.13: FISSION CROSS SECTION VS MODERATOR TEMPERATURE ..... 98**

**FIGURE 5.14: FISSION CROSS SECTION VS MODERATOR ISOTOPIC PURITY ..... 100**

**FIGURE 5.15: FISSION CROSS SECTION VS MODERATOR BORON CONTENT ..... 101**  
**FIGURE 5.16: PERCENTAGE OF GAMMA RAY ENERGY RECOVERABLE WITH CHANGES IN BORON  
 CONTENT..... 103**  
**FIGURE 5.17: SORO ERROR VS RELATIVE REGION POWERS ..... 106**  
**FIGURE 5.18: HISTOGRAM OF THE COMBINED EFFECTS OF VARIABILITY OF BURNUP AND MODERATOR  
 TEMPERATURE ON THE CONVERSION OF FLUX TO POWER..... 109**

## List of Tables:

**TABLE 3.1: SUMMARY OF THE GEOMETRY OF THE CANDU BUNDLE USED IN WIMS[] ..... 26**

**TABLE 4.1: ENERGY RELEASED FROM FISSION ..... 36**  
**TABLE 4.2: RANGE OF FISSION FRAGMENTS IN ZIRCONIUM AND URANIUM ..... 39**  
**TABLE 4.3: CAPTURE ENERGY IN CANDU FUEL FOR THE MAJOR FISSIONABLE ISOTOPES..... 48**  
**TABLE 4.4: CAPTURE PROBABILITY IN A CANDU LATTICE AT MIDBURNUP, CALCULATED USING WIMS  
 2.5D ..... 49**  
**TABLE 4.5: TABLE OF MAJOR GAMMA RAYS FROM NEUTRON CAPTURE ..... 50**  
**TABLE 4.6: RADIAL FLUX DEPRESSION FACTORS AT VARIOUS BURNUPS ..... 58**  
**TABLE 4.7: ENERGY GROUP INTERVALS FOR MULTIGROUP MICROSCOPIC PHOTON CROSS SECTIONS 63**  
**TABLE 4.8: COMPARISON OF GAMMA RAY ENERGY DEPOSITION RESULTS ..... 70**

**TABLE 5.1: PARAMETERS EXAMINED IN SUBSEQUENT ANALYSIS ..... 73**  
**TABLE 5.2: VARIATION OF AVERAGE THERMODYNAMIC PROPERTIES A CHANNEL, AS A RESULT OF  
 CHANGING(DECREASING) ROH PRESSURE..... 94**  
**TABLE 5.3: SENSITIVITY OF THE COMPONENTS OF THE H FACTOR TO ROH PRESSURE ..... 95**  
**TABLE 5.4: VARIATION OF AVERAGE THERMODYNAMIC PROPERTIES IN A CHANNEL, AS A RESULT OF  
 CHANGING(INCREASING) RIH TEMPERATURE ..... 96**  
**TABLE 5.5: SENSITIVITY OF H FACTOR TO RIH TEMPERATURE, VIA THERMODYNAMIC PROPERTIES ..... 96**  
**TABLE 5.6: COMPARISON OF MEASURED REGION POWERS VS CALCULATED SORO POWERS. .... 105**  
**TABLE 5.7: SUMMARY OF EFFECTS ON H FACTOR..... 107**  
**TABLE 5.8: RANKING OF EXAMINED PHENOMENA ..... 108**  
**TABLE 5.9: ESTIMATE OF THE MAGNITUDE OF THE CONSTITUENT UNCERTAINTY COMPONENTS PRESENT  
 IN THE H FACTOR ESTIMATE. .... 111**

## Nomenclature

### Acronym

BEAU	Best estimate and analysis of uncertainty
CANDU	Canada uranium deuterium
CDF	Cumulative distribution function
FINCH	Fully instrumented channel
FRS	Functional response surface
LOCA	Loss of coolant accident
LOE	Limit of operating envelope
PDF	Probability distribution function
PID	Parameter interaction diagram
PIFR	Physical interdependency functional relationship
PKPIRT	Phenomena and key parameter identification and ranking table
RFSP	Reactor fuelling simulation program
RIH	Reactor inlet header
ROH	Reactor outlet header
SORO	Simulation of Reactor Operation
WIMS	Winfrith Improved Multigrid Scheme

### Variables

Symbol	Description	Units
$A$	Atomic mass number	Dimensionless
$E_f^i$	Energy released from fission of isotope i	MeV
$F$	Flux depression factor	Dimensionless
$H$	Conversion of flux to power factor	MeV/cm
$h$	Planks constant	eV * s
$h$	Enthalpy	J/kg
$h_f$	Heat transfer coefficient of the fluid	W/(m <sup>2</sup> *k)
$h_v$	Enthalpy of vaporization	J/kg
$K_b$	Hydraulic loss coefficient of a fuel bundle	Dimensionless
$k_C$	Conductivity of fuel cladding	W/(m*k)
$k_F$	Conductivity of fuel	W/(m*k)
$m_g$	Mass of gas	kg
$m_l$	Mass of liquid	kg
$N$	Neutron density	$\frac{\text{Neutrons}}{\text{cm}^3 * \text{s} * \text{MeV} * \text{steridian}}$
$Q_A$	Energy of Anti-Neutrinos	MeV
$Q_{Beta}$	Energy of Fission product $\beta$ decay	MeV

$Q_C$	Energy of Capture gamma rays	<i>MeV</i>
$Q_{DG}$	Energy of delayed gamma rays	<i>MeV</i>
$Q_{FP}$	Kinetic Energy of fission products	<i>MeV</i>
$Q_N$	Kinetic Energy of the neutrons generated	<i>MeV</i>
$Q_{PG}$	Energy of prompt gamma rays	<i>MeV</i>
<b>R</b>	Range of a charged particle	<i>cm</i>
$r_F$	Radius of fuel	<i>cm</i>
<b>S</b>	Stopping power of a charged particle	<i>MeV / cm</i>
$t_C$	Thickness of fuel cladding	<i>cm</i>
$T_{CL}$	Fuel centre line temperature	$^{\circ}\text{C}$
$T_{Cool}$	Coolant temperature	$^{\circ}\text{C}$
<b>V</b>	Velocity	<i>cm/s</i>
<b>W</b>	Mass flow	<i>kg/s</i>
$w_f^i$	Recoverable energy from fission of isotope i	<i>MeV</i>
<b>Z</b>	Atomic number	Dimensionless
$\chi$	Quality of fluid	Dimensionless
$\Sigma$	Macroscopic cross section	<i>cm<sup>-1</sup></i>
$\Phi$	Scalar neutron flux	$\frac{\text{Neutrons}}{\text{cm}^2 * \text{s} * \text{MeV}}$
$\phi$	Angular neutron flux	$\frac{\text{Neutrons}}{\text{cm}^2 * \text{s} * \text{MeV} * \text{Steradian}}$
$\Psi$	Percentage of gamma ray energy recoverable	%
$v$	Neutron velocity	<i>cm/s</i>
$\sigma$	Microscopic cross section	<i>cm<sup>2</sup></i>
$\omega$	Burnup	<i>MWh/kg</i>

# Chapter One

## 1.0 Introduction

Operating margin in a nuclear power plant is directly related to accurate calculations of reactor power distributions. The steady state reactor power distribution, which is the result of the fuel management scheme employed, impacts reactor operations in the long term, while in the short term, the steady state power distribution serves as part of the initial conditions in plant upsets and postulated accident scenarios.

The power distribution in a CANDU reactor is calculated using core physics codes, such as SORO (Simulation of Reactor Operation) and RFSP (Reactor Fuelling Simulation Program). The power calibration, which is based on a heat balance calculation, is an attempt to match the true power with the power calculated by the modeling codes. A mismatch of theoretical and measured power, is indicative of propagated errors. The errors may stem from instrumentation, computer models and parameter inputs to the models. The accuracy of the computational results is affected by both the uncertainties in the models, as well as the uncertainty in the parameter inputs to the models. Often conservatism appears in both the models and the parameters. This conservatism is seldom a reflection of the current state of knowledge, but more often is implemented to satisfy a regulatory viewpoint in which it appears acceptable to discard a result with a higher accuracy in favor of a result which was calculated using a less accurate but conservative model.

This thesis will draw upon the procedures outlined in best estimate and analysis of uncertainty (BEAU)[1] methodology. The objective is to extend the BEAU methodology to the analysis of steady state channel power, focusing primarily on the uncertainty associated with the conversion of neutron flux to power. This conversion is directly related to the spatial location of the deposition of energy from fission. The BEAU methods are structured such that the analyzed parameters are broken down into their constituent components, allowing each component to be separately analyzed and updated. In this way BEAU methods are incremental, given that as the knowledge of the models and parameters improve, the analysis can be easily refined to yield a rapid update of results.

Chapter two outlines the best estimate and analysis of uncertainty methodology and describes the BEAU techniques employed in this thesis, including parameter interaction diagrams, functional response surfaces, and integrated uncertainty analysis.

Chapter three introduces the equations for flux and power. The coupling of a lattice cell code with a three dimensional diffusion codes is presented, as well as a summary of the methods which can be used to calculate the power in a CANDU reactor.

Chapter four outlines the types of energy produced during fission. Subsequently the location of the energy deposition in a lattice cell is examined. Based on the location of deposition the energy is classified as recoverable, if it deposited in the heat transport system, or non-recoverable, if the energy is deposited elsewhere.

Chapter five develops the parameter interaction diagrams for the reactor power systems. WIMS is used to examine the sensitivity of the macroscopic fission cross

sections to perturbations of various parameters. A developmental gamma ray code is used to evaluate the effects of the parameters on the location of the gamma ray energy deposition in the CANDU lattice.

Chapter six will outline the conclusions derived from this thesis as well as outline future work in this area.

## **1.1 Literature Review**

The assumption of a constant H factor has not been extensively studied in existing literature. The H-factor was originally the output of the code POWDERPUFS-V[2] which was used previously for lattice cell calculations, in CANDU reactors, and was a function of irradiation. Sermer et al[18] fit a seventh order polynomial to the relationship between the H factor and irradiation for the purpose of estimating bundle power error along a channel. The underlying physics of the H factor vs. irradiation relationship was not examined.

An complete analysis of the gamma ray energy deposition for the MASURCA reactor was done by Luthi[25], however, the MASURCA reactor is a plutonium burning fast reactor which is not similar to the current CANDU design.

The location of the gamma ray energy deposition in a CANDU reactor lattice was calculated by Boss[36] using the assumption of homogeneous fuel rings, in place of the true geometry, a 37 element configuration. Boss's work was re-examined by Abdelbaky et al[3] where it was determined that the geometric assumptions introduced in the Boss

model was a source of error, which affected the gamma ray energy deposited in the coolant.

An algorithm of a simple Monte Carlo simulation was given by Blomquist and Gelbard[35]. The algorithm did not consider pair production events. MCNP[4] has been used to model gamma ray transport for many US reactors, however it is to some extent a black box.

In this work, the algorithm outline by Blomquist and Gelbard is modified to model the two dimensional CANDU reactor lattice and will also take into account pair production events. The results are then compared against those previously presented by Boss. The model is designed such that the lattice conditions can be easily modified, for the purpose of determining the sensitivity of the location of gamma ray energy deposition.

## Chapter Two

# 2.0 Outline of Best Estimate and Analysis of Uncertainty Methodology

In the past, the Canadian nuclear industry has employed conservative models to compensate for a deficiency in both knowledge and uncertainty in plant conditions and modeling parameters. This resulted in the creation of the Limit of Operating Envelope (LOE) methodology [5], primarily employed in nuclear safety analysis of accident scenarios. The LOE methodology used models in which important input parameters are biased to conservative bounding values. An example of this is to assume that at the start of a loss of coolant accident (LOCA), all fuel elements have powers that conform to a bounding envelope of power-burnup history. Not surprisingly the LOE methods often indicate small or negative safety margins. The results, which were not indicative of the true safety margins, became part of the Canadian nuclear culture and influenced subsequent analysis, regulatory acceptance, as well as new designs.

As might be expected, the nuclear industry is continuously advancing its state of knowledge. Years of experience gained from R&D programs and from nuclear plant operation and design have led to both improved computer models, and better definitions of uncertainties associated with parameters; however, the increase of knowledge is often not reflected in the LOE methods, since more representative models for treatment of uncertainties are discarded in favor of older conservative models, which, are more likely to gain regulatory acceptance. The inflexibility of LOE methods has led to difficulty

incorporating improvements in engineering knowledge into previous LOE analysis. As a result, costly reanalysis is often performed, which can impose an economic penalty on scientific progress. A new method of analysis is replacing the LOE methods; a methodology that motivates improvements in models, and knowledge of parameters. This new methodology is referred to as Best Estimate and Analysis of Uncertainty Methods (BEAU).

In BEAU methods, as the name implies, the analysis assigns each parameter a best estimate value. A best estimate of a parameter corresponds to the parameter's most probable value given the state of the system. The uncertainty associated with each parameter value is quantified, and this uncertainty is subsequently propagated throughout the analysis.

The goal of the analysis is to ascertain a best estimate of a key safety parameter of interest, and to quantify the uncertainty of the estimate. An example of the application of BEAU methods follows. Referring back to the LOE LOCA example, in best estimate methods, the power of each fuel element would be set to its calculated best estimate value, consistent with its position along a channel and the assumed averaged burnup of the channel. The calculated element powers would each have some uncertainty, related to the variability of the power-burnup relationship derived from fuel management calculations. The powers of each fuel element would be sampled about the probability distribution that characterizes the power-burnup relationship for the relevant channel location in the core. The result is a probability distribution of the calculated parameter, in this case fuel element power. Thus, the BEAU analysis encourages accurate calculation of

the parameters and the probability distributions that characterize the variability in the parameters. The uncertainties are, as expected, related to the state of knowledge, i.e. validity of computer codes, models, and measured parameters. As knowledge is gained through more accurate modeling and measurement, the uncertainty tends to decrease. This may appear trivial, but the necessity to maintain continued operation or obtain licenses has at times stifled change and improvement in the nuclear industry, in favor of the status quo. Thus, the best estimate method is an attempt not only to regain operating margin through better quantification and treated of uncertainty components, but also endeavors to ultimately change the regulatory nuclear culture.

## **2.1 Phenomena and Key Parameter Identification and Ranking**

In BEAU methods an important first step is to identify the fundamental parameters and phenomena that the analysis will focus on. These key parameters are those that significantly influence the calculations of the parameters of interest (such as channel power). The parameter evaluation process is done with the assistance of Phenomena and Key Parameter Identification and Ranking Tables (PKPIRT) and Parameter Interaction Diagrams (PID)[6]. The PKPIRT lists each system of interest and the relative phenomena associated with each system. The use of PKPIRT is a comprehensive reference of the parameters that were included in the analysis, which lends itself to refinement. Included in the PKPIRT is a ranking of the importance of both the parameter, and the associated phenomena. The PID is a visual reference that allows for quick identification of the interdependencies between the relevant parameters in the

system of interest. An example of a PID for the reactor physics system is shown in Figure 2.1 [7]

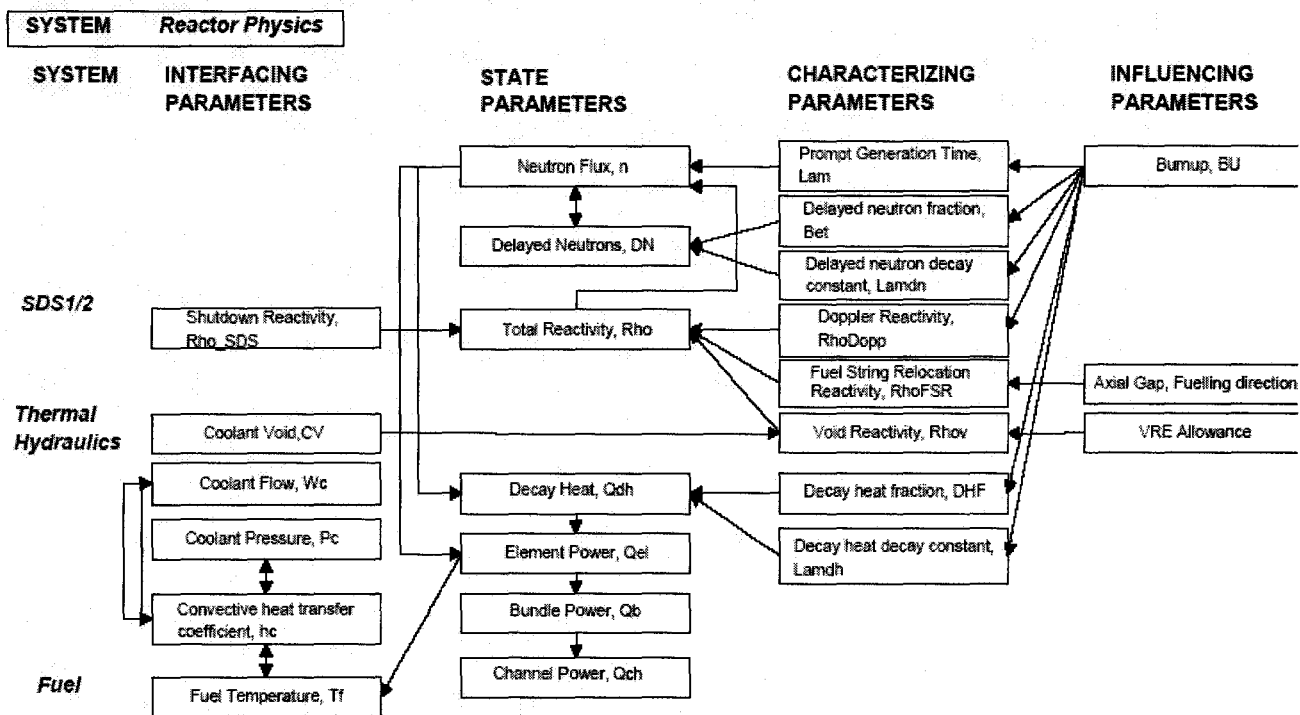


**Figure 2.1: Example of a Parameter Interaction Diagram for the Reactor Physics System[7]**

Figure 2.1 gives a visualization of the interdependencies between the parameters examined. For example, Figure 2.1 shows that the axial gap between the fuel string and end shield plug influences the fuel string relocation reactivity, which is a component of the total reactivity.

The PID distinguishes between parameters by grouping them into four broad classes based upon their relationships in modeling physical processes, as will be described in the subsequent section.

## 2.2 Parameter Classification

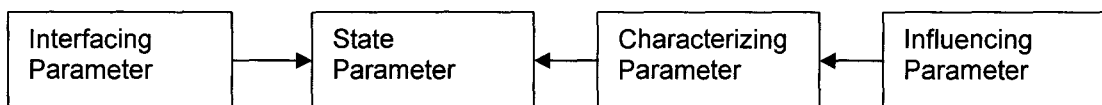
The parameters in the systems can be lumped into four broad groups, State parameters, Interfacing parameters, Characterizing parameters, and Influencing parameters. These groups define the underlying relationships associated with modeling of physical processes.

**State Parameters:** Are parameters that can be described by a differential equation. The analysis is centered on calculating the probability distribution of the state parameters. An example of a state parameter is channel power.

**Interfacing Parameters:** Are state parameters from other systems. An example is coolant flow, which is a state parameter of the heat transport system.

**Characterizing Parameters:** Are parameters that appear as coefficients of the differential equations used to calculate the state parameters. Examples are the diffusion coefficient and the macroscopic cross sections, which are coefficients required to calculate neutron flux.

**Influencing Parameters:** Are parameters that the characterizing parameters are dependent on. An example is the moderator temperature, which affects the diffusion coefficient.



In the subsequent analysis, the characterizing parameters are the coefficients of the equation used in the calculation of channel power. The parameters that are not measured but are implicit in the calculation of the characterizing parameters are the

interfacing parameters. The parameters that are measured values, which affect either the characterizing or interfacing parameters, are the influencing parameters.

## 2.3 Sensitivity Study of Parameters

A component of the PKPIRT is an index of the importance of each parameter, which gives an indication of the relative impact of the parameter on the calculated outcome. The importance is ascertained from a sensitivity study of the state parameter. The sensitivity study involves varying each of the operating parameters about their best estimate values. Typically the variation extends over  $\pm 3.5$  standard deviations about the best estimate value. The operating parameters are varied parametrically, while the other parameters are each set to their best estimate values. This allows for an estimate of the sensitivity,  $\left(\frac{dy}{dx}\right)$ , where y represents the state parameter and x represents the influencing parameter. The ranking of the parameter is defined as the absolute value of the product of the sensitivity and the range of variation of the parameter ( $\Delta x$ ).

$$Rank = abs\left(\frac{dy}{dx} * \Delta x\right) \quad (2.1)$$

Other ranking schemes are used [11] to evaluate the importance of the parameters, the most common being to evaluate the square of the product of sensitivity and uncertainty, as shown in equation (2.2).

$$Rank = \left(\frac{dy}{dx} * \Delta x\right)^2 \quad (2.2)$$

The ranking scheme of equation (2.1) is used since in the previous formulation, equation (2.2), a parameter that has half the impact of another parameter, will receive a ranking equal to a quarter of the previous effect. This nonlinear behavior tends to discount the importance of less sensitive parameters.

Once the rankings are obtained they are then normalized, which consists of dividing by the highest ranking and multiplying by 100.

$$Rank_i = \frac{Rank_i}{Max\{Rank_i\}} * 100 \quad (2.3)$$

This results in a table in which parameters are listed in order of their relative ranking and from which the relative importance of each parameter is readily apparent. The parameters are then further distinguished based upon the ranking value into categories of High, Medium and Low.

The values for the rankings are as follows:

$$\mathbf{High} \geq 20 \quad || \quad \mathbf{20} > \mathbf{Medium} \geq 1 \quad || \quad \mathbf{1} > \mathbf{Low}$$

The parameters that have a High ranking are included in the analysis along with the interdependencies between other High ranked parameters. The parameters ranked Medium are set to their best estimate values during the analysis, while the Low ranked parameters will have a negligible impact and are often set to bounding values when determining the parameter of interest.

Once the parameters are ranked, the analysis can then focus on a smaller subset of the Medium and High ranked parameters. A revised PID can then be created which displays a visual link of the interactions between relevant parameters. The PKPIRT and

PID can be refined during the course of an analysis and should be created with the aid of expert input and supported by relevant references.

## 2.4 Physical Interdependency Functional Relationships

Physical Interdependency Functional Relationships (PIFR) relate a composite parameter to a number of underlying physical parameters.

PIFR can be determined in the following ways[8]:

- A differential equation relating a state parameter to characterizing and influencing parameters.
- An algebraic function relating the dependent parameter to a number of independent parameters.
- A computer generated mathematical polynomial function, which correlates a dependent variable to a set of independent variables.

A PIFR generated using the last two methods is also called a functional response surface (FRS).

An example of generating a FRS, is to use the lattice cell code WIMS[9,10] to relate a characterizing parameter such as the axial diffusion coefficient to underlying modeling parameters such as, fuel temperature, moderator purity, and burnup. The FRS is used as a replacement to continually running the computer codes from each individual case. The code is run for a fixed number of cases and a multidimensional curve fit is made, typically the regression method of least squares is used[11].

$$M = \beta_0 + \sum_{i=1}^k \beta_i P_i + \sum_{j=1}^k \sum_{i \geq j}^k \beta_{ij} P_i P_j \quad (2.4)$$

Where  $M$  is the acceptance parameter,  $P$  are the key parameters identified in the sensitivity analysis,  $k$  is the number of key parameters, and  $\beta$  are the fitting coefficients.

The use of the functional response surface will introduce additional error into the best estimate procedure. This error is quantified by running the computer code for random cases and then calculating the error between the generated FRS and the random points.

## **2.5 Integrated Uncertainty Analysis**

Once the FRS has been generated, each of the influencing parameters ranked high are sampled about their respective probability distributions. The variation in the state parameters is obtained through the use of the FRS. Once a sufficient number of runs have been completed, the state parameter results are grouped into bins and plotted as histograms. From the histograms, the best estimate of the state parameter as well as the confidence interval is extracted. Confidence intervals are generally 95/95.

The 95/95 intervals are a result of requiring an estimate of probability using imperfect information[12].

## Chapter Three

### **3.0 Model for the Calculation of Power in a CANDU Reactor**

This chapter introduces the parameters used to quantify the neutron population in the reactor, and discusses how neutrons interact with matter. The equations used to calculate power and flux in a nuclear reactor are outlined. The lattice cell approximation used in CANDU reactors is introduced, which utilizes the repetitive geometry of the reactor. The integration of the lattice code with a three dimensional diffusion code to calculate the macroscopic flux distribution is described. The purpose of this section is to provide background on how the neutron flux is calculated, as well as to highlight the relationship between flux and power.

### **3.1 Equations Relating Nuclear Fission and Power**

Power in a nuclear reactor is primarily generated through the process of nuclear fission. Fission is, to a first order approximation, a process in which a neutron is captured by a heavy element; the binding energy of the added neutron causes the element to break into two smaller elements, accompanied by a release of energy, as depicted in Figure 3.1 [13].

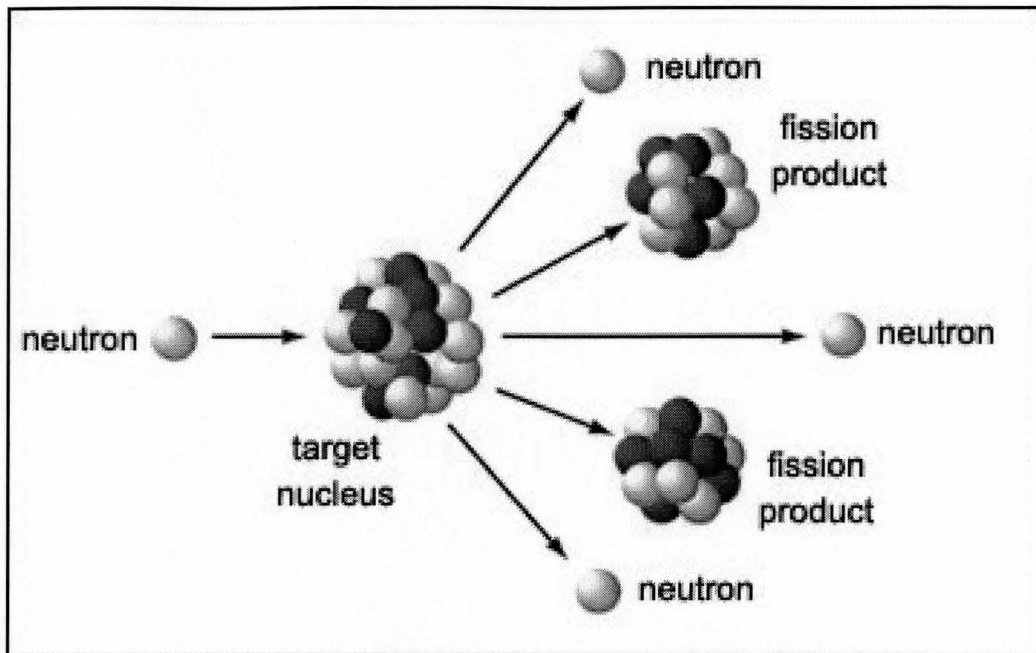


**Figure 3.1: Depiction of the Particles Involved in a Fission Event[13].**

Although fission can also occur by the absorption of other nuclei, protons, or high energy photons, these events are of relatively low probability and will be considered negligible in this dissertation.

In a typical thermal nuclear reactor the fuel is comprised of elements containing fissionable material at relatively low concentrations, the most common being Uranium 235, which has a relatively high fission probability at thermal neutron energies. In all current CANDU reactors in service the fuel used is natural Uranium which contains 0.7% U235, and 99.3% U238 by weight. Commonly in other reactors, and in future CANDU reactors, the Uranium 235 content is increased through a process known as enrichment.

To induce a fission event, the fuel must be immersed in a neutron field.

Mathematically, the neutron field is described by the variable  $N(r, E, \Omega, t)$ , depicted in

Figure 3.2[15], is known as the angular density of the neutrons[17].  $N(r, E, \Omega, t)$  is defined as the number of neutrons per unit volume,  $\left(\frac{\text{Neutrons}}{\text{cm}^3}\right)$ , at a point  $r$ , with energy  $E$ , moving in a direction with a solid angle  $\Omega$ , at a time  $t$ .

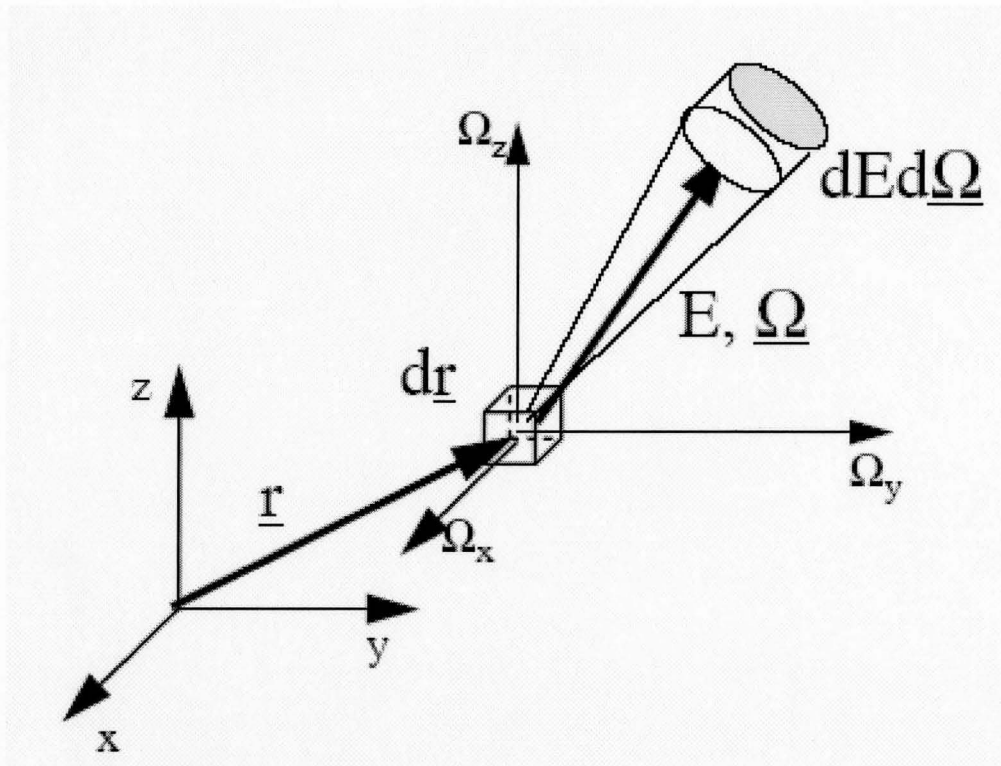


**Figure 3.2: Depiction of the Neutron Density [15]**

In order to quantify the amount of fission occurring in the reactor, and thus the rate of energy release, the interaction rate between the neutron field and the fissionable material must be evaluated. The interaction rate will be proportional to the rate that the neutrons move through an area of the material. The rate,  $\left(\frac{\text{Neutrons}}{\text{cm}^2 \text{ s} * \text{MeV} * \text{Steradian}}\right)$ , is equal to the product of the angular neutron density,  $\left(\frac{\text{Neutrons}}{\text{cm}^3 * \text{s} * \text{MeV} * \text{steradian}}\right)$ , with the average neutron velocity  $v$ ,  $\left(\frac{\text{cm}}{\text{s}}\right)$ . This quantity is referred to as the angular neutron flux  $\phi$ .

$$\varphi(r, E, \Omega, t) = v(E)N(r, E, \Omega, t) \left\| \left[ \frac{\text{Neutrons}}{\text{cm}^2 * \text{s} * \text{MeV} * \text{Steradian}} \right] \right. \quad (3.1)$$

The reaction rates are weakly dependent on angle of the incident neutrons, so it is often appropriate to work with a measure of the number of neutrons moving through an area, independent of the angle at which the neutrons move. By integrating the angular neutron flux over the solid angle  $\Omega$ , a flux independent of angle is obtained, known as the scalar neutron flux,  $\phi(r, E, t)$ .

$$\phi(r, E, t) = \int_{\Omega} \varphi(r, E, \Omega, t) d\Omega \left\| \left[ \frac{\text{Neutrons}}{\text{cm}^2 * \text{s} * \text{MeV}} \right] \right. \quad (3.2)$$

The scalar neutron flux, also referred to as simply the neutron flux, measures the number of neutrons passing through an area ( $\text{cm}^2$ ) per unit of time ( $\text{sec}^{-1}$ ). The probability of a neutron with an energy,  $E$ , inducing fission of a material  $i$ , when passing through the material, is given by  $\sigma_f^i(E)$ , which is the energy dependent microscopic cross section of fission, for the element  $i$ . The fission rate is therefore equal to the product of the rate that neutrons pass through a fissionable element with number density,  $N_i(r, t)$ , and probability of a fission interaction denoted by  $\sigma_f^i(E)$ :

$$\text{FissionRate} = \sigma_f^i(E)N_i(r, t)\phi(r, E, t) \quad (3.3)$$

The above equation can also be expressed in terms of the macroscopic cross section of fission  $\Sigma_f$ , which is equal to the product of the number density and interaction probability:

$$\Sigma_f^i(r, E, t) = \sigma_f^i(E)N_i(r, t) \quad (3.4)$$

Each fission event of an isotope  $i$ , will be accompanied by a release of energy  $E_f^i$ , where  $E_f^i$  is the average amount of energy released per fission of isotope  $i$ . The energy will be released in the various forms listed below.

$$E_f^i = Q_{FP} + Q_N + Q_{PG} + Q_{DG} + Q_{Beta} + Q_A \quad (3.5)$$

Where the terms are defined below:

$Q_{FP}$  : *Kinetic Energy of fission products*

$Q_N$  : *Kinetic Energy of the neutrons generated*

$Q_{PG}$  : *Energy of prompt gamma rays*

$Q_{DG}$  : *Energy of delayed gamma rays*

$Q_{Beta}$  : *Energy of Fission product  $\beta$  decay*

$Q_A$  : *Energy of Anti-neutrinos*

An additional source of energy that is present is the energy released from the capture of the excess neutrons. This energy, denoted as  $Q_C$ , although is not a direct product of fission, must be added to equation (3.5) as the binding energy of the excess neutrons is primarily converted to capture gammas as will be subsequently discussed.

Only a portion of the total energy emitted from fission will be recoverable. Neutrinos, which rarely interact with matter, escape the heat transport system, as will some of the energy from both the gamma rays and the neutrons. Thus, the amount of energy released  $E_f^i$  that is recoverable is denoted as  $w_f^i$ . When the superscript  $i$  is dropped,  $w_f$  represents the average recoverable energy released, calculated by weighting the

averaged released per fission of each isotope by the amount of fission that occurs in each isotope.

Using the previously defined expression for the rate of fission, as well as the energy released from fission, a relationship between the flux and the useable power generated in a reactor can be defined. The volumetric heat generation rate is given by equation (3.6) which is the product of the fission rate integrated over energy multiplied by the amount of recoverable energy released, summed over all elements which fission.

$$q'''(r) = \sum_i w_f^i N_i(r,t) \int_0^\infty dE \sigma_f^i(E) \phi(r,E) \quad (3.6)$$

Where  $q'''(r)$  is the recoverable volumetric fission heat source. Equation (3.6) when integrated over the volume of the core, gives the total recoverable thermal energy that the reactor generates. The neutron flux, however, must be known in order to evaluate the amount of power being generated by the reactor.

## 3.2 Equations for Neutron Flux

### 3.2.1 Transport Equation

As stated in the previous section, the spatial distribution of the neutron flux is required to evaluate the power distribution. The neutron density is described in detail by the Boltzman neutron transport equation shown in equation (3.7). The transport equation relates the time rate of change of the neutron density to the number of neutrons entering and leaving a control volume, plus any neutrons generated by a source within the control volume. Ultimately the equation is equivalent to the accounting of neutrons.

$$\frac{\partial N}{\partial t} = -v\Omega \cdot \nabla N - v\Sigma_t(r, E)N + \int_{4\pi} d\Omega \int_0^\infty dE' v' \Sigma_s(E' \rightarrow E, \Omega' \rightarrow \Omega)N + S \quad (3.7)$$

Where  $N(r, E, \Omega, t)$  is written as  $N$ , for simplicity. The physical significance of the terms in the neutron transport equation is described below.

**First Term:**  $\frac{\partial N}{\partial t}$ , Time rate of change of the neutron density. This term is set to zero in the case of steady state calculations.

**Second Term:**  $-v\Omega \cdot \nabla N$ , The net leakage of neutrons through the surface of the control volume. Where  $v$  is the velocity of the neutrons.

**Third Term:**  $-v\Sigma_t(r, E)N$ , A loss term that accounts for neutron absorption, and the rate at which neutrons are scattered out of energy  $E$ , and angle  $\Omega$ .

**Fourth Term:**  $\int_{4\pi} d\Omega \int_0^\infty dE' v' \Sigma_s(E' \rightarrow E, \Omega' \rightarrow \Omega)N$ , An inscattering term which quantifies the rate at which neutrons of energy  $E'$  and angle  $\Omega'$  scatter into energy  $E$  and angle  $\Omega$ .

**Fifth Term:**  $S$ , A neutron source term. Usually corresponds to the neutrons that are generated in the control volume by fission.

The neutron transport equation has no analytical solution, as it is a single equation that is a function of seven unknown variables; three spatial, two angular, one energy, and one temporal. The temporal derivative is reduced to zero for the case of steady state operation, which will be all cases examined in this work. The transport equation can be solved numerically by discretizing each of the variables.

An example of a numerical solution process is to divide the continuous energy variable into intervals. In each energy interval, the variables in the transport equation are

treated as constants. The value of the constant is determined by an appropriate weighted average of the variable over an energy interval. Typically the cross sections are weighted by the flux (which is unknown), thus conserving reaction rates in each energy interval. The energy dependent flux used to calculate the weighted average, is the current best estimate of the flux; in the case where a hypothesis of the flux cannot be formulated an energy independent flux can be used, however, in most situations a more educated guess can be formulated, for example a Maxwellian distribution in the thermal range.

Using the outlined energy discretization scheme the average absorption cross section over an energy  $E_1$  to an energy  $E_2$  is given by equation (3.8),

$$\Sigma_{a1} = \frac{\int_{E_1}^{E_2} dE \Sigma_a(E) \phi(E)}{\int_{E_1}^{E_2} dE \phi(E)} \quad (3.8)$$

If energy, space, and angular dependence, are each treated as discrete variables then the number of equations to be solved can become computationally difficult. To illustrate this, if a 100 by 100 by 100 spatial grid were to be chosen, then one million equations would need to be solved, to know the flux in each of the volume elements. Discretizing each of the volume elements into 10 energy groups, would increase the number of equations to be solved to 10 million. 10 discretizations of the two angular variables, at each position and energy would increase the number of equations to one billion. Furthermore if a time dependent calculation was required, then one billion equations for each time step are required. If a reactor has a volume of  $230,000,000 \text{cm}^3$  ( $230 \text{m}^3$ ), typical of a CANDU 900MW reactor, displayed in Figure 3.3,

then a 100 by 100 by 100 grid may be inadequate since the maximum spatial resolution that can be obtained is about  $230 \text{ cm}^3$ , which is approximately the volume of half of a single fuel bundle. i.e. still relatively low spatial resolution as an individual fuel element cannot be resolved. To increase the spatial resolution, the repetitive nature of the reactor is used, where the transport equation is solved over a small repeating area known as a Lattice Cell.

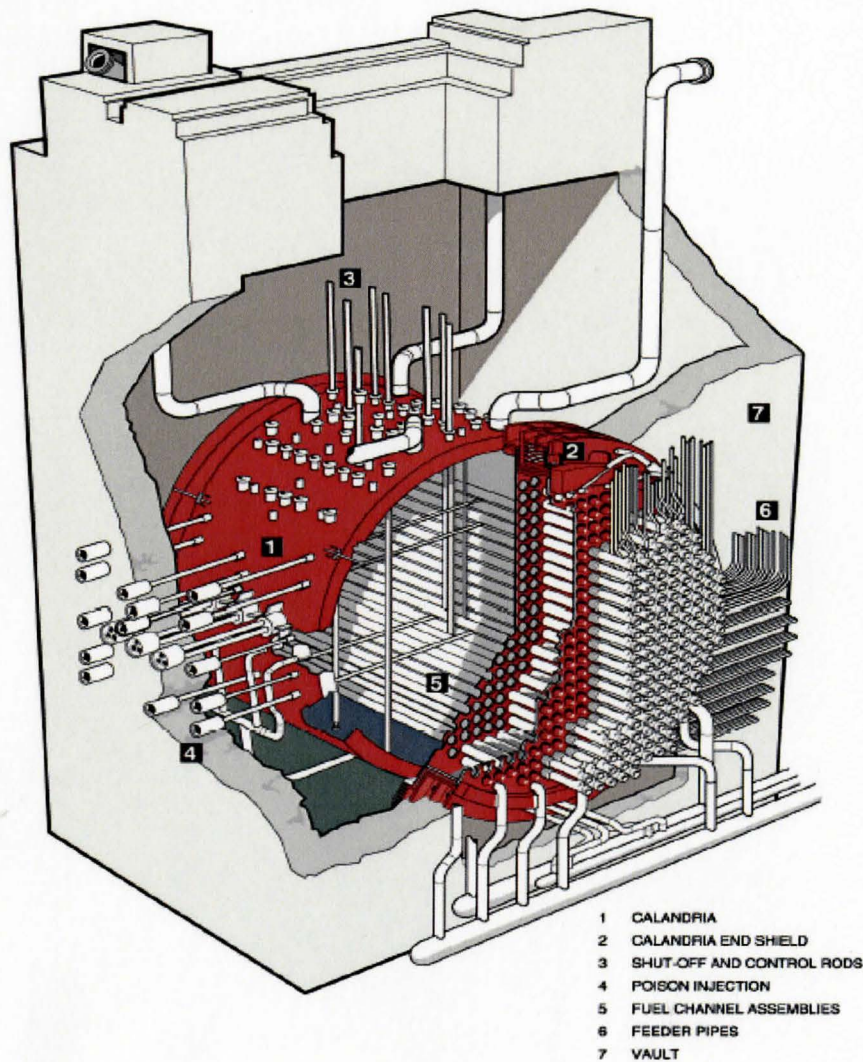


**Figure 3.3: Depiction of a CANDU Reactor Core[14]**

### 3.2.2 CANDU Lattice Cell Approximation

A typical CANDU 900MW reactor has 480 fuel channels, each of which contains 13 fuel bundles with 37 elements per bundle. To circumvent the computer limitations of modeling each fuel element, the lattice cell approximation is used, where each fuel bundle is modeled as a two dimensional lattice cell. The lattice cell is treated as an infinite repeating array of unit cells, where the assumption is made that each unit cell has a reflective boundary condition. The reflective condition is reasonable in the regions of the core not situated on a boundary, since the neutron leakage out of each cell would be balanced by the neutron leakage into the cell from the adjacent lattice cells.

A standard 37 element fuel bundle is shown in Figure 3.4.

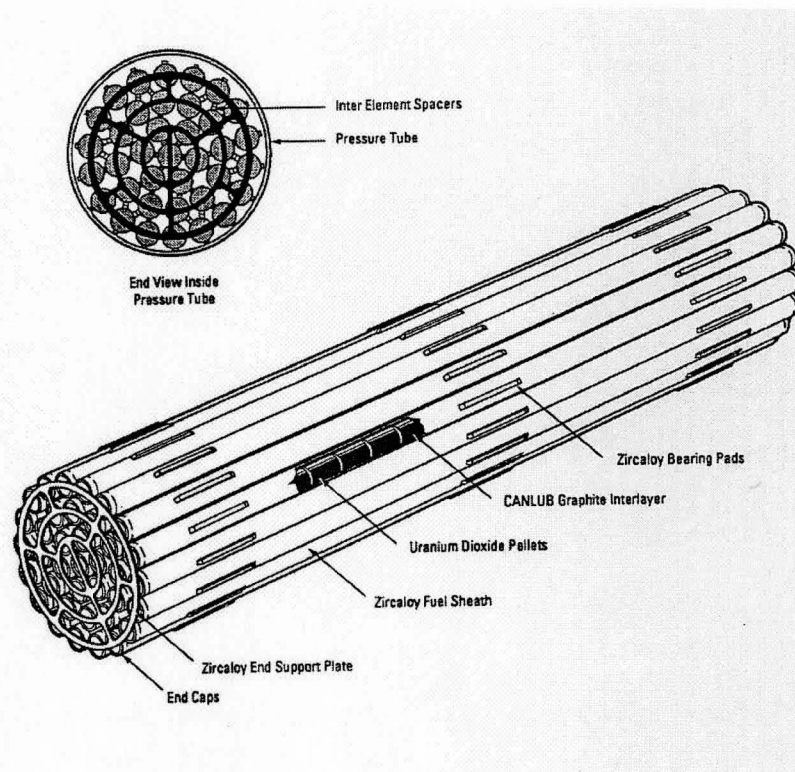


**Figure 3.4: CANDU Fuel Bundle [15]**

The fuel bundles consist of natural  $\text{UO}_2$  surrounded by a zirconium-4 cladding, which, is a material with high corrosion resistance. If each element in the reactor core were to be modeled, the number of elements that would require modeling would be the product of the fuel channel  $\times$  bundles per channel  $\times$  elements per bundle, or  $480 \times 13 \times 37 = 230880$ . The overwhelming number of elements, combined with the process of solving the transport equation in multiple neutron energy groups, illustrates the computational difficulty of obtaining a solution within a reasonable time and computational resources.

The CANDU lattice cell that corresponds to the 37-element fuel bundle is shown in Figure 3.5 . The fuel elements are separated by element spacers (not shown) that allow the heavy water coolant,  $\text{D}_2\text{O}$ , to flow through subchannels between elements. A zirconium pressure tube made of Zr-2.5%Nb houses the fuel bundle. The pressure tube is surrounded by a gap which has a gas circulated to provide thermal insulation between the pressure tube and the Zirconium-2 Calandria tube.

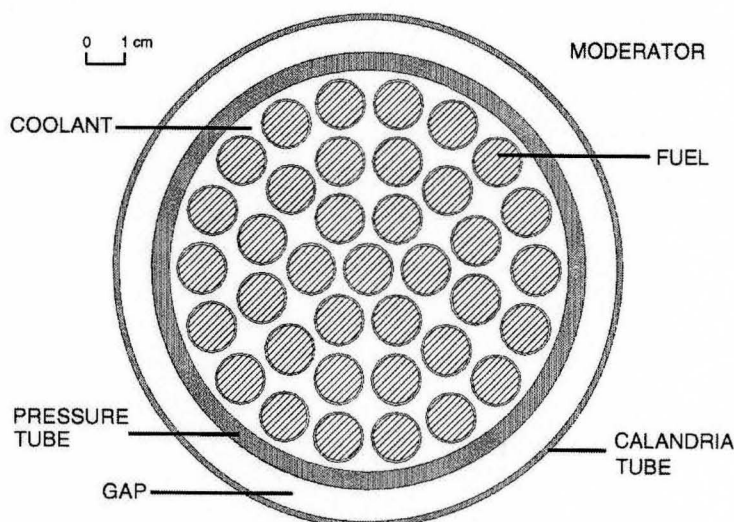


**Figure 3.5: CANDU Lattice Cell [15]**

The transport equation is discretized and solved over the relatively small dimensions of the lattice. The result is a solution of the transport equation, which is accurate with regards to the spatial and energy dependence of parameters within the lattice. To obtain the solution over the lattice cell, various industry codes have been developed, such as DRAGON, and WIMS 2.5d. The latter code is used in this work.

WIMS solves the angular dependent transport equation for steady state by evaluating the integral transport equation, using collision probability methods[9]. The major approximation that is made is that the scattering cross section is isotropic. Normally the angular dependence of the scattering cross section is expanded in a series of Legendre polynomials. In a thermal reactor however, the series is truncated at the zeroeth term, since in thermal reactors the primary source of anisotropic scattering only occurs in the case of neutrons scattering off light atoms.

The solution of the lattice code is clearly dependent on the input into the code, correspondingly the more accurate the input, the more accurate the output. WIMS requires the input of the materials present in the lattice cell, the temperatures and densities of the materials, and the relevant geometric dimensions. The geometry of the lattice cell is summarized in Table 3.1. The selection of the material parameters will be discussed in the subsequent chapter. The output of the code is the neutron flux profile within the lattice cell, known as the microscopic flux profile, as well as the lattice coefficients averaged over the area of the lattice in two energy intervals, which will be used to calculate the macroscopic flux profile in a reactor core physics code. This subsequent calculation

yields the flux profile in the reactor, which takes into account the boundary conditions on the lattice cells at the edge of the reactor.

**Table 3.1: Summary of the Geometry of The CANDU Bundle used in WIMS[16]**

Parameter	37 CANDU-Element Bundle
Fuel Bundle Length	Infinite
UO <sub>2</sub> Pellet Radius	0.6075 cm
Cladding Outer Radius	0.654 cm
Pitch Circle Radius of Inner 6 Elements	1.48845 cm
Angular Offset of Inner Elements	0 radians
Pitch Circle Radius of Middle 12 Elements	2.8753 cm
Angular Offset of Middle Elements	0.2617994 radians
Pitch Circle Radius of Outer 18 Elements	4.3307 cm
Angular Offset of Outer Elements	0 radians
Inner Radius of Pressure Tube	5.180 cm
Outer Radius of Pressure Tube	5.590 cm
Inner Radius of Calandria Tube	6.540 cm
Outer Radius of Calandria Tube	6.696 cm
Lattice Pitch	28.575 cm

### 3.2.3 Two Group Diffusion Equation

In the case where a lower amount of spatial resolution is required, such as the flux profile over the entire reactor core, the multigroup neutron diffusion equation is employed. For the derivation of the diffusion equation, the reader is referred to [17] or almost any introductory text of reactor physics.

The diffusion equation introduces a constant familiar from studies of the movement of gaseous particles. The approximation is made that neutrons diffuse from regions of high concentration towards regions of low concentration, i.e. the movement is dependent on the neutron concentration gradient between regions as governed by Ficks law. The multiple energy group diffusion equation is summarized below:

$$\frac{1}{v_g} \frac{\partial \phi_g}{\partial t} = \nabla \cdot D_g \nabla \phi - \Sigma_{ag} \phi_g + \chi_g \sum_{g'=1}^G \nu_{g'} \Sigma_{fg'} \phi_{g'} - \Sigma_{sg} \phi_g + \sum_{g'=1}^G \Sigma_{sg'g} \phi_{g'} \quad g=1,2,\dots,G \quad (3.9)$$

Where the subscript  $g$  refers to the energy group,  $D$  is the diffusion coefficient,  $\chi$  is the fraction of neutrons emitted,  $\Sigma_{sg'g}$  refers to the scattering from group  $g$  into group  $g'$ .

In a well thermalized reactor such as the CANDU a two energy group approximation is reasonable, so the multigroup diffusion equations reduce to the two energy group diffusion equations

$$\begin{aligned} \frac{1}{v_1} \frac{\partial \phi_1}{\partial t} &= \nabla \cdot D_1 \nabla \phi_1 - \Sigma_{R1} \phi_1 + \chi_1 [\nu_1 \Sigma_{f1} \phi_1 + \nu_2 \Sigma_{f2} \phi_2] \\ \frac{1}{v_2} \frac{\partial \phi_2}{\partial t} &= \nabla \cdot D_2 \nabla \phi_2 - \Sigma_{a2} \phi_2 + \chi_2 [\nu_1 \Sigma_{f1} \phi_1 + \nu_2 \Sigma_{f2} \phi_2] + \Sigma_{s12} \phi_1 \end{aligned} \quad (3.10)$$

In the above equation it is assumed that neutrons do not gain enough energy from scattering to move them from the thermal group to the fast group. This is known as no upscattering.

The coefficients of the neutron diffusion equation are obtained from the transport calculation over the lattice cell. Each lattice cell is treated as a homogeneous region in the diffusion calculation. The transport parameters are dependent on the input of various variables, such as fuel temperature, moderator temperature, coolant voiding etc, which is dependent on the macroscopic flux profile and geometric location of the lattice in the reactor. The diffusion coefficients generated from the transport code serve as input to a diffusion calculation over the reactor, which yields the macroscopic flux profile. The macroscopic flux profile can then be used to obtain a better estimate of the input parameters of the lattice cell calculation.

Thus a procedure of calculating the flux profile in the reactor is established:

1. A lattice cell code is used to solve the transport equation over a small unit volume of the core. The code obtains a microscopic flux profile in the lattice.
2. The lattice cell code then generates cell averaged coefficients which serve as input to the two group diffusion equation.
3. The diffusion equation is solved over the core. This gives the macroscopic flux profile, which is normalized to the power distribution of the reactor. This gives an estimate of the channel and bundle powers throughout the reactor. The normalization process assumes a constant linear mapping between flux and power.
4. The power distribution obtained can be used to obtain a better estimate of the input parameters of the lattice cell calculation. For example, the power will affect the temperature of the fuel, which is an input to the lattice cell code.

### **3.3 Estimating CANDU Channel Power**

In a generic CANDU 900MW reactor the channel power is measured in selected fully instrumented channels, or **FINCH**'s. There are 22 FINCH's in the Bruce Power reactors, and 44 at Darlington. In the FINCH channels, variables such as inlet temperature, outlet temperature, flow, and quality of the fluid are monitored; these values are used to compute the energy transferred to the coolant, which is representative of the steady state power delivered to the coolant flowing through the channel. The power calculated using the FINCH measurements is used to estimate the normalized average total power in the reactor[18].

$$ReactorPower = \frac{1}{F} \sum_{c \in F} \frac{M_c}{N_c} \quad (3.11)$$

Where  $M_c$  is the channel power obtained from the FINCH  $c$ ,  $F$  is the number of FINCH's and  $N_c$  are the 100% full power FINCH nominals that are used to normalize the measurements to the total reactor power. The reactor power calculated is compared to the power measured using a secondary side heat balance. Error between the calculated and measured power is compensated for by adjusting the FINCH nominals. Thus, FINCHs are a tool, which are used to give calibrated estimates of the reactor power.

The total power calculated from the set of FINCH's, is used in conjunction with the flux profile of the reactor generated from a three dimensional diffusion code, to obtain a power profile over the entire reactor. From this simulation with a fuel management code, such as SORO, the channel power and bundle powers can be evaluated. This process is displayed in Figure 3.6.

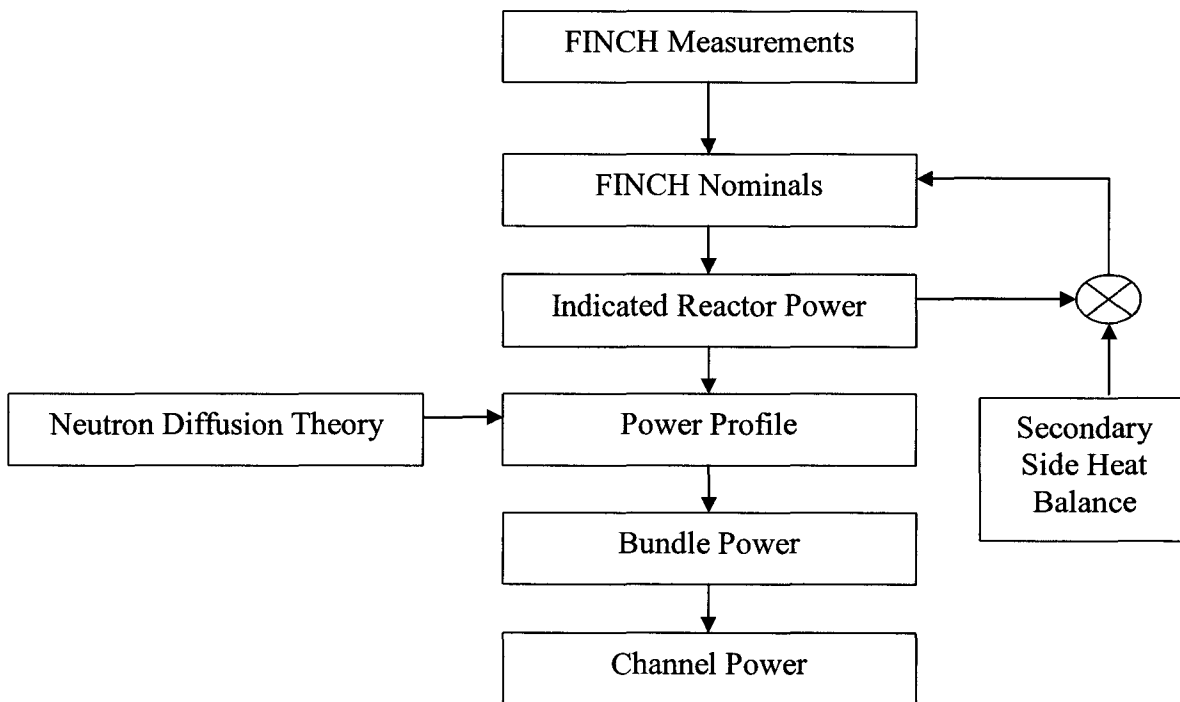


**Figure 3.6: Depiction of the Measurement and Computational Scheme to Calculate Channel and Bundle Power**

The assumption implicit in the above computational scheme is that the flux profile created using the diffusion code, is identical to the power profile. In fact in most computational efforts the assumption is made that the power profile calculated is identical to the thermal flux profile. The mapping of flux to power is carried out through a constant known as the H factor. The H factor originates from a predecessor of WIMS, the lattice code POWDERPUFFS which output the conversion of flux to power as a function of the irradiation of the lattice cell.

In order to analyze the H factor in closer detail, refer back to the conversion of flux to fission power. The basic equation for the power released from fission is shown in

equation (3.12), where  $w_f^i$  is the recoverable energy released per fission of isotope  $i$ ,  $V^{fuel}$  is the fuel volume,  $N_i(r)$  is the spatially dependent number density of isotope  $i$ ,  $\sigma_f^i$  is the microscopic fission cross section of isotope  $i$ , and  $\phi(r, E)$  is the energy and spatial dependent flux.

$$FissionPower = V^{fuel} \sum_i w_f^i N_i(r) \int_0^\infty dE \sigma_f^i(E) \phi(r, E) \quad (3.12)$$

In the two group approximation used in CANDU, the microscopic fission cross sections are replaced with their flux weighted averages, and multiplied by their respective number densities to yield the two group macroscopic fission cross sections  $\Sigma_{1,f}^i$ , and  $\Sigma_{2,f}^i$ , where the subscript 1 refers to the fast group and the subscript 2 refers to the thermal group. Substituting the two group macroscopic fission cross sections into equation (3.12) gives,

$$FissionPower = V^{fuel} \sum_i w_f^i (\Sigma_{1,f}^i \phi_1^{fuel} + \Sigma_{2,f}^i \phi_2^{fuel}) \quad (3.13)$$

The diffusion code will yield the cell averaged flux, which must be related to the flux in the fuel used in equation (3.13). The flux in the fuel can differ appreciably from that of the cell average due to the process in which the outer fuel elements shield the inner elements from thermal neutrons diffusing from the moderator. The difference between the cell averaged flux and the flux in the fuel is accounted for by the use of the F factor, which is the ratio of flux in the fuel to the cell averaged flux.

$$F_1 = \frac{\phi_1^{fuel}}{\phi_1^{cellav}} \quad F_2 = \frac{\phi_2^{fuel}}{\phi_2^{cellav}} \quad (3.14)$$

The F factor encapsulates a flux depression in the thermal group since the fuel is a net sink of thermal neutrons. Since the fuel is a source of fast neutrons the fast F factor will be greater than one, representing a higher fast flux in the fuel than the cell average. The power can be written using the F factors, by substituting equation (3.14) into equation (3.13). The use of the F factors allows the cell averaged flux from the diffusion code to be used in equation (3.15)

$$FissionPower = V^{fuel} \sum_i w_f^i (F_1 \Sigma_{1,f}^i \phi_1^{cellav} + F_2 \Sigma_{2,f}^i \phi_2^{cellav}) \quad (3.15)$$

Often in CANDU reactor calculations, the fission power is taken to be, directly proportional to the cell averaged thermal flux in the reactor. The proportionality factor H is a factor which is defined as the ratio of the fission power to cell averaged thermal flux.

$$FissionPower = H * \phi_2^{cellav} \quad (3.16)$$

Equation (3.16) will hold if the cell averaged thermal flux is linearly proportional to the cell averaged fast flux, which is true for steady state thermal reactors. Thus by comparing equation (3.15) and equation (3.16), and introducing the proportionality constant  $\gamma$ , which relates the cell averaged thermal flux to cell averaged fast flux and fast F<sub>1</sub> factor, the H factor can be expressed as in equation (3.18)

$$\gamma = F_1 \frac{\phi_1^{cellav}}{\phi_2^{cellav}} \quad (3.17)$$

$$H = V^{fuel} \sum_i w_f^i (\gamma \Sigma_{1,f}^i + F_2 \Sigma_{2,f}^i) \quad (3.18)$$

Thus the H factor is the product of the energy released from fission multiplied by the adjusted fission cross section, which takes into account the F factors and the differences between the fast and thermal flux. As the term will be subsequently used throughout this work, the adjusted fission cross section is defined here as;

$$\text{AdjustedFissionCross section} = \sum_i [\gamma \Sigma_{1,f}^i + F_2 \Sigma_{2,f}^i] \quad (3.19)$$

As stated previously, in simulations used to calculate channel and bundle power, the H factor is to a first order approximation, assumed to be constant and equal to the core averaged fission power divided by the core averaged flux. Upon closer examination equation 3.18 shows the H factor will be dependent upon any variable which affects the reaction rate of fission, or the recoverable energy released from fission.

Often there is a mismatch between the calculated and measured power distribution. The variability may occur in part due to the assumption of an average constant H-factor, since clearly the components of equation 3.18 are indeed variable. The error can also stem from the uncertainty in the macroscopic flux profile, for instance the use of the diffusion approximation to calculate the flux profile. The error in the fission power,  $\xi_{FissionPower}$ , will be a function of the error in the H factor and the error in the flux calculation. This work will make no attempt to quantify the error in the flux profile, and will focus solely on the H factor uncertainty.

$$\xi_{FissionPower} = f(\xi_{Hfactor}, \xi_{Flux}) \quad (3.20)$$

Using WIMS, a detailed analysis of the reaction rates in the fuel can be obtained. This will allow the adjusted fission cross section to be evaluated for various states of

lattice cells. The sensitivity of the adjusted fission cross section to various perturbations will be examined in chapter five. A limitation of WIMS for the assessment of the H factor is that the code makes no distinction where the energy released from fission will be deposited. The next section analyzes the modes of energy deposition in the CANDU lattice cell.

## Chapter Four

# 4.0 Examination of The Energy Released From Fission

“During World War II physicists at the Los Alamos Scientific Laboratory came to a knotty problem on the behavior of neutrons. How far would neutrons travel through various materials? The question had a vital bearing on shielding and other practical considerations. But it was an extremely complicated one to answer. To explore it by experimental trial and error would have been expensive, time-consuming and hazardous. On the other hand, the problem seemed beyond the reach of theoretical calculations. The physicists had most of the necessary basic data: they knew the average distance a neutron of a given speed would travel in a given substance before it collided with an atomic nucleus, what the probabilities were that the neutron would bounce off instead of being absorbed by the nucleus, how much energy the neutron was likely to lose after a given collision, and so on. However, to sum all of this up in a practicable formula for predicting the outcome of a whole sequence of such events was impossible.

At this crisis the mathematicians John von Neumann and Stanislaus Ulam cut the Gordian knot with a remarkably simple stroke. They suggested a solution which in effect amounts to submitting the problem to a roulette wheel. Step by step the probabilities of the separate events are merged into a composite picture which gives an approximate but workable answer to the problem.

The mathematical technique von Neumann and Ulam applied had been known for many years. When it was revived for the secret work at Los Alamos, von Neumann gave it the code name “Monte Carlo.” The Monte Carlo method was so successful on neutron diffusion problems that its popularity later spread. It is now being used in various fields, notably in operations research.”

Excerpt from the beginning of:

D.D. McCracken, “The Monte Carlo Method”, *Scientific American*, vol. 192, 1955, pp 90-95.

As seen in chapter three, the conversion between reactor flux and power is dependent upon the energy that can be recovered from a fission event. Energy from fission is released in different forms, and each form has its own mechanisms that govern the transport of the energy. This chapter examines the location of the energy deposition within the lattice cell.

## 4.1 Exploring the Energy Emitted from Fission

Equation (3.5) lists the forms of energy which can be emitted from the fission process. The major fissionable isotopes in a CANDU reactor are Uranium 235 and Plutonium 239. A summary of the averaged energy released, from fission of Uranium and

Plutonium is shown in Table 4.1, omitted is the energy released in the form of neutrinos, due to their high probability of escaping the reactor. Observation of the values in Table 4.1 a general statement can be made that the fission of a plutonium atom releases more energy than fission of a Uranium atom.

**Table 4.1: Energy Released from Fission[16]**

Energy Component	U235(MeV)	U238(MeV)	Pu239(MeV)	Pu241(MeV)
Fragment Kinetic Energy	169.12	169.57	175.78	175.36
Kinetic Energy Neutrons	4.79	5.51	5.9	5.99
Prompt $\gamma$ rays	6.97	6.64	7.76	7.65
$\beta$ Ray Energy	6.5	8.25	5.31	6.58
Delayed $\gamma$ 's of Daughter Nuclei	6.33	8.02	5.17	6.4
Total	193.7	198.0	199.9	202.0

The location of the energy deposition will determine whether the energy is recoverable. Recoverable energy is that which is deposited in the *Fuel, Cladding, Coolant, and Pressure Tube* of the lattice cell. Recoverable refers to the fact that the heat transport system under steady state conditions will remove the energy in these regions primarily through conduction and convection. Energy that is considered unrecoverable is that which is deposited in the *Annulus gas, Calandria Tube, and Moderator*. The heat transport system tends to capture very little energy from these areas due to the insulation that the annulus gas provides.

Each component of fission energy has a different mechanism for energy loss in a material, which will affect the location of the energy deposition. The following sections explore the amount of energy from fission that can be recovered.

## 4.2 Kinetic Energy of Fission Fragments

To test the assumption that the kinetic energy of the fission fragments is confined to the fuel, the energy deposition mechanisms of charged fission products is analyzed.

When fission occurs the nucleus breaks into two highly energetic nuclei, fission fragments, each of which has an excess of positive charge. As the positively charged fragment moves through the material, the columbic force results in the fission fragment ionizing the atoms of the material in which it is moving. The ionization process causes the fission fragment to lose kinetic energy. As the fragment slows, it picks up electrons, which decrease the net charge of the fission fragment; the result is that the ionizing power of the fragment decreases as it traverses the medium, resulting in an ionization density distribution known as a Bragg curve. The linear stopping power is the rate at which the particle energy varies as it transverses a medium[19]

$$S = -\frac{dE}{dX} \quad (4.1)$$

Where S is the stopping power,  $dE$  is the incremental kinetic energy loss per unit of distance traveled,  $dX$ . A detailed derivation of the equation for stopping power is beyond the scope of this work, see[20,21] for details. The Bohr formula for the stopping power[20] of fission fragments is used to derive equation (4.2)[21] for the stopping power of a medium, for a fission fragment. The kinetic energy has been replaced by velocity in equation (4.2):

$$\frac{dV}{dX} = \frac{127.3 \times 10^{11} Z_2^{\frac{1}{2}} \left[ 4.7622 (kZ_1^{\frac{5}{2}})^3 + kZ_1^{\frac{1}{2}} \right]}{\rho A_1 A_2} \quad (4.2)$$

Where  $A_1, Z_1$  are the mass number and atomic number of the fission fragment,  $A_2, Z_2$  are the mass and atomic number of the medium which the fragment is transversing, and  $k$  is a constant equal to 1 in a solid and 1.5 in a gas. The initial charge  $Z_1$  of the fission fragment immediately after a fission event is related to the mass of a heavy fission fragment by the formula:

$$Z_1(A_1) = \frac{A_1}{2.587} \quad (4.3)$$

To find the range of the fragments, which will indicate whether the fragment is contained in the fuel, the inverse of stopping power is integrated over velocity as the fragment slows.

$$Range = \int \left( \frac{dV}{dx} \right)^{-1} dV \quad (4.4)$$

It is sufficient to evaluate the above integral from the initial fragment velocity  $V_i$  to the velocity at which the fragment has a neutral charge  $V_0$ , which is equal to  $\frac{e^2}{h_{bar}}$  since at  $V_0$  the orbital electrons are then moving at a velocity similar to that of the fragment. Once the fragment becomes neutral it will primarily experience interactions which result in large deflections which contribute negligibly to the range.

Integrating the inverse of equation (4.2) the range in  $\left( \frac{mg}{cm^2} \right)$  is then given by

$$R = \frac{A_1 A_2 (V_i - V_0)}{127.3 Z_2^3 \left[ 4.7622 (k Z_1^3)^{\frac{1}{5}} + k Z_1^{\frac{1}{3}} \right]} \quad (4.5)$$

Dividing equation (4.5) will yield the absolute range in cm.

Using the above formula for range, along with the density of the material, the distance of two common fission fragments in Uranium and Zirconium are calculated and displayed in Table 4.2 .

**Table 4.2: Range of Fission Fragments in Zirconium and Uranium**

Fragment	Energy	Medium	Density(g/cm <sup>3</sup> )	Range(cm)
A=96	50MeV	Zirconium	6.44	7.02E-04
A=131	50MeV	Zirconium	6.44	6.38E-04
A=96	100MeV	Zirconium	6.44	9.92E-04
A=131	100MeV	Zirconium	6.44	9.02E-04
A=96	50MeV	Uranium	10.358	8.28E-04
A=131	50MeV	Uranium	10.358	7.52E-04
A=96	100MeV	Uranium	10.358	1.17E-03
A=131	100MeV	Uranium	10.358	1.06E-03

The above Table shows that the fission fragments are indeed primarily confined to the fuel. Even if a fragment is generated at the very edge of the fuel pellet, the 0.04cm Zirconium cladding is sufficient to prevent the fragment from leaving the fuel, thus confining the fragment energy to the fuel, and hence, to the heat transport system.

Similar results to those in Table 4.2 can be obtained from a freely available code SRIM(Stopping and Range of Ions in Matter)[22], however, SRIM does not deal specifically with fission fragments, and thus does not account for the probable number of electrons on an ion after fission.

## 4.2 Energy from Beta Particles

Beta particles like fission fragments are charged particles, thus the primary energy loss mechanism is from columbic interaction. When a high energy beta particle passes near an atomic shell, a columbic impulse is often sufficient to liberate an orbital electron from the atomic shell, creating an ion pair. The average energy that the beta particle loses by creating an ion pair in air is approximately 33eV[23]. The ion pair energy for other materials is similar to that of air.

The maximum range of a beta particle in a material is given by an empirical equation useful for hand calculations known as Feathers rule, shown in equation (4.6) [23]

$$R = \frac{0.543E - 0.16}{d} \quad (4.6)$$

Where R is the range in cm, E is the energy in MeV, d is the density in  $\text{g/cm}^3$

If the maximum energy of a beta particle is taken, conservatively, to be 6.5MeV and the material that the beta particle is traveling through is the fuel with density  $10.2 \text{ g/cm}^3$ , then using the equation above the maximum range of the beta particle by an application of Feathers rule is 0.33cm. This implies that most of the energy of beta particles created from fission would be deposited in the fuel region, and the energy that escapes the fuel would surely be dissipated in the fuel cladding. Thus, the assumption that the beta energy from fission is confined to the fuel elements, and is recoverable, is deemed acceptable.

## 4.3 Energy from Neutrons

Neutrons interact with materials in a nuclear reactor primarily in three ways, fission, capture and scattering. The fission process has been explored in section 3.1 and to avoid redundancy will not be reiterated here. In neutron capture the neutron is absorbed by another atom without a subsequent fission event occurring. Neutrons can also scatter off the nucleus of various materials in the reactor, transferring some portion of their energy to the nucleus involved in the collision. The location of these modes of neutron interaction will be explored.

### 4.3.1 Elastic Scattering

Elastic scattering, displayed in Figure 4.1 , also referred to as potential scattering, is essentially the process of neutrons involved in “billiard ball” scattering events with heavy nuclei. Elastic scattering predominantly occurs with neutrons of energy below 1MeV.

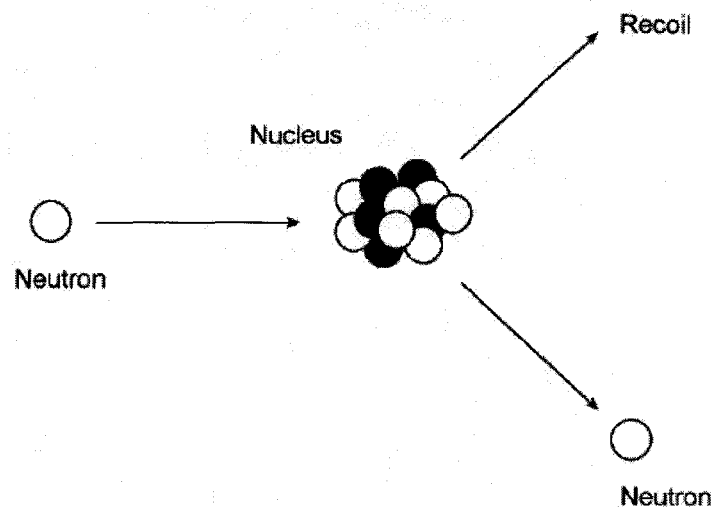


**Figure 4.1: Depiction of Elastic Scattering of Neutrons[24]**

The energy that is lost by a neutron in elastic scattering will be dependent on the mass of the atom and the angle of scatter. An equation for the energy of the scattered neutron is[17]:

$$E_f = \left[ \frac{(1 + \alpha) + (1 - \alpha) \cos \theta_c}{2} \right] E_i \quad (4.7)$$

Where,

$$\alpha = \left( \frac{A - 1}{A + 1} \right)^2 \quad (4.8)$$

In the above expression A is the mass number.

This formula displays the relationship that on average the energy lost by a neutron will increase as the mass of the collision target approaches the mass of the neutron. A comparison of the energy loss of a 180 degree scatter of a neutron with Uranium and with Deuterium shows that  $\alpha = 0.9831$  for a scattering event with U235 and  $\alpha = 0.111$  for Deuterium. Substituting in the respective values of alpha into equation (4.7), shows that an elastic scattering event with a Deuterium atom a neutron can lose up to 88.99% of its energy, while the neutron loses only up to 1.69% when scattering with a U235 atom. This supports an assumption that most of the energy lost from the elastic scatter of neutrons will be deposited in the moderator.

### 4.3.2 Inelastic Scattering

Inelastic scattering, Figure 4.2, occurs when an element absorbs a neutron and then quickly re-emits the neutron at a lower energy. This type of scattering will occur primarily with neutrons of energy greater than 1MeV. The incident neutron leaves the

atom in an excited state, from which it will subsequently decay. The most common decay mechanism is the emission of high energy gamma rays.

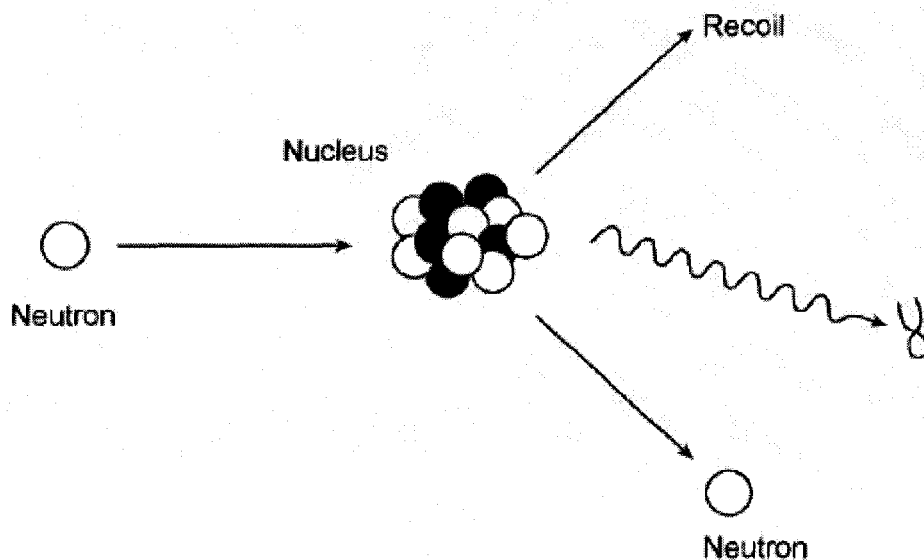


**Figure 4.2: Depiction of Inelastic Scattering of Neutrons[24]**

The large energy threshold of inelastic scattering implies this mechanism will be more relevant in the fuel, since on average neutrons are at higher energies within the fuel.

The location of the energy deposition of gamma rays will be explored in section 4.4.

### 4.3.3 Neutron Capture

Similar to inelastic scattering, neutron capture occurs when an element absorbs a neutron. The distinguishing feature is that in neutron capture the neutron is not remitted. A series of gamma rays are emitted which are equal to the incident neutron energy plus the binding energy of the additional neutron, of the particular element in which the capture event occurred. Neutron capture is shown in Figure 4.3 .

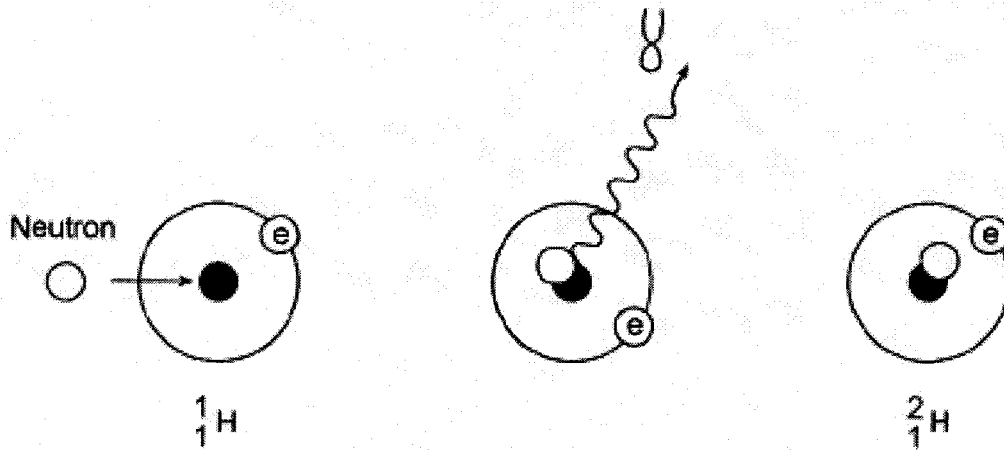


**Figure 4.3: Example of Neutron Capture in a Hydrogen Atom[24]**

## 4.4 Energy Emitted from Gamma's

The location the energy deposition from gamma rays will be correlated to the initial energy of the emitted gamma. The energy is in turn a function of the mode of gamma ray generation. The three most significant sources of gamma rays are prompt, delayed and capture gammas each of which is subsequently examined.

### 4.4.1 Prompt Gamma Rays

Prompt gamma rays occur as a result of a fission reaction and appear within  $10^{-8}$  seconds of a fission event. The energy spectrum of the prompt gamma rays, will depend upon the isotope which undergoes fission, as well as the incident neutron energy. A typical prompt gamma ray energy spectrum from the fission of a U235 nucleus is seen in Figure 4.4[16].

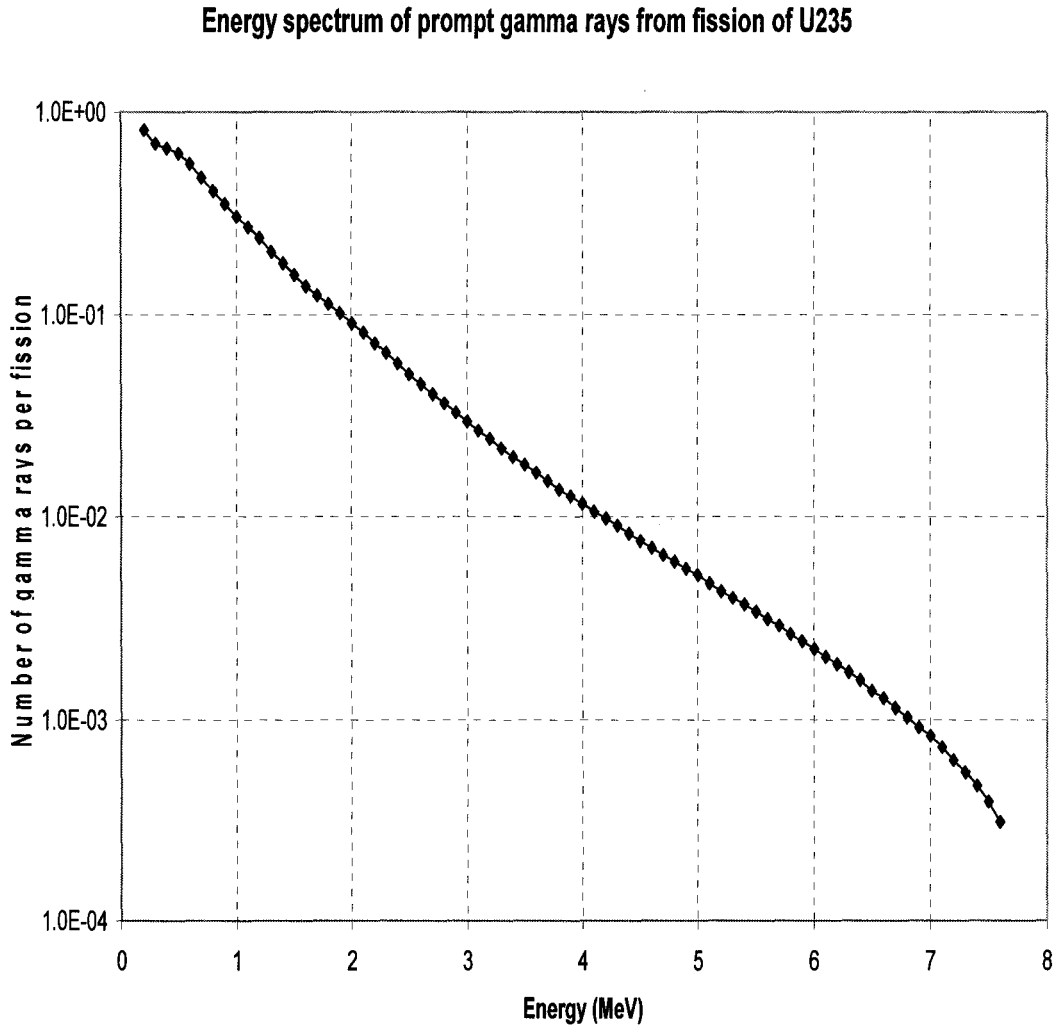


**Figure 4.4: Energy Spectrum for Prompt Gamma Rays from U235[23]**

A theoretical shape for the emission of prompt gamma rays was proposed[25], which, is dependent on the isotope and the average number of prompt neutrons emitted.

$$P(E_\gamma) = \frac{e^{-E_\gamma / \langle E_\gamma \rangle}}{\langle E_\gamma \rangle} \text{ for } E_\gamma > 0.7 \text{ MeV} \quad (4.9)$$

$$P(E_\gamma) = P(0.7 \text{ MeV}) \text{ for } E_\gamma < 0.7 \text{ MeV}$$

Where ,

$$\langle E_\gamma \rangle = \text{average energy of the emitted gamma's} = \frac{\langle E_{\gamma,t} \rangle}{\langle N_\gamma \rangle}$$

$$\langle E_{\gamma,t} \rangle = \text{average emitted total prompt gamma energy} = C_1 \nu_p + C_2$$

$$\langle N_\gamma \rangle = \text{average number of emitted gamma's}$$

$C_1$  and  $C_2$  are constants which are dependent on the isotope that undergoes fission, and  $\nu_p$  is the average number of prompt neutrons emitted.

Examining Table 4.1 the total energy released from prompt gamma's is higher for Pu 239. To illustrate the relative amounts of Pu239 fission to U235 fission at a burnup of 4217MWd/t, which is approximately midburnup of the fuel, the amount of Pu239 fission is roughly equal to the U235 fission.

#### 4.4.2 Delayed Gamma Rays

Delayed gammas occur as a result of the decay of unstable elements created by the fission process. Although the delayed gamma ray energy is the result of decay events in which the gammas emitted are at specific quanta, the large number of unique decay events that occur allows the spectrum to be treated as continuous, for steady state operation. Upon shutdown of the reactor the spectrum will begin to shift to lower intensities, since the quanta emitted by the decay of short lived isotopes will begin to disappear. It is interesting to note that the spectrum retains the same shape with time, and that the spectrum appears to be relatively independent of the isotope which has undergone

fission. Figure 4.5 displays the delayed gamma ray spectrum of the major fissionable isotopes[16].

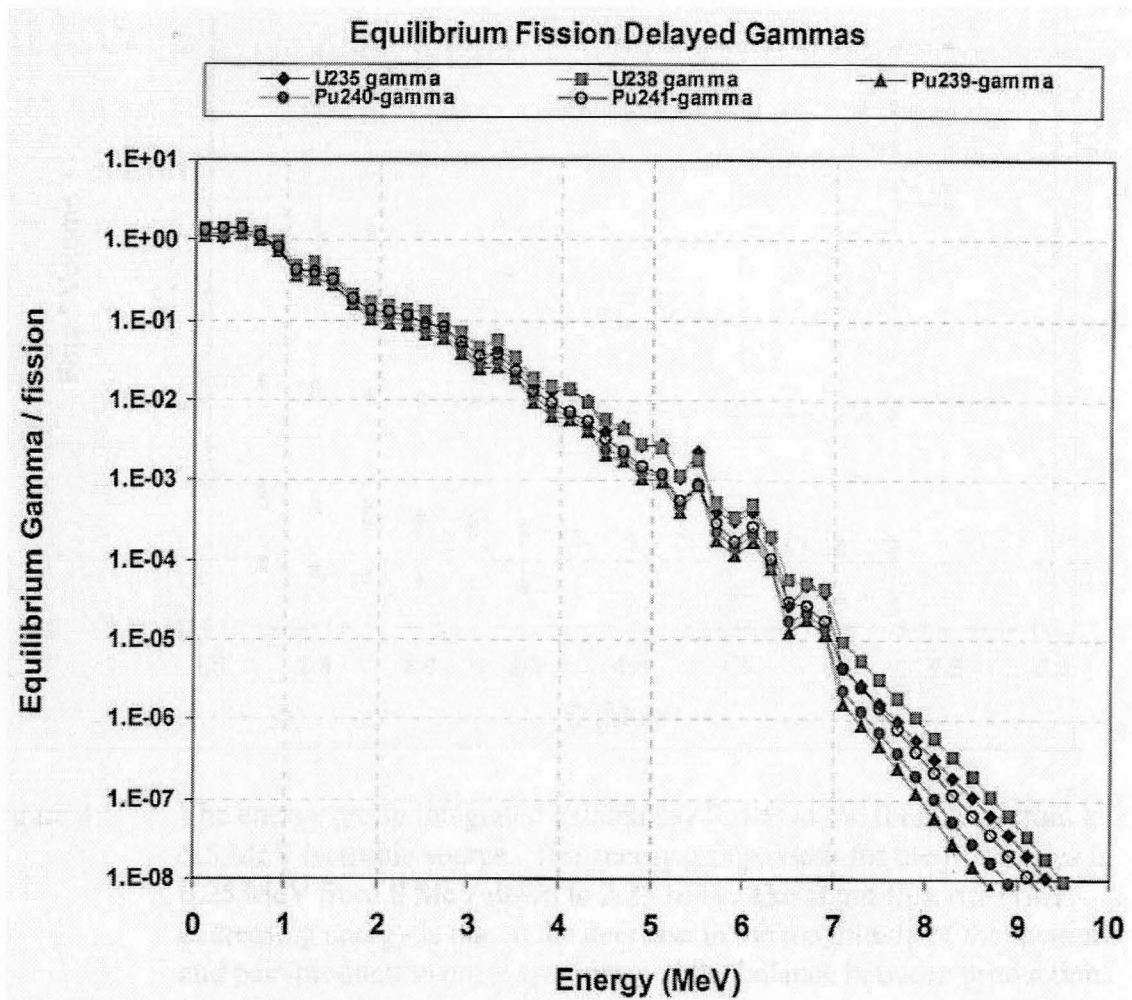


**Figure 4.5: The Delayed Gamma Ray Yield for Major Fissionable Isotopes[16]**

Although the shape of Figure 4.5 is similar for each isotope, the intensity of the delayed gamma rays is slightly lower for fission of Pu239 than U235. This is in agreement with the data presented in Table 4.1 which indicates that the delayed gamma from Pu239 should be less than that of U235.

### 4.4.3 Gamma rays from Neutron Capture

When a neutron is captured by an atom, there is a difference between the sum of the rest mass energy of the neutron and the incident atom. The mass defect between the two states results in a release of energy, most commonly in the form of 1-4 gamma rays. If the decay occurs slowly via gamma ray emission, the neutron capture is referred to as radiative capture. The exact energy of the emitted gammas will be dependent upon both the isotope and energy of the incident neutron, however, Table 4.3 shows that for major fuel isotopes this energy is approximately 5.99 MeV. Thus, the gamma ray spectrum from radiative capture is significantly harder than the spectrum from both prompt and delayed gamma rays.

**Table 4.3: Capture Energy in CANDU Fuel for the Major Fissionable Isotopes[26]**

Isotope	$\nu - 1$ (#/fission)	Energy Released Single in Capture(MeV)	Total Capture Energy(MeV)
U-235	1.437 $\pm$ 0.0034	5.99 $\pm$ 0.5	8.608 $\pm$ 0.72
U-238	1.822* $\pm$ 0.01**	5.99 $\pm$ 0.5	10.914 $\pm$ 0.91
Pu-239	1.879 $\pm$ 0.006	5.99 $\pm$ 0.5	11.255 $\pm$ 0.94
Pu-241	1.945 $\pm$ 0.007	5.99 $\pm$ 0.5	11.651 $\pm$ 0.97

\*This value has been adjusted to account for the (n,2n) reaction in U-238, which increase the neutron production by about 1.5%. The adjustment was calculated using WIMS-AECL for a 37-element bundle.

\*\*This value is estimated based on the nuubar values for the other fissionable isotopes. Note that the uncertainties in the nuubar value are negligible compared to the uncertainty in the energy released from a single capture.

The location of the neutron capture will determine where the gamma ray was generated and subsequently the probability that the energy will be recovered in the heat transport system. Table 4.4, which was composed for a CANDU reactor lattice at midburnup using WIMS, shows that over 85% of neutron captures occur in the fuel. The

amount of capture that occurs in the fuel is inevitably higher than 85% since a significant amount of the remaining neutron capture takes place in other fission fragments, located in the fuel. This illustrates that the assumption of capture gamma rays originating in the fuel is reasonable.

**Table 4.4: Capture Probability in a CANDU Lattice at Midburnup, Calculated Using WIMS 2.5d**

Material	Capture Probability %	Material	Capture Probability %
$^{235}\text{U}$	21.2	Heavy Water	0.2
$^{238}\text{U}$	36.6	Zirconium Pressure	1.3
$^{239}\text{Pu}$	26.3	Zirconium Calandria	0.6
$^{241}\text{Pu}$	1.3	Light Water	1.1
$^{135}\text{Xe}$	2.4	Other Materials	9.0

As displayed above, the major contribution of capture gamma rays are from neutron capture which occurs in  $^{235}\text{U}$ ,  $^{238}\text{U}$ , and  $^{239}\text{Pu}$ . Table 4.6 displays the most important gamma rays which occur during a capture event of the aforementioned isotopes, as well as their intensity relative to the most intense gamma ray. In the case where multiple gamma rays are present in an energy group the intensities are summed. The gamma ray capture spectrum cannot in general be approximated as continuous as there is a large variation in the energy of the gamma rays emitted.

**Table 4.5: Table of Major Gamma Rays From Neutron Capture[27]**

Material	Energy(keV)	Intensity Relative to Isotopes Most Intense Gamma Ray	Material	Energy(keV)	Intensity Relative to Isotopes Most Intense Gamma ray
<b>U238</b>	10-200	100	<b>235U</b>	642.2	100
	400-600	79.5		687.5	31.03
	600-800	60.7		909.1	13.1
	800-1000	19.4		912.7	5.52
	1000-1200	21.6		915.1	6.9
	3000-3200	3.9		922.1	9.31
	3200-3400	3.6		943.0	16.21
	3400-3600	5.2		956.2	17.76
	3600-3800	3.2		958.3	7.76
	3800-4000	5.0		959.9	5.52
<b>239Pu</b>	4000-4200	12.0	977.4	10.17	
	5123.80	58.00	1006.0	7.59	
	5292.70	38.00	1014.1	13.1	
	5575.00	100.00	6395.7	5.52	
	5633.60	10.00			
	5673.30	9.00			
	5936.60	13.00			
	6491.20	30.00			

Table 4.5 indicates that the gamma ray spectrum as a result of neutron capture, can be significantly harder than the gamma ray spectrum from prompt and delayed neutrons. In the case of U235 and U238 the probability of a gamma ray of high energy being emitted generally decreases, as the energy increases. However, the energy dependence does not decrease exponentially, as is the case for fission and delayed gammas. Table 4.6 also shows that the hardest spectrum is a result of capture from Pu239, and it is seen that all of the significant gamma rays have energies greater than 5MeV. Thus, as the fuel begins to burnup, creating more plutonium, the neutron capture spectrum will shift to higher gamma ray energies. A general rule is that higher energy gamma rays are more penetrating, increasing the probability that the gammas will escape the fuel.

## 4.5 Gamma ray Interactions with matter

Gamma rays interact with matter primarily in three different ways, *Photoelectric effect*, *Compton scattering*, and *Pair production*. Although there are other types of gamma ray interactions with matter, these interactions are negligible for gamma ray energies below 10MeV.

### 4.5.1 Photoelectric Effect

The photoelectric effect occurs when a relatively low energy gamma ray (energy less than 1MeV) interacts with the atomic shell. This interaction causes the gamma ray to vanish and an electron to be emitted, with kinetic energy equal to that of the incident gamma ray minus the binding energy of the electron, as shown in equation (4.10). Where  $h$  is Plank's constant, and  $\nu$  is the frequency of the emitted photon.

$$E_e = h\nu - \text{Binding Energy} \quad (4.10)$$

The absorption spectrum for the photoelectric effect, exhibits peaks when the energy of the incident gamma ray is equal to the difference between two quantum states in the atomic shell. Absorption of electrons in the K shell ( $1s$ )<sup>2</sup> is the most significant in terms of energy transfer from gamma rays to electrons, since the K shell electrons are the most tightly bound, as shown in Figure 4.6. If the gamma ray energy is just below the energy needed to eject a K shell electron, the probability for photoelectric effect drops off rapidly, this effect is known as the K edge. The other atomic shells L, M depicted in Figure 4.6 each have similar edges, which occur at progressively lower energies, since the electrons have a lower binding energy.

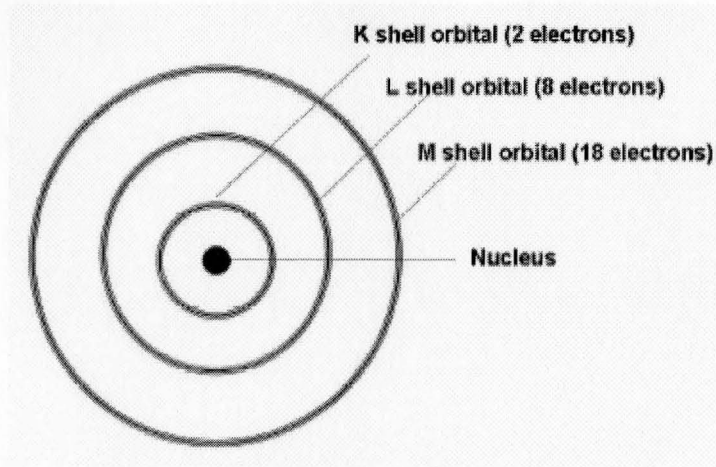


**Figure 4.6: Depiction of Atomic Shells[28]**

The energy range over which the photoelectric effect occurs is limited by the binding energy of the K shell electrons. Typically photoelectric interactions are the dominant mode of interaction until near 1MeV. The photoelectric effect cross section decreases as the energy of the photon increases, as the probability of an interaction occurring is proportional to the wavelength of the photon. The photoelectric effect is shown in Figure 4.7.

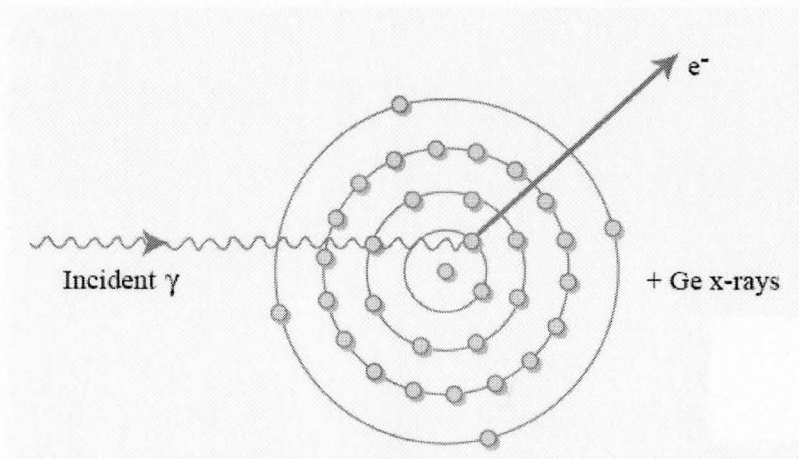


**Figure 4.7: Depiction of Photoelectric Effect[28]**

## 4.5.2 Compton Scattering

Compton scattering[19,29], shown in Figure 4.8, occurs when a photon interacts with an individual electron. The interaction between the photon and electron in Compton scattering is treated as a two body collision process. The photon imparts a fraction of its energy to the recoil electron, and is deflected by an angle  $\theta$  in the centre of mass coordinate system. The energy of the deflected photon is given by equation (4.11).

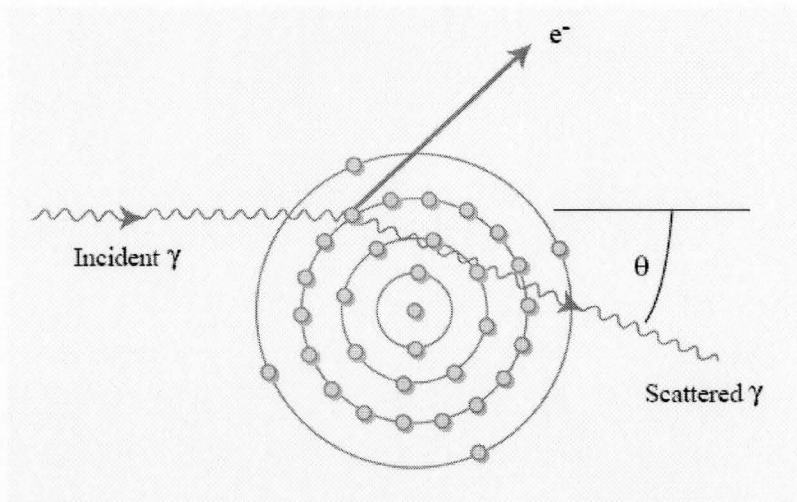


**Figure 4.8: Depiction of Compton Scattering[28]**

$$h\nu' = \frac{h\nu_0}{1 + \gamma(1 - \cos \theta)} \quad (4.11)$$

$$\gamma = \frac{h\nu_0}{m_e c^2} \quad (4.12)$$

Where  $h\nu'$  is the energy of the deflected photon,  $h\nu_0$  is the energy of the incident photon,  $\theta$  is the angle of scatter of the photon, and  $\gamma$  is a ratio of the energy of the incident

photon to the rest mass energy of the electron. The energy lost in the collision will be dependent upon the angle of scatter in the collision.

The probability distribution of the scattering angle of the photon is given by the Klien-Nishima cross section:

$$\frac{d\sigma_{KN}}{d\Omega} = \frac{r_e^2}{2} \frac{1}{[1 + \gamma(1 - \cos\theta)]^2} \left[ 1 + \cos^2\theta + \frac{\gamma^2(1 - \cos\theta)^2}{1 + \gamma(1 - \cos\theta)} \right] \quad (4.13)$$

In the above equation  $r_e$  is the classical electron radius 2.82E-15.

When the Klien-Nishima distribution is integrated over the angular coordinate the expression for the total Compton cross section is[30]:

$$\mathcal{G}_{KN} = 2\pi r_e^2 \left[ \frac{1 + 2\gamma}{\gamma^2} \left( \frac{2(1 + \gamma)}{1 + 2\gamma} - \frac{\ln(1 + 2\gamma)}{\gamma} \right) + \frac{\ln(1 + 2\gamma)}{2\gamma} - \frac{1 + 3\gamma}{(1 + 2\gamma)^2} \right] \quad (4.14)$$

Using equation (4.11), with equation (4.14) the energy that the photon imparts to the electron can be computed. The electron will subsequently interact in a short distance as shown in the previous section, thus in this work the energy is considered deposited at the point of interaction. Compton scattering is generally the primary interaction at energies between 1MeV and 5MeV.

### 4.5.3 Pair Production

Pair production, shown in Figure 4.9, occurs when a gamma ray transforms into a positron electron pair. Pair production can only occur in the vicinity of an electric field and when the gamma ray energy is greater than 1.022 MeV, which is the sum of the rest mass energy of the positron and electron. Thus, pair production is only of interest for high

energy gamma rays in the CANDU reactor. The positron will slow within a short distance through coulombic interaction. Once the positron loses its excess kinetic energy, it will recombine with an electron producing two 511keV gamma rays, which will travel in opposite directions, required by momentum conservation.

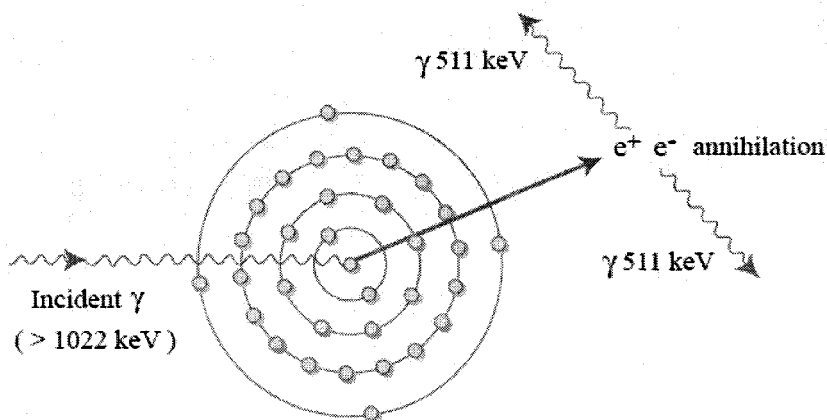


**Figure 4.9: Depiction of Pair Production[28]**

Pair production is the dominant mode of interaction for energies over 5MeV.

## **4.6 Monte Carlo Simulation of Gamma Ray Energy Deposition in A CANDU Lattice Cell**

Monte Carlo methods are an effective means for solving problems for which an analytical solution is difficult or impossible, but underlying probability distributions are known. To calculate the energy deposition within a CANDU lattice cell a Monte Carlo simulation of gamma ray transport was created using MATLAB 7. The gamma ray code uses simple models to obtain pertinent results, for example the sensitivity of the location of the energy deposition to parameters such as the moderator density.

The geometry of the CANDU lattice, as listed in Table 3.1, was modeled; modeling consisted of entering the photon cross section of the material in the Cartesian coordinates that the material occupied. Shown below is an example of the modeling demonstrated by an excerpt from the code; The (x,y) position of the gamma ray is checked, in the example below if the location is found to be a particular fuel element, then a flag is set to one. This flag's purpose is to indicate which material the gamma ray is traveling in. The next step is to determine the energy of the gamma ray in order to assign a photon electron cross section, which will be subsequently discussed. A cross section is assigned for each significant element present in the fuel.

```
elseif (((((x-ring3*cos(0*pi/6 + ang))^2)+(y-ring3*sin(0*pi/6 +
ang))^2)^0.5)<0.6075) %checks the location of the photon
flagfuel=1;

%Assigning Photon Cross Sections to Fuel Materials
elseif (energy>=group3 & energy<group4 & flagfuel==1) %100ev-1000ev
RhophotoU=2796957.84;RhocomptonU=0.78366;RhopairU=0;
RhophotoOxy=272261.607;RhocomptonOxy=.086196170;RhopairOxy=0;
RhophotoTh=2888499.31;RhocomptonTh=.809426708;RhopairTh=0;
RhophotoNp=2734360.26;RhocomptonNp=.777215822;RhopairNp=0;
RhophotoPu=2761053.34;RhocomptonPu=.774534757;RhopairPu=0;
```

Each material with a non negligible isotopic concentration, was programmed into the simulation. A non-negligible concentration in each region was defined as the product of the relative density of the material  $\frac{\rho_x}{\rho_m}$ , multiplied by the number of electrons,  $Z_x$  being greater than a fixed value of  $1e-2$ .

$$\frac{\rho_x}{\rho_m} \times Z_x > 1e-2 \quad (4.15)$$

Where  $\rho_x$  is the density of the isotope x,  $\rho_m$  is the density of the compound. Since the gamma rays primarily interact with the electrons in the materials atoms, equation (4.15)

was used to ascertain the relative importance of each of the materials. In the fuel region the above rule was relaxed somewhat and more elements were programmed, namely Neptunium, Thorium, and Plutonium. The addition of these isotopes had a negligible impact; the addition of these isotopes solely to allow a greater flexibility of the code for future applications, such as testing the effects of high burnup fuel on the gamma ray energy.

Examining the location in which the gamma rays are generated, Table 4.4 indicates a majority of the neutron capture occurs in the fuel. The fission assuredly occurs in the fuel as well, so the approximation was made that each of the gamma rays were generated in the fuel.

The probability of a gamma ray being generated in the individual fuel elements was assumed to vary with the radial thermal flux profile. Using WIMS, the relative flux in the fuel elements was found. In a CANDU lattice cell the outer fuel elements shield the inner elements from the thermal neutrons generated in the moderator, as shown in Figure 4.10.

The fuel ring in which the gamma ray originates was chosen by weighting the number of fuel elements in the ring, by the radial depression factor obtained through WIMS.

$$P(RE_y) = F_y \times \frac{N_y}{N_{Burn}} \quad (4.16)$$

Where  $P(RE_y)$  is the probability that a gamma will be generated in ring  $y$ , and  $y$  can equal 1,2,3 or 4 corresponding to the four fuel rings,  $F_y$  is the radial flux depression factor

obtained from WIMS at midburnup,  $N_y$  is equal to the number of elements in a particular ring, and  $N_{burn}$  is the number of elements in the bundle, 37 in this case.

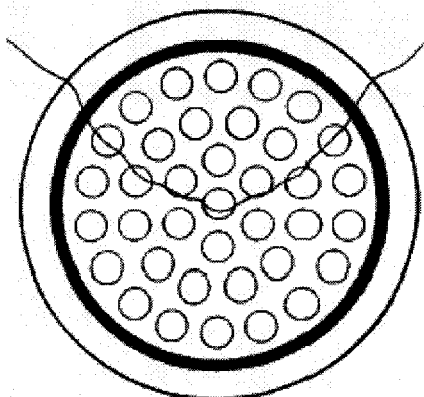


**Figure 4.10: Depiction of the Shielding Effect of the Outer Elements[31]**

**Table 4.6: Radial Flux Depression Factors at Various Burnups**

<b>Location</b>	<b><math>N_y</math></b>	<b>F-factor Zero Burnup</b>	<b>F-Factor Mid Burnup</b>	<b>F-Factor Full Burnup</b>
<b>Ring One</b>	1	0.81	0.78	0.76
<b>Ring Two</b>	6	0.84	0.81	0.80
<b>Ring Three</b>	12	0.93	0.92	0.91
<b>Ring Four</b>	18	1.12	1.13	1.14

Once the element was selected, the next step is to determine the radial position in the element in which the gamma ray is generated. The approximation was made that the flux profile within the fuel elements was spatially independent. The true flux profile within the elements should resemble a Bessel function[32], so the impact of the flat flux approximation would be to bias high the number of gamma rays generated near the centre

of the fuel pin. The result is that the final result will have a slight systematic bias towards gamma rays being captured by the fuel.

To obtain an equally distributed radial sampling, a first attempt was to simply generate a random number between zero and the radius of the fuel element. This sampling technique was found to be inadequate as it is biased towards over sampling the inner portion of the fuel element. Figure 4.11 illustrates the problem with the aforementioned sampling technique; the inner circle represents the inner half of the fuel element, which has an area equal to  $\frac{1}{4}$  the area of the circle. The outer portion of the circle has an area equal to  $\frac{3}{4}$  of the total circle area. The sampling should be proportional to the area of the circle. If the radial sampling is done linearly between zero and  $r$ , gamma rays will be generated in the inner circle  $\frac{1}{2}$  of sampling events, and in the outer portion  $\frac{1}{2}$  of sampling events, which does not conform with area proportional sampling. The solution is to generate a random number linearly between zero and  $r^2$  which is equivalent to area proportional sampling, and subsequently take the root of the random number, thereby skewing the radial sampling toward the outer portion of the circle.

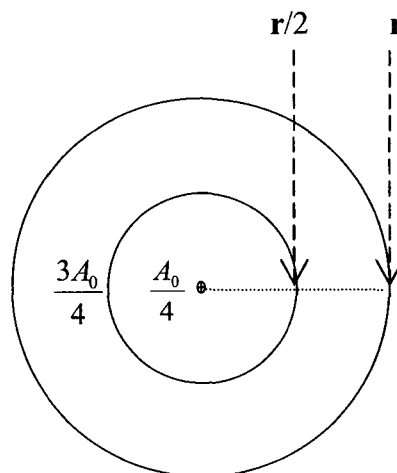


**Figure 4.11: Depiction of fuel element sampling**

Subsequently another random number was chosen evenly between 0 and 360, corresponding to the angle in degrees in which the photon would travel. An assumption was made that the gamma rays are emitted isotropically. Once this is done the gamma ray has both a position as well as a direction.

The next step was to determine the energy of the generated photon. The three spectra from which the gamma rays could be chosen, as previously discussed are the prompt spectrum, the delayed spectrum, and the capture spectrum. The probability distributions for each spectra was chosen from the data previously displayed in Section 4.4 which outlined the generation of gamma rays.

With regards to capture gamma rays, the amount of capture is slightly greater than the amount of fission. Also the energy released from each capture event is greater than that of a delayed or prompt gamma emission from each fission event. Intuitively this may indicate that the capture spectrum should be sampled more often, however, since the capture spectrum is harder, when the capture spectrum is sampled it is more likely that a high energy gamma will be chosen.

Since the prompt and delayed gamma curves for the major fissionable isotopes are similar, a reasonable first approximation was to sample from the U235 gamma ray spectrum.

If a capture event was chosen, then the capture spectrum was sampled from a gamma ray in either the U235, U235 or Pu239 capture spectrum.

Once the energy of the gamma ray was determined, the microscopic cross section for photon interaction in the region could be selected. The total microscopic cross section

was found by summing the cross sections of photoelectric effect, Compton scattering, and pair production.

$$\mathcal{J}_{total} = \sigma_{photo} + \sigma_{compton} + \sigma_{pair} \quad (4.17)$$

The cross section data was obtained from processing the Evaluated Photon Data Library(EPDL97), which is publicly available through the IAEA websites[33]. The EPDL data is in a format which must be manipulated into a usable form. The processing of the EPDL97 library into a usable form was done through the use of a freely available code suite named PREPRO2004[34], which can be used to process all of the libraries with ENDFB-VI format. The routine GROUPIE, which is part of the PREPRO code suite was used to create group averaged energy photon cross sections. A 22 energy group scheme was selected. At low energies the group intervals increase by decades until 100keV. This coarse energy grid for low energies was thought to be sufficient since the errors introduced in photon cross sections for low energy photons would have less of an impact on the energy deposition than cross section errors for high energy photons. Between 100KeV and 1MeV the group spacing is 100KeV, and between 1MeV and 8MeV the group spacing is 1MeV. The group structure is displayed in Table 4.7. These energy group weighted cross sections were then directly hard coded into the Monte Carlo simulation. The values of the photon cross sections for each isotope considered in the code can be found in appendix B. A graphical illustration of the cross sections for Uranium is depicted in Figure 4.12.

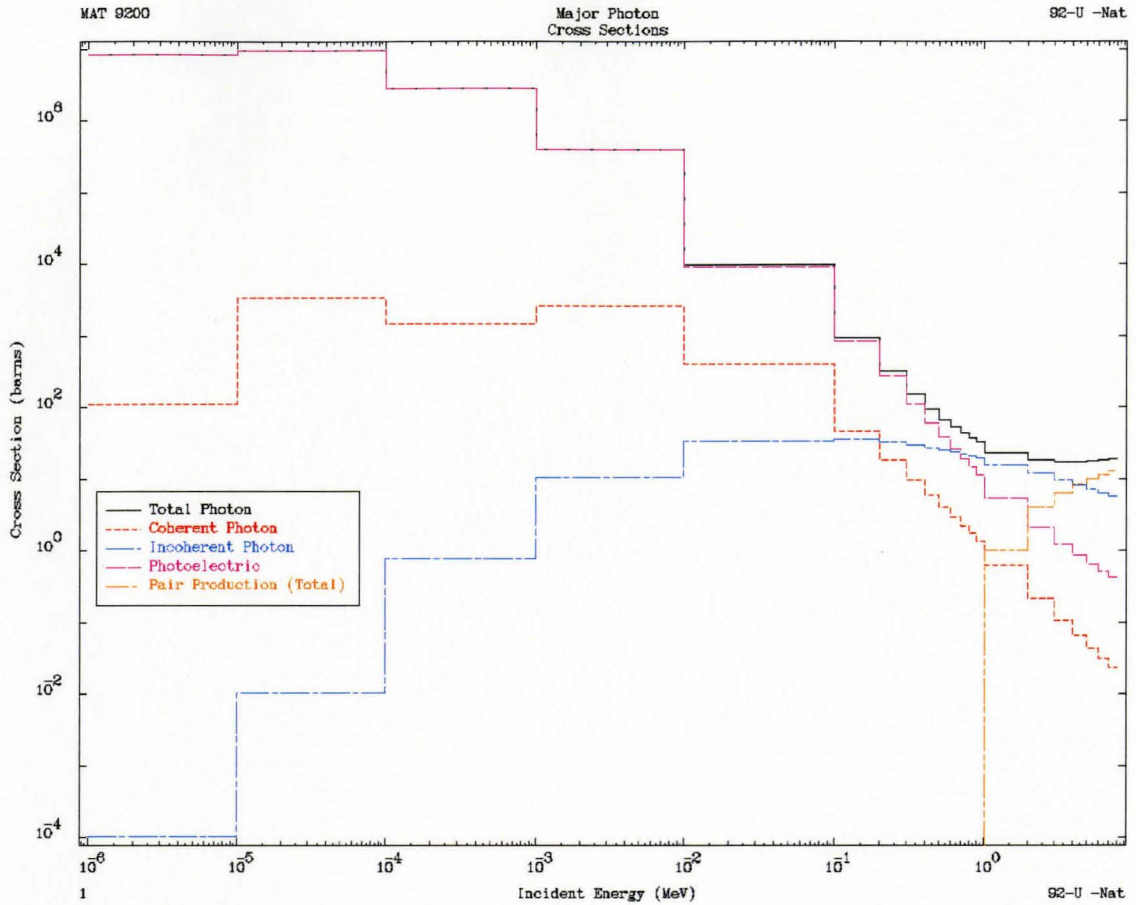


**Figure 4.12: PREPRO Plot of Photon Interaction Cross Sections For Uranium Using the PREPRO Routine EVALPLOT**

**Table 4.7: Energy Group Intervals for Multigroup Microscopic Photon Cross Sections**

Group	Upper Energy Limit eV	Group	Upper Energy Limit eV	Group	Upper Energy Limit eV
1	1E+01	8	4E+05	15	2E+06
2	1E+02	9	5E+05	16	3E+06
3	1E+03	10	6E+05	17	4E+06
4	1E+04	11	7E+05	18	5E+06
5	1E+05	12	8E+05	19	6E+06
6	2E+05	13	9E+05	20	7E+06
7	3E+05	14	1E+06	21	8E+06

The microscopic photon interaction cross sections obtained for each of the groups were then multiplied by the material density, to obtain the macroscopic cross section. In compound materials the microscopic cross section times the density was summed, to yield the total photon macroscopic cross section of the compound.

$$\Sigma_{total} = \sum_i \sigma_{total}^i * \rho^i \quad (4.18)$$

An interaction distance was set to 0.01cm. Thus every 0.01cm a check is performed to assess if an interaction has occurred. Decreasing the interaction distance by an order of magnitude will roughly increase the run time by an order of magnitude since the photon will run through many more checks before an interaction occurs. To check for an interaction a random number between zero and unity was generated and compared to the probability of the gamma ray undergoing an interaction in that distance. For an infinite material with total photon macroscopic cross section  $\Sigma_{total}$  the probability distribution for collision dx is:

$$\begin{aligned} f(x)dx &\equiv Pr\{Travels\_To\_x\_without\_collision\} \times Pr\{Collides\_in\_dx\} \\ &= (e^{-\Sigma_i x}) \times (\Sigma_i dx) \end{aligned} \quad (4.19)$$

Therefore the probability distribution function (PDF) is:

$$f(x) = \Sigma_i e^{-\Sigma_i x} \quad (4.20)$$

While the cumulative distribution function (CDF) is the integral of  $f(x)$  from zero to x is:

$$F(x) = 1 - e^{-\Sigma_i x} \quad (4.21)$$

The interaction probability can then be evaluated via the difference of the CDF between two points. The interaction probability between zero and some point labeled distance is,

$$InteractionProbability = e^{-\Sigma_{total} * distance} \quad (4.22)$$

At this point a random number, denoted *rand*, can be used to test whether an interaction has occurred in the interval distance.

IF,

*rand* > *InteractionProbability*, then an interaction has occurred

*rand* <= *InteractionProbability*, then no interaction has occurred

If the random number was greater than the value of the interaction probability, then no interaction was assumed to have occurred. The gamma ray would continue along the current trajectory, and a check would be performed as to whether the gamma ray had entered into another material; If the gamma ray entered a region with a new material, the photon interaction cross sections were altered to that of the new material.

If the random number was less than the value for the above equation, then an interaction was assumed to have occurred. The type of interaction was then determined by taking the ratio of the photon cross sections and dividing them into intervals. A random number was once again generated to select the interaction which occurred. If a photoelectric interaction occurred, then all of the energy was taken to be deposited at the point of the interaction. In a Compton scattering event a fraction of the energy was taken to be deposited based on the angle of scatter. The angle was calculated using an algorithm[35] which calculated the scattering angle based on the Klien-Nishima distribution as previously discussed. If a pair production interaction occurred then all of the energy except 1.022 MeV was taken to be deposited, and two 511keV gamma rays were generated at the point of the pair production interaction. The pair production gamma

rays were generated with direction vectors 180 degrees apart to ensure conservation of momentum. The following is an excerpt from the code, where a decision is made which interaction has taken place, and subsequently calculations are performed for the new photon energy, as well as the energy deposited and the location of the energy deposition (enstor variable).

The first *if* statement is for the photoelectric effect, the energy of the photon is stored as well as the location. Subsequently the energy is set to zero, and a flag is set to indicate that the photoelectric effect has occurred. This will cause the code to generate a new photon in the fuel.

```
if (dice2>=0 &dice2<PphotoFuel) %Photoelectric Effect
    enstor(ecount,1)=energy;
    enstor(ecount,2)=x;
    enstor(ecount,3)=y;
    ecount=ecount+1;
    energy=0;
    Photocount=1;
```

The second *if* statement is for a pair production event. The (x,y) position at which the interaction takes place is stored. The energy of the photon minus 1.022MeV is stored at this (x,y) location. This assumption neglects the energy transport from the created electron and positron. The annihilation photons are approximated as being created at the point of pair production. The flag *PairProCount* is used to remind the code that once the first photon experiences the photoelectric effect, another photon must be generated at the same x,y coordinate, but with a 180 degree rotation of the position vector.

```
elseif (dice2>=PphotoFuel & dice2<=(PphotoFuel+PpairFuel))
    %PairProduction

    enstor(ecount,2)=x;
    enstor(ecount,3)=y;
```

```
xpair=x;
ypair=y;
angpair=direct;
energynew=511000;
enstor(ecount,1)=energy-2*energynew;
ecount=ecount+1;
energy=energynew;
PairProCount=1;
pairgam=1;
```

The third *if* statement is for the occurrence of a Compton scattering event. The Klein Nishima distribution (kman subroutine) is used to compute the energy of the photon after the scattering event, as well as the angle of scatter. The difference between the incident photons energy and the energy of the scattered photon is the amount of energy deposited at (x,y). A flag named `comptonanglepreservation` is triggered so the code does not reset the angle at which the photon is traveling.

```
else %Compton Scatter

    enstor(ecount,2)=x;
    enstor(ecount,3)=y;
    %kman is a function which returns r(the ratio of incident photon
    %energy to scattered photon energy, and the scattering angle of
    %the photon, based on the Klien-Nishima distribution)
    [scatterangle,r]=kman(energy);
    energynew=energy/r;
    enstor(ecount,1)=energy-energynew;
    ecount=ecount+1;
    energy=energynew;
    direct=direct+scatterangle;
    comptonanglepreservation=1;
end
```

The flow chart seen in Figure 4.13 gives a simplified outline of the code.

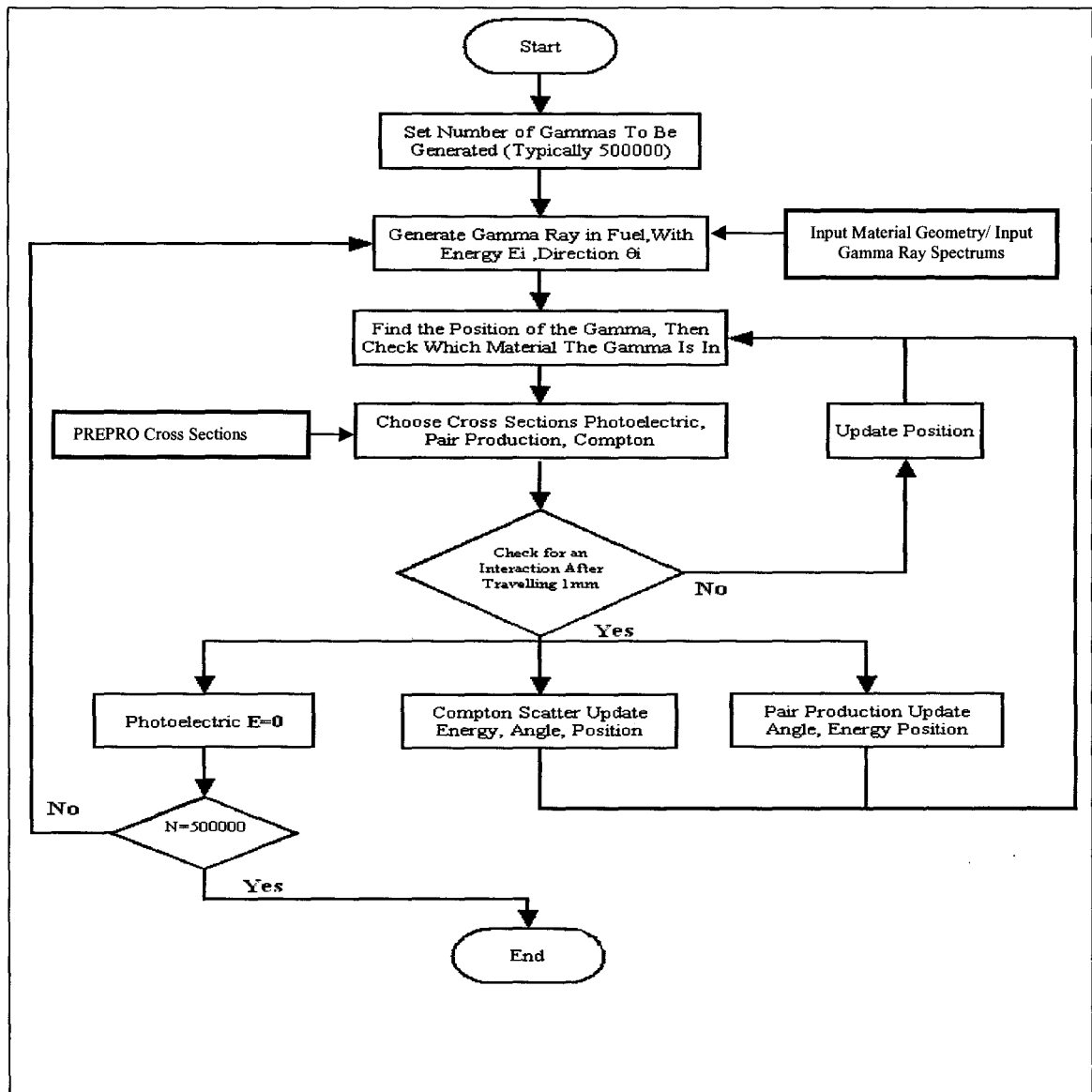


**Figure 4.13: Flow Chart of Gamma Ray Code**

Since the code stores the location of the energy deposition of each of the gamma rays, a plot can be created of the energy deposition in the lattice cell, seen in Figure 4.14. The plot of the energy deposition closely resembles that of the actual lattice cell. This is expected since the fuel elements are of high  $Z$  and thus are more likely to have photon-

electron interactions. Conversely heavy water is a low  $Z$  material, and although heavy water is near 85% of lattice volume, roughly 10% of the energy is deposited within it. Table 4.8 shows the location of the energy deposition in the CANDU lattice. The picture corresponds well to the prediction that most of the energy will be deposited in regions of high  $Z$ . The highest amount of energy deposition appears in the centre of the fuel bundles.

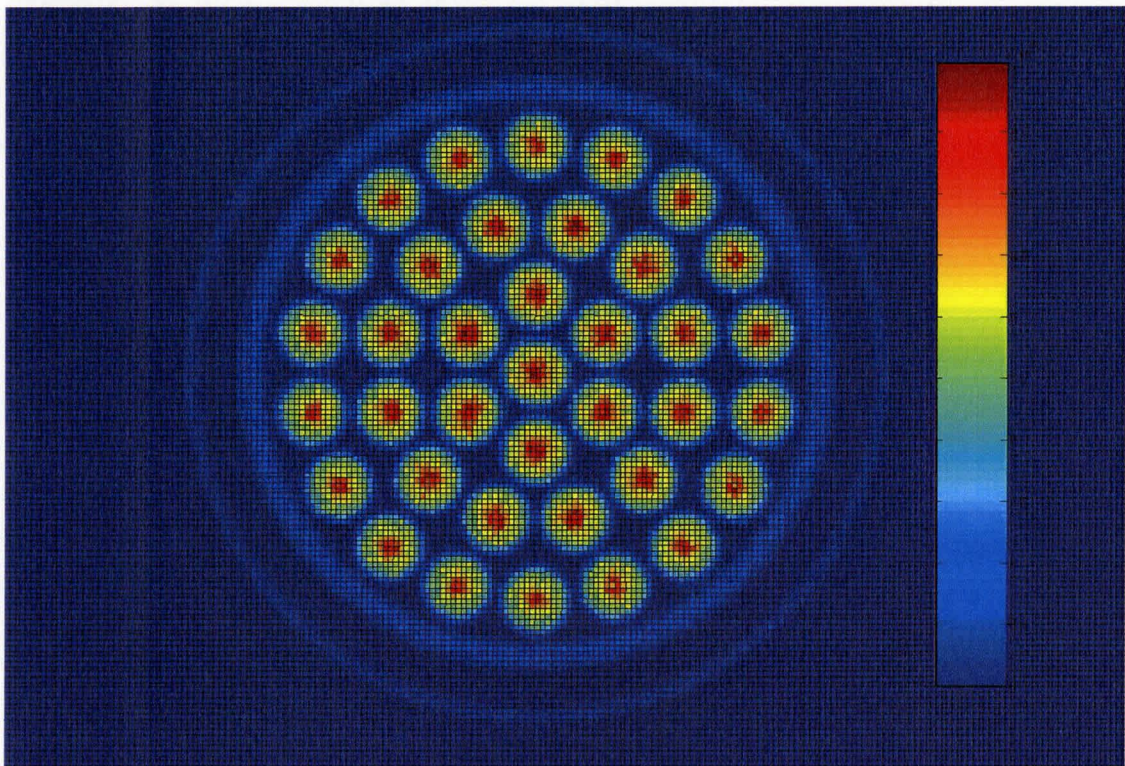


**Figure 4.14: Monte Carlo Gamma Ray Energy Deposition Simulation, For A CANDU Lattice, For A BE Case**

In order to provided some degree of verification of the code, the results are compared to those of Boss[36].

**Table 4.8: Comparison of Gamma Ray Energy Deposition Results**

Location	Percent of Total Delayed and Prompt Gamma Ray Energy Deposited in Components of CANDU Lattice	
	Boss[36]	This Work
<b>Fuel</b>	69.7	64.1
<b>Clad</b>	2.9	11.1
<b>Coolant</b>	2.0	1.4
<b>Pressure Tube</b>	5.1	7.0
<b>Gas Annulus</b>	N/A	0.1
<b>Calandria Tube</b>	1.8	2.3
<b>Moderator</b>	18.5	13.8
<b>RECOVERABLE</b>	79.7	83.7

The amount of gamma ray energy recoverable,  $\Psi$ , was found to be in reasonable agreement with the work of Boss, with the exception of the energy deposited in the cladding and the moderator. This is likely a result in the differences between the models used, as Boss treated the fuel elements as a small number of annular fuel rings.

## Chapter FIVE

The young specialist in English Lit, ...lectured me severely on the fact that in *every* century people have thought they understood the Universe at last, and in *every* century they were proved to be wrong. It follows that the one thing we can say about our modern "knowledge" is that it is *wrong*.

... My answer to him was, "... when people thought the Earth was flat, they were wrong. When people thought the Earth was spherical they were wrong. But if you think that thinking the Earth is spherical is just as wrong as thinking the Earth is flat, then your view is more wrong than both of them put together."

Isaac Asimov

### 5.0 Applying BEUA Methods to the Reactor Physics System

In the previous chapter a scheme for the calculation of the power profile in the reactor was outlined. This chapter will apply best estimate methods to obtain a prediction of the sensitivity of the H factor to various input parameters.

The sensitivity of the H factor to a variable x is defined as:

$$\frac{\partial H}{\partial x} = \frac{\partial w_f}{\partial x} (\gamma \Sigma_{1,f} + F_2 \Sigma_{2,f}) + \frac{\partial (F_2 \Sigma_{2,f} + \gamma \Sigma_{1,f})}{\partial x} w_f \quad (5.1)$$

Equation (5.1) shows how the variation of the H factor will be evaluated in terms of the variation of the recoverable energy, and the variability of the total adjusted fission cross sections

### 5.1 Parameter Interaction Table for Reactor Power System

A summary of the parameters for which the sensitivity of the H factor will be computed, are as follows:

**Coolant Inlet Temperature:** The coolant inlet temperature will influence the coolant temperature at each of the fuel elements in the bundle. Using an assumed steady state power profile, the axial coolant temperature profile can be calculated. The axial temperature in combination with the axial pressure profile can be used to determine the thermodynamic properties of the coolant.

**Outlet Pressure:** The outlet pressure in combination with the temperature can be used to determine the thermodynamic properties of the coolant. The pressure will affect the saturation conditions of the coolant, thus is a factor in determining the quality of the coolant.

**Burnup at Outlet:** Since the composition of the fuel element varies with irradiation, lattice parameters and recoverable energy release per fission will be functions of the irradiation. A homogeneous model for refueling will be used in this paper, which is described later.

**Moderator Temperature:** The moderator temperature will affect the thermal spectrum of the neutrons. As moderator temperature decreases the thermal neutrons will on average be at lower energies, which increases the fission probability. Also the temperature variation will have an effect on the moderator density which will subsequently affect the amount of gamma ray absorption.

**Moderator Purity:** As the moderator purity decreases from increased light water content, the amount of absorption in the lattice cell will increase.

**Moderator Poison:** The amount of Boron in the moderator will affect the amount of absorption in the lattice. Also the presence of Boron will influence the spectrum of

neutrons in the moderator as certain neutron energies corresponding to resonance absorption bands in Boron will be preferentially absorbed.

Table 5.1 summarizes the parameters that will be analyzed as well as their best estimate values and random variability. The phenomena refers to the expected mechanism of influence on the H factor.

**Table 5.1: Parameters examined in subsequent analysis**

<b>Operating Parameter</b>	<b>System</b>	<b>Phenomena</b>	<b>Best Estimate</b>	<b>Standard Deviation</b>
RIH Temperature (°C)	Reactor Cooling System	Changes coolant density Impacts fission spectrum and fuel temperature	267.1	0.11
ROH Pressure (MPa)	Reactor Cooling System	Similar to RIH temperature	9.853	0.016
Exit Burnup (MW h/kg U)	Fueling System	Impacts the fuel composition.	208.8	2.48
Moderator Temperature (°C)	Moderator System	Changes the neutron spectrum. Influences the electron density	68	4.4
Moderator Poison (ppm Boron)	Moderator System	Changes the neutron spectrum. Influences the electron density	0.105	0.058
Moderator Isotopic Purity(%wt)	Moderator System	Changes the neutron spectrum.	99.7	0.009

## 5.2 Parameter Interaction Diagram for the Reactor Channel Power

The parameters discussed in the previous section will influence either the fission cross sections, or the energy released from fission.

The moderator purity was hypothesized to have no influence on the recoverable energy from fission, since the gamma ray energy deposition is insensitive to changes between heavy and light water. The moderator temperature and moderator poison

concentration, were each suspected to influence both the fission cross sections, and recoverable energy from a fission event. The Boron would impact the electron density of the water, however the effect should be negligible since the atomic number of Boron is near that of Oxygen. The moderator temperature would impact the density of the moderator, which effects the electron density.

The burnup was suspected to impact both the cross sections and the recoverable energy. The recoverable energy was hypothesized to be influenced by the hardening of the gamma ray spectrum, due to the creation of Plutonium as the fuel burns.

The RIH temperature and ROH pressure would affect both the adjusted fission cross section, as well as the recoverable energy. These parameters would primarily influence the characterizing parameters via their effect on coolant temperature, void fraction, and fuel temperature.

In an attempt to display the interdependencies between parameters in the power calculation a PID has been created as seen in Figure 5.1. The parameters that are analyzed in this work have blue arrows linking them, while the parameters that were not examined have green arrows. Each of the parameters will be discussed in depth in the subsequent sections.

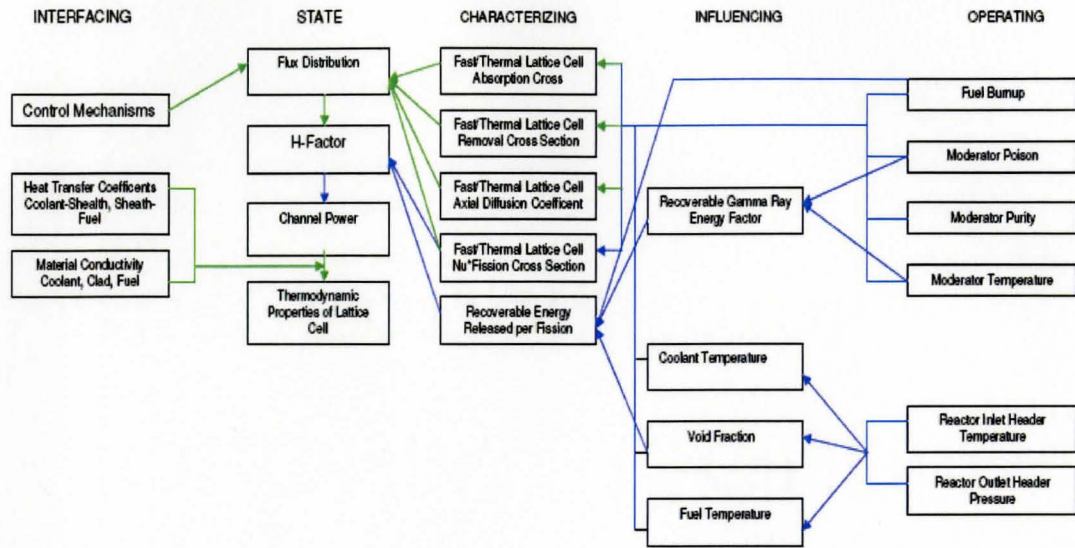


**Figure 5.1: Parameter Interaction Diagram for the Calculation of Channel Power. The Parameters in Blue are Examined in This Work.**

### 5.2.1 Exit Burnup

Burnup in the fuel is defined as the quantity of energy the fuel produces over an amount of time, relative to a unit mass. The burnup is linearly related to the integral of the flux in the fuel over time, known as the irradiation. The burnup impacts the fissile content of the fuel, which results in three effects that influence the H factor:

- 1) Changes in the isotopic composition of the fuel. The probability of an isotope fissioning is proportional to the density of the isotope. In a CANDU reactor as the fuel burns, the U235 content decreases, while the Pu239 content increases.
- 2) As different isotopes fission, the total energy released from fission will change. Pu239 releases a larger amount of energy than U235 when fissioned; therefore the energy released from fission is expected to increase with burnup.

- 3) The recoverable energy from a fission event will be altered. This is a result of changes in the form in which the fission energy is released, as well as the spectrum of the gamma rays.

Examining  $w_f$ , the amount of recoverable fission energy will be the sum of the kinetic energy of the fission fragments, beta particles, and the gamma ray energy deposited in the heat transport system:

$$w_f = Q_{FP} + \Psi * Q_{PG} + \Psi * Q_{DG} + \Psi * Q_{CG} + Q_{beta} \quad (5.2)$$

Where  $\Psi$  is the percentage of gamma ray energy recoverable. Collapsing the gamma ray energy into  $Q_{gamma}$ :

$$w_f = Q_{FP} + Q_{beta} + \Psi * Q_{gamma} \quad (5.3)$$

Since the energy released is dependent on the isotope which fissions, each component of the energy released from fission is weighted by the relative amount of fission that occurs. An example of the weighted average of the kinetic energy that appears in the fission fragments is shown below:

$$Q_{FP} = \frac{1}{\xi} \left( N^{U235} \sigma_f^{U235} Q_{FP}^{U235} + N^{U238} \sigma_f^{U238} Q_{FP}^{U238} + N^{Pu239} \sigma_f^{Pu239} Q_{FP}^{Pu239} + N^{Pu241} \sigma_f^{Pu241} Q_{FP}^{Pu241} \right) \quad (5.4)$$

Where,

$$\xi = N^{U235} \sigma_f^{U235} + N^{U238} \sigma_f^{U238} + N^{Pu239} \sigma_f^{Pu239} + N^{Pu241} \sigma_f^{Pu241} \quad (5.5)$$

The exception to the above weighting, is the energy release from neutron capture,  $Q_{CG}$ , which is taken to be linearly proportional to the concentration of the isotope.

The sensitivity of the recoverable energy to the burnup of the fuel  $\omega$ , is evaluated through the change in isotope concentration of the fissile isotopes in the fuel.

$$\frac{\partial w_f}{\partial \omega} = \sum_i \frac{\partial w_f}{\partial N^i} \frac{\partial N^i}{\partial \omega} \quad (5.6)$$

Of course variations in fuel isotopic composition will influence both the energy released from fission, as well as the spectrum of the gamma rays released in fission, which subsequently affects the fraction of gamma energy that is recoverable,  $\Psi$ .

Inserting equation (5.3) into equation (5.6) to identify how the components of  $w_f$  vary with burnup,

$$\frac{\partial w_f}{\partial \omega} = \sum_i \frac{\partial(Q_{FP} + Q_{beta} + \Psi * Q_{gamma})}{\partial N^i} \frac{\partial N^i}{\partial \omega} \quad (5.7)$$

Separating the contributions of energy from particles from the contributions of recoverable energy from gammas,

$$\frac{\partial w_f}{\partial \omega} = \sum_i \frac{\partial(Q_{FP} + Q_{beta})}{\partial N^i} \frac{\partial N^i}{\partial \omega} + Q_{gamma} \frac{\partial \Psi}{\partial N^i} \frac{\partial N^i}{\partial \omega} + \Psi \frac{\partial Q_{gamma}}{\partial N^i} \frac{\partial N^i}{\partial \omega} \quad (5.8)$$

So the sensitivity of the H factor will be equal to the change in the energy released, added to the change in the fission cross section of the fuel. Substituting burnup into equation (5.1):

$$\frac{\partial H}{\partial \omega} = \frac{\partial w_f}{\partial \omega} (\gamma \Sigma_{1,f} + F_2 \Sigma_{2,f}) + \frac{\partial(F_2 \Sigma_{2,f} + \gamma \Sigma_{1,f})}{\partial \omega} w_f \quad (5.9)$$

Inserting equation (5.8) into equation (5.9) the sensitivity of the H factor to burnup is shown,

$$\begin{aligned} \frac{\partial H}{\partial \omega} = & \left[ \sum_i \frac{\partial(Q_{FP} + Q_{beta})}{\partial N^i} \frac{\partial N^i}{\partial \omega} + Q_{gamma} \frac{\partial \Psi}{\partial N^i} \frac{\partial N^i}{\partial \omega} + \Psi \frac{\partial Q_{gamma}}{\partial N^i} \frac{\partial N^i}{\partial \omega} \right] [\gamma \Sigma_{1,f} + F_2 \Sigma_{2,f}] \\ & + w_f \left[ \frac{\partial(F_2 \Sigma_{2,f} + \gamma \Sigma_{1,f})}{\partial \omega} \right] \end{aligned} \quad (5.10)$$

The change in the H factor with the change in burnup can now be evaluated in terms of the constituent components. Figure 5.2 illustrates  $\frac{\partial N^i}{\partial \omega}$  for the major fissionable isotopes in the fuel. Figure 5.3 illustrates the variation of the adjusted fission cross section with burnup  $\frac{\partial (F_2 \Sigma_{2,f} + \gamma \Sigma_{1,f})}{\partial \omega}$  and Figure 5.4 illustrates the sensitivity of the gamma energy recoverable to changes in isotope concentration  $\frac{\partial \Psi}{\partial N^i}$ .

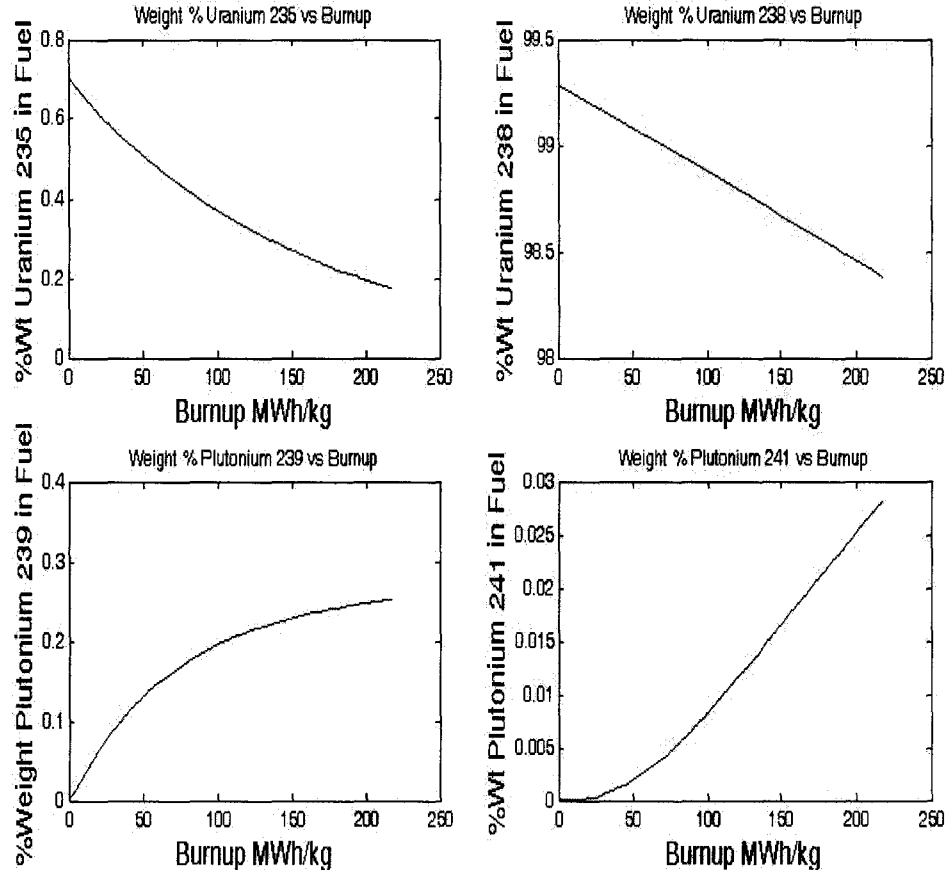


**Figure 5.2: Variation of Major Fissionable Isotopes in the Fuel vs Burnup**

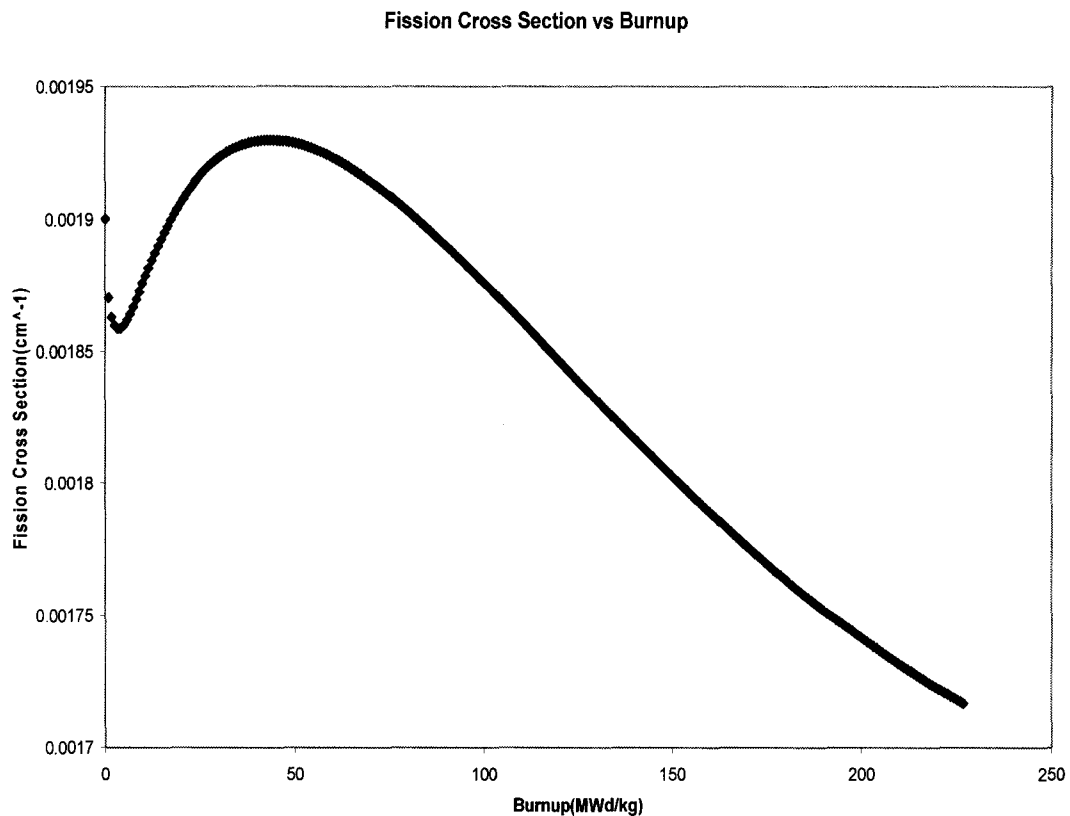


**Figure 5.3: Total Adjusted Fission Cross Section vs Burnup**

Observing Figure 5.3 the sensitivity or slope of the adjusted fission cross section vs. burnup varies over the range of burnup. The average exit channel burnup, however, is confined to a small range of values. If the homogeneous model is employed as discussed in the subsequent section, then the fuel bundles can be approximated to be at half the exit burnup. Examining the variation about this small range of values, the approximation can be made that the sensitivity of burnup is linear over this range. Bundles in regions of the highest flux will have the largest impact on the channel power. The high flux bundles will be near the centre of the core, and typically the bundles will have burnup values near

midburnup. The linear dependence of the total adjusted fission cross section near midburnup is shown in Figure 5.4.

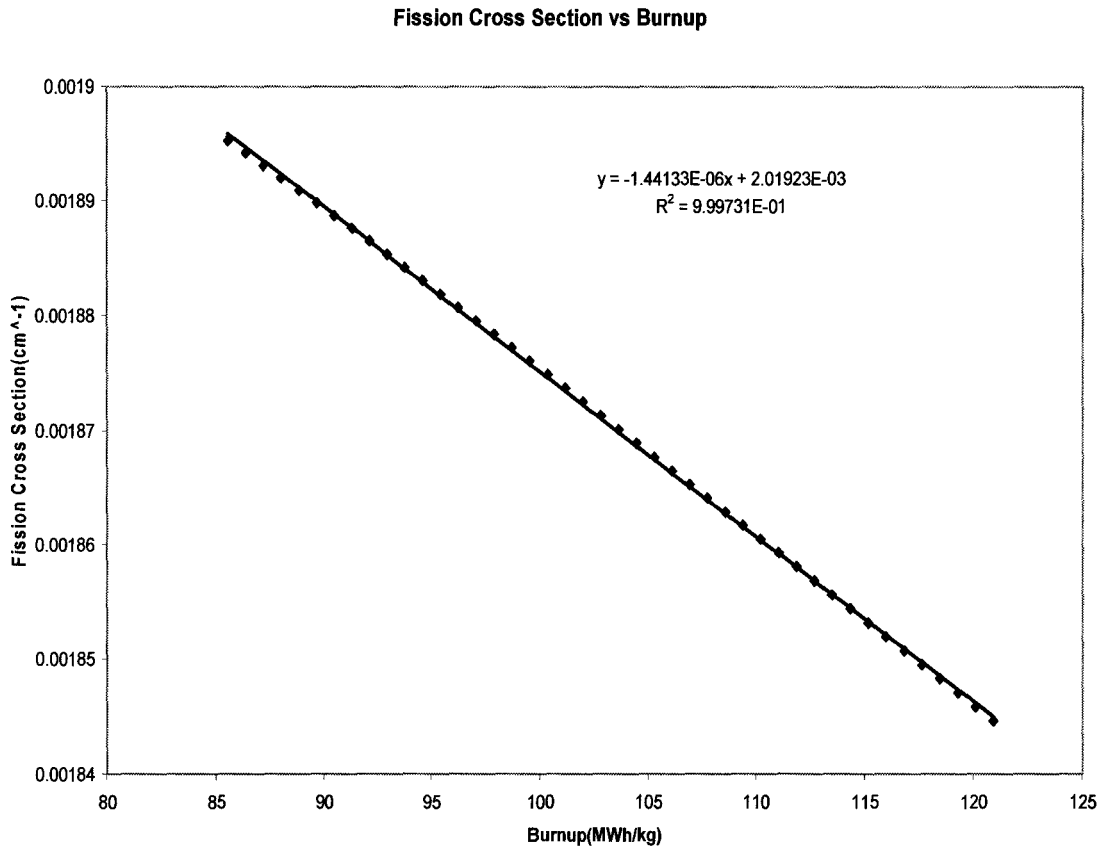


**Figure 5.4: Close Up View of the Variation of the Adjusted Fission Cross Section Over a Small Range of Burnup**

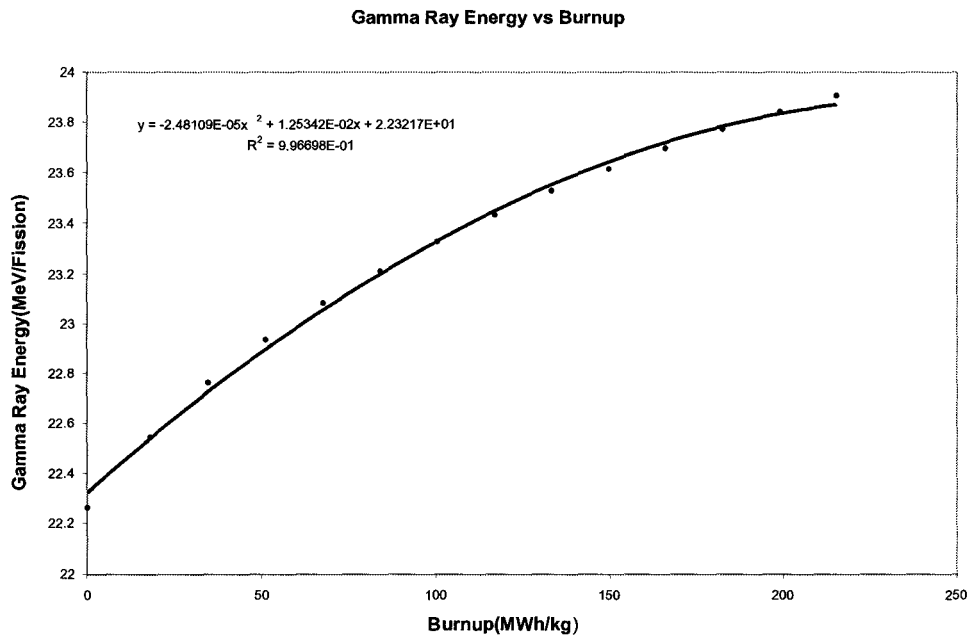


**Figure 5.5: Gamma Ray Energy Released Per Fission Event vs Burnup**

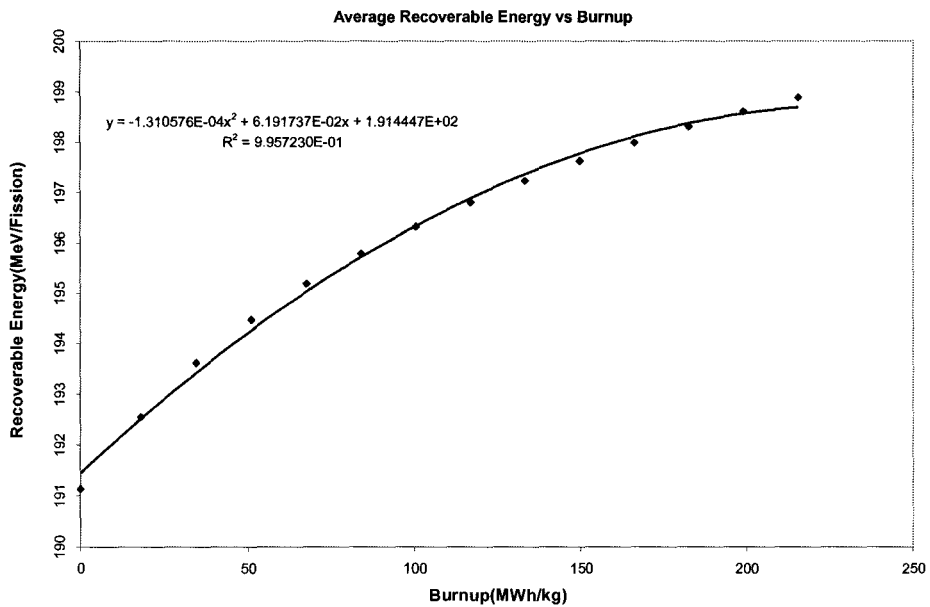


**Figure 5.6: Variation of Recoverable Energy vs Burnup**

Adjacent channels in a CANDU reactor are fueled in opposite directions, referred to as bidirectional fueling. Because of bidirectional fuelling, a bundle of high burnup is adjacent to four bundles of low burnup, and vice versa. This configuration causes the macroscopic flux profile to “smooth out” since without bidirectional fuelling large flux tilts would arise as one side of the core would have fresh fuel, while the other side would have high burnup fuel.

When calculating the average channel power as a function of the channel burnup, the curve will on average resemble that of Figure 5.3. The position in the channel of each bundle will represent a small line segment on Figure 5.3, corresponding to the burnup of that channel position. The channel power will be the sum of each of the corresponding segments weighted by the flux in the region, since bundles in high flux regions will contribute more to the power than bundles in low flux regions. Thus the burnup in each channel position has little variation. The average channel power can be approximated as sensitive only to the average exit burnup of the channel, since the exit burnup is directly related to the burnup in each channel position. This allows the channel to power to burnup relationship to be quantified solely by the exit burnup in the channel.

Applying the same argument to the calculation of the H factor implies that the flux to power relationship on average in the channel can be evaluated via the exit burnup of the channel. It should be stressed that evaluating the sensitivity of the H factor in terms of an exit burnup is reasonable for average channel properties, but should not be taken to

correspond to the variation of the H factor between individual fuel bundles in a channel.

This would result in a much larger range of variation of the H factor.

The average burnup in the channel is taken to be half of the exit burnup. This corresponds to the homogeneous approximation of fuel burnup used in CANDU reactors.

### ***Homogeneous Approximation***[37]

In the homogeneous approximation the fuel is assumed to move along the channel at a constant rate, denoted by R. Since a CANDU reactor has bi-directional fuelling, each channel will have four adjacent channels fuelled in the opposite direction.

The irradiation  $\omega$  at a point z along the channel, for a channel fuelled from Z=0 is given by

$$\omega_1 = \int_0^z \frac{\Phi(z)}{R} dz \quad (5.11)$$

And for a channel fuelled from the Z=L end

$$\omega_2 = \int_z^L \frac{\Phi(z)}{R} dz \quad (5.12)$$

The average irradiation at a spatial point z in the channel, is then the sum of the irradiations divided by two.

$$\omega(z) = \frac{1}{2}[\omega_1(z) + \omega_2(z)] \quad (5.13)$$

Since the flux is the same in both equation (5.11) and equation (5.12) the integrals can be combined.

$$= \frac{1}{2} \int_0^L \frac{\Phi(z)}{R} dz = \frac{1}{2} \omega(L) = \text{a constant} \quad (5.14)$$

The result is that the irradiation at each point in the channel can be related to the exit irradiation.

### 5.2.2 Thermalhydraulic Model

The temperature of the fuel elements is primarily the result of the power level of the fuel bundle, which is determined from the measured channel power and modeled flux distribution. To evaluate the effect of RIH temperature and ROH pressure on the flux to power conversion, via the thermodynamic properties of the fuel bundle, a thermalhydraulics model of a single channel was created. The model is meant to provide a survey calculation to gauge the effect of RIH temperature and ROH pressure fluctuations. The accuracy of the model can undoubtedly be improved upon, as it was outside the scope of this work to construct a full coupled reactor neutronics/thermalhydraulics code. The code is described below.

The properties of the heavy water coolant were modeled in the code using Hill's fits of Hermite polynomials given in [38].

In the thermohydraulic model, the channel power distribution was approximated as a sine curve. The specified channel power was distributed over the flux profile, which gave a bundle power.

$$\Phi \approx \sin\left(\frac{\pi x}{L}\right) \quad (5.15)$$

Assuming that flux maps onto power in an approximately linear fashion, which will be the case for small perturbations, as this is equivalent to the constant H factor assumption, the power of any bundle  $P_n$  is

$$P_n = P_0 \sin\left(\frac{n\pi}{L}\right) \text{ for } n=1:13, L=14 \quad (5.16)$$

Note, if a thermohydraulic parameter is found to have a substantial effect on the H factor, then equation (5.16) will need to have an adjustment term added, taking into account the variability of the H-factor. The current best estimate of the H factor will be used, and the code would be repeated to produce an updated value of the H factor.

The normalization constant  $P_0$  is equal to

$$P_0 = \frac{\text{channel power}}{\sum_{n=1}^{13} \sin\left(\frac{n\pi}{L}\right)} \quad (5.17)$$

The input of coolant mass flow is matched to the channel power. Using the mass flow and the outlet pressure, an estimate of the pressure profile in the channel was obtained.

$$p_i = p_{i-1} + \frac{K_b \rho(h, p) V^2}{2} \quad (5.18)$$

Equation (5.18) makes the assumption that pressure drop across a bundle is completely given by  $K_b$ , where  $K_b$  is the total bundle resistance,  $\rho(h, p)$  is the density of heavy water as a function of enthalpy and pressure,  $V$  is the velocity of the fluid, and  $p_{i-1}$  is the pressure at the previous bundle. The calculation begins at the ROH end of the channel where the exit pressure is known. The velocity of the fluid is computed using the mass flow  $w$ , and the flow area of the bundle  $A$ .

$$V = W / \rho(h, p)A \quad (5.19)$$

Using the estimate of the pressure profile, a saturation enthalpy of the fluid at a given pressure is computed, which allows the code to adjust the thermodynamic properties of the fluid depending on its thermodynamic state.

**If  $h < h_{sat}$**

The axial enthalpy profile of the fluid can be calculated using the power of the previous bundle, the mass flow, and the enthalpy of vaporization.

$$h_n = h_{n-1} + \frac{P_{n-1}}{W} \quad (5.20)$$

The remaining thermodynamic properties are found as functions of the current pressure, and enthalpy.

**If  $h \geq h_{sat}$**

The additional heat load to the coolant cause vaporization in the fluid. The results is a change in the water quality  $\chi$  defined as the ratio of the mass of liquid to the sum of mass of liquid and steam.

$$\chi = \frac{m_l}{m_l + m_g} \quad (5.21)$$

The quality at the next bundle can be computed using equation (5.22), where  $h_v$  is the heat of vaporization. This equation assumes that once the fluid is at saturation all additional energy will result in vaporization.

$$\chi_n = \chi_{n-1} + \frac{P_{n-1}}{h_v W} \quad (5.22)$$

The thermodynamic state of the fluid, as well as the velocity, allows a average heat transfer coefficient of the fuel to be computed.

The change in density of the coolant will have a feedback effect on the velocity of the fluid, which subsequently effects the pressure profile. Thus an iteration is preformed until the convergence of the pressure profile occurs.

The RIH temperature and ROH pressure will influence the H factor via the influence on coolant temperature, fuel temperature and coolant density. The thermodynamic properties of the coolant are calculated as described above. The knowledge of the thermodynamic properties of the fluid allows the average temperature of the fuel elements to be determined.

The centerline temperature,  $T_{CL}$ , is given by equation (5.23)

$$T_{CL} = T_{Cool} + \frac{q'}{2\pi r_F} \left[ \frac{r_F}{2k_F} + \frac{t_c}{k_C} + \frac{r_F}{h_f(r_F + t_C)} \right] \quad (5.23)$$

Where  $T_{Cool}$  is the temperature of the heavy water coolant,  $q'$  is the linear heat generation which will depend upon the neutron flux in the element,  $r_F$  is the radius of the fuel,  $t_c$  is the thickness of the zirconium cladding,  $k_F$  is the conductivity of the fuel,  $k_C$  is the conductivity of the clad, and  $h_f$  [32] is the heat transfer coefficient of the fluid which is dependent on the thermodynamic state of the fluid.

The temperature drop across the fuel is given by

$$\Delta T = \frac{q'}{4\pi k_F} \quad (5.24)$$

Thus the effects of RIH temperature and ROH pressure on the average temperature of the fuel elements can be obtained.

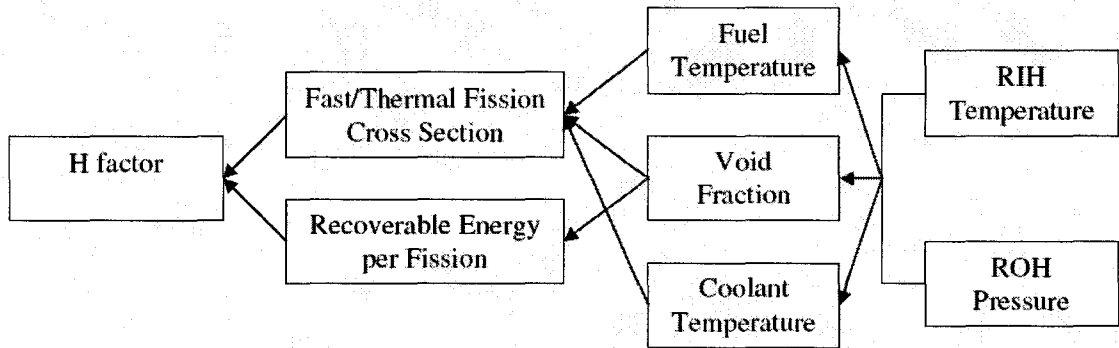


**Figure 5.7: Illustration of the Interaction of H factor with RIH temperature and ROH pressure**

### 5.2.3 Fuel Temperature

The corresponding variation of the H factor to the temperature of the fuel is

$$\frac{\partial H}{\partial T_{fuel}} = \left[ \frac{\partial w_f}{\partial T_{fuel}} (\gamma \Sigma_{1,f}^i + F_2 \Sigma_{2,f}^i) + w_f \frac{\partial (\gamma \Sigma_{1,f}^i + F_2 \Sigma_{2,f}^i)}{\partial T_{fuel}} \right] \quad (5.25)$$

Figure 5.8 captures the variation of the adjusted fission cross section with changes in the fuel temperature.

The amount of recoverable energy released from fission vs fuel

temperature,  $\frac{\partial w_f}{\partial T_{fuel}}$  was hypothesized to be influenced by the of the Doppler broadening of

the fission cross sections of U235 and Pu239.

Doppler broadening also occurs in resonance absorption cross section of U238. Since a constant macroscopic flux profile is assumed, the broadening of the resonance absorption cross section influences the H factor in two ways; The first is the effect of the increased absorption on the spatial flux profile, as U238 increases the amount neutron shielding between the moderator and the fuel grows, which lowers the F factor; the second effect is the broadening of the U238 absorption cross section will impact the spectrum of neutrons within the fuel, this effect is implicitly captured in the macroscopic fission cross sections.

Another effect from an increased fuel temperature which can be hypothesized, is the effect on the amount of energy recoverable, via the density of the fuel. This effect is not examined primarily for two reasons, the first being that the expansion of ceramic fuel elements is relatively small, and the second being that the two dimensional Monte Carlo code developed would not correctly capture the three dimensional anisotropic expansion.

The effect of fuel temperature is examined through its effect on the adjusted fission cross section as seen in Figure 5.8.

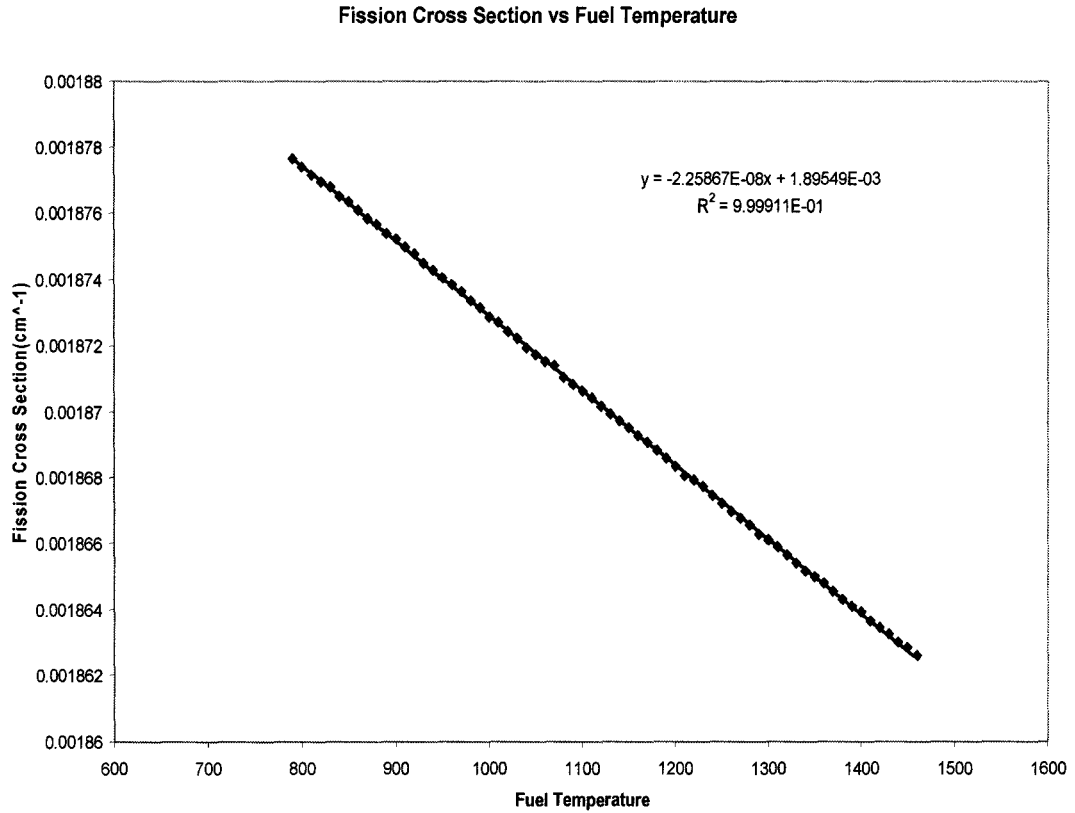


**Figure 5.8: Fission Cross Section vs Fuel Temperature**

### 5.2.4 Coolant Temperature

The effect of the coolant temperature on the H factor is given by equation (5.26)

$$\frac{\partial H}{\partial T_{cool}} = \left[ \frac{\partial w_f}{\partial T_{cool}} (\gamma \Sigma_{1,f}^i + F_2 \Sigma_{2,f}^i) + w_f \frac{\partial (\gamma \Sigma_{1,f}^i + F_2 \Sigma_{2,f}^i)}{\partial T_{cool}} \right] \quad (5.26)$$

Figure 5.9 shows the effect of the coolant temperature on the adjusted fission cross section. As the trend illustrates, as the coolant temperature increases the fission cross section decreases. This is primarily due to upscattering which occurs when thermal neutrons reenter from the moderator, and collide with hot coolant. When the neutrons

collide with the relatively rapidly moving heavy water molecules of the coolant, they tend to gain energy, since the Maxwellian distribution of neutron energies is centered about the temperature of the medium in which they reside. The increased neutron energy decreases the probability of fission, in the fuel.

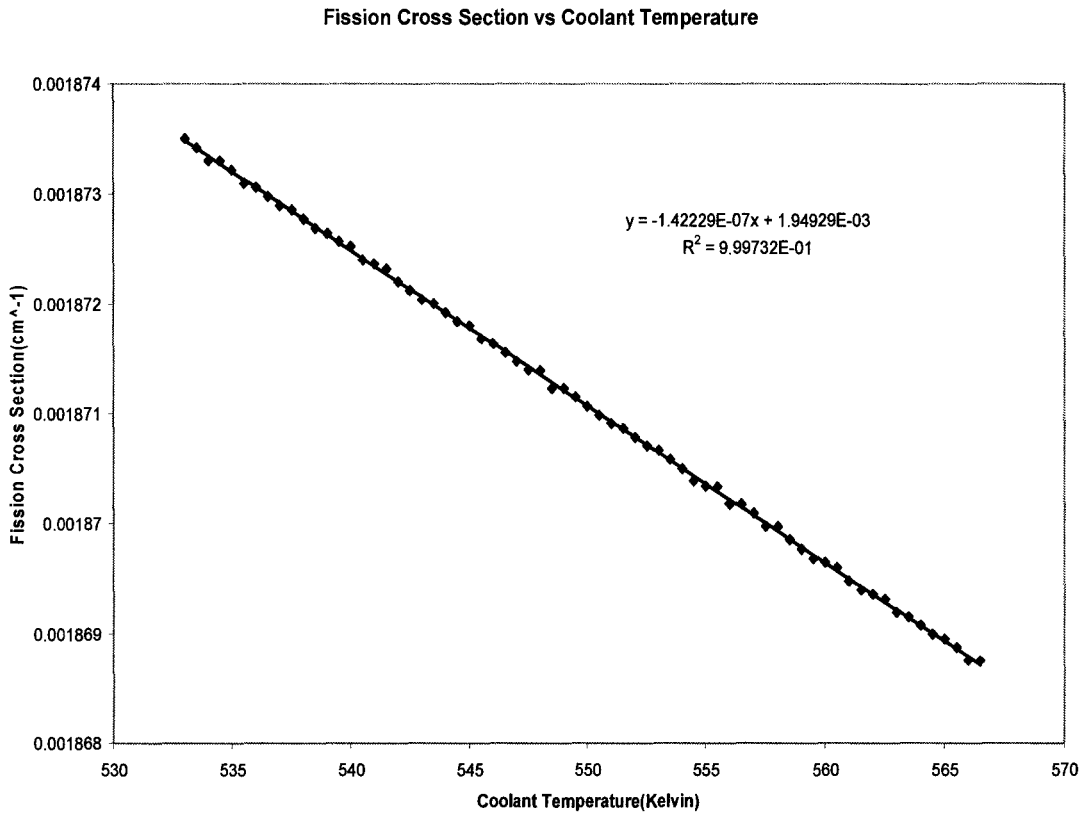


**Figure 5.9: Fission Cross Section vs Coolant Temperature**

### 5.2.4 Void Fraction

The void fraction is defined as the total volume of vapour divided by the total volume of the liquid vapour mixture.

$$\alpha_v = \frac{V_g}{V_l + V_g}$$

The effect of void fraction is evaluated through changes in the coolant density. The void fraction in the reactor is dependent upon a number of input parameters. An increase in void fraction will lead to a decrease in the coolant density. The coolant density decrease will result in less gamma ray energy being directly deposited in the coolant. The change in void fraction was the result of other factors, in the previous section the effect of RIH temperature and ROH pressure was determined, the results were averaged over the channel, and the amount of voiding was found to be negligible except in the case of the exit bundles of a high powered channel. For the purpose of future analysis of bundle to bundle variations of H factor, the effect of voiding on fuel bundles is examined separately.

The effect of changes in coolant density on the adjusted fission cross section is shown in Figure 5.10. The trend displayed is that as the coolant density decreases the fission cross section increases, at midburnup. This is consistent with other CANDU reactor result which show a positive void reactivity.

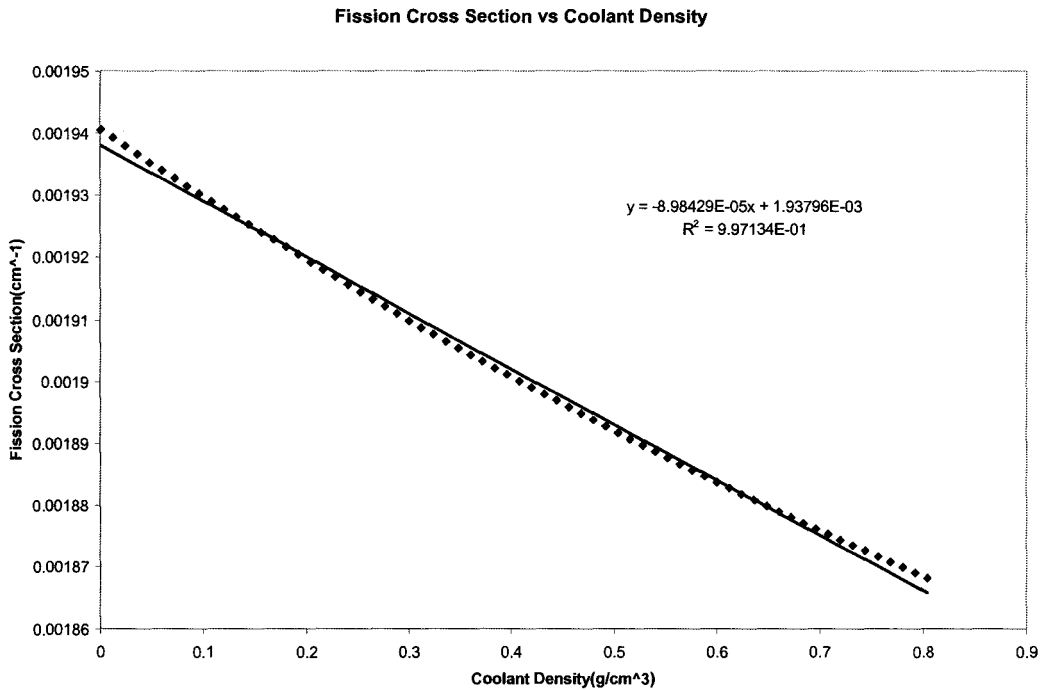


**Figure 5.10: Fission vs Coolant Density**

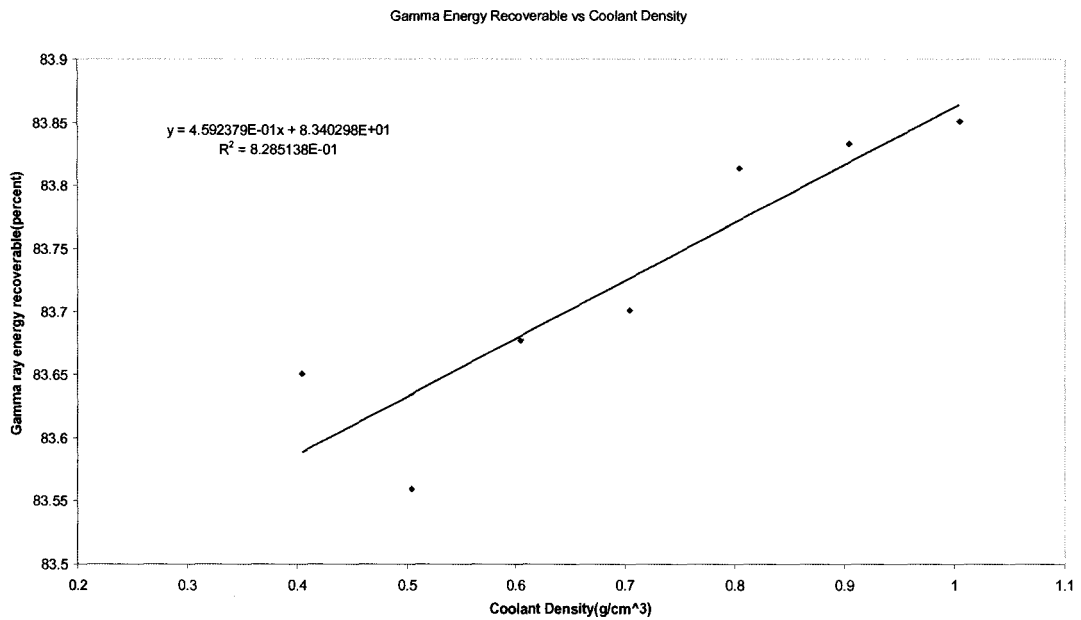


**Figure 5.11: Percentage of Gamma Ray Energy Recoverable vs Coolant Density**

Figure 5.11 shows that as the density of the coolant decreases the amount of recoverable energy decreases. As more gamma rays escape the coolant region, the amount of energy deposited in the moderator, and hence lost, increases as might be expected.

### 5.2.5 Cladding Temperature

The cladding temperature was input into WIMS to obtain the sensitivity of the fission cross sections to perturbations in cladding temperature. The results from WIMS gave a constant output regardless of cladding temperature. Therefore the effect of cladding temperature on H factor was excluded from the model.

### 5.2.6 ROH Pressure

The ROH pressure was varied, and the change in the mean thermodynamic properties of the fuel bundle were recorded. The results are briefly summarized in Table 5.2

**Table 5.2: Variation of Average Thermodynamic Properties a Channel, as a result of Changing(decreasing) ROH pressure.**

Parameter	Variation(+/-3.5 $\sigma$ )
Fuel Temperature	+0.007 (C)
Coolant Temperature	+0.006 (C)
Coolant Density	-0.938(kg/m <sup>3</sup> )

Thus the small range of variation in the ROH pressure results in only small variations of the thermodynamic properties. The sensitivity of the H factor is determined by the standard equation

$$\frac{\partial H}{\partial P_{ROH}} = \left[ \frac{\partial w_f}{\partial P_{ROH}} (\gamma \Sigma_{1,f} + F_2) + w_f \frac{\partial (\gamma \Sigma_{1,f} + F_2)}{\partial P_{ROH}} \right] \quad (5.27)$$

The impact of the ROH pressure is evaluated through the pressures effect on the thermodynamic properties. Substituting in for the effects of ROH pressure on the thermodynamic properties of the lattice, the following sensitivity equation is obtained.

$$\frac{\partial H}{\partial P_{ROH}} = \left[ \begin{aligned} & \frac{\partial w_f}{\partial \rho_{cool}} \frac{\partial \rho_{cool}}{\partial P_{ROH}} (\gamma \Sigma_{1,f}^i + F_2 \Sigma_{2,f}^i) + w_f \frac{\partial (\gamma \Sigma_{1,f}^i + F_2 \Sigma_{2,f}^i)}{\partial \rho_{cool}} \frac{\partial \rho_{cool}}{\partial P_{ROH}} + \frac{\partial w_f}{\partial T_{fuel}} \frac{\partial T_{fuel}}{\partial P_{ROH}} (\gamma \Sigma_{1,f}^i + F_2 \Sigma_{2,f}^i) \\ & + w_f \frac{\partial (\gamma \Sigma_{1,f}^i + F_2 \Sigma_{2,f}^i)}{\partial T_{fuel}} \frac{\partial T_{fuel}}{\partial P_{ROH}} + \frac{\partial w_f}{\partial \alpha_v} \frac{\partial \alpha_v}{\partial P_{ROH}} (\gamma \Sigma_{1,f}^i + F_2 \Sigma_{2,f}^i) + w_f \frac{\partial (\gamma \Sigma_{1,f}^i + F_2 \Sigma_{2,f}^i)}{\partial \alpha_v} \frac{\partial \alpha_v}{\partial P_{ROH}} \end{aligned} \right] \quad (5.28)$$

**Table 5.3: Sensitivity of the components of the H factor to ROH Pressure**

Parameter	$\frac{\partial x}{\partial P_{ROH}}$	$w_f$	$\frac{\partial w_f}{\partial x}$	$\frac{\partial (\gamma \Sigma_{1,f}^i + F_2 \Sigma_{2,f}^i)}{\partial x}$	$\frac{\partial x}{\partial P_{ROH}} \frac{\partial (\gamma \Sigma_{1,f}^i + F_2 \Sigma_{2,f}^i)}{\partial x}$
Fuel Temperature	+0.0068	196.33	0	-2.26E-08	-1.54E-10
Coolant Temperature	+0.0062	196.33	0	-1.42E-08	-8.80E-11
Coolant Density	-0.9377	196.33	-4.30E-04	-8.98E-08	+8.42E-08

### 5.2.7 RIH Temperature

The inlet coolant temperature at the ROH was obtained from plant measurement data. The ROH temperature distribution was input into the survey thermalhydraulics code to determine the between channel variations of the H factor, due to variations in ROH temperature.

**Table 5.4: Variation of Average Thermodynamic Properties in a Channel, as a Result of Changing(increasing) RIH Temperature**

Parameter	Variation(+/-3.5σ)
Fuel Temperature	+0.823 C
Coolant Temperature	+0.702 C
Coolant Density	-0.963 (kg/m <sup>3</sup> )

The RIH temperature, similarly to the ROH pressure, has only a small effect on the channel averaged thermodynamic properties of the fuel bundle. Examining the relationship between the H factor and the RIH temperature

$$\frac{\partial H}{\partial T_{RIH}} = \left[ \frac{\partial w_f}{\partial T_{RIH}} (\gamma \Sigma_{1,f}^i + F_2 \Sigma_{2,f}^i) + w_f \frac{\partial (\gamma \Sigma_{1,f}^i + F_2 \Sigma_{2,f}^i)}{\partial T_{RIH}} \right] \quad (5.29)$$

Subbing in for the effects of the RIH temperature on the thermodynamics of the lattice

$$\frac{\partial H}{\partial T_{RIH}} = \left[ \begin{aligned} & \frac{\partial w_f}{\partial \rho_{cool}} \frac{\partial \rho_{cool}}{\partial T_{RIH}} (\gamma \Sigma_{1,f}^i + F_2 \Sigma_{2,f}^i) + w_f \frac{\partial (\gamma \Sigma_{1,f}^i + F_2 \Sigma_{2,f}^i)}{\partial \rho_{cool}} \frac{\partial \rho_{cool}}{\partial T_{RIH}} + \frac{\partial w_f}{\partial T_{fuel}} \frac{\partial T_{fuel}}{\partial T_{RIH}} (\gamma \Sigma_{1,f}^i + F_2 \Sigma_{2,f}^i) \\ & + w_f \frac{\partial (\gamma \Sigma_{1,f}^i + F_2 \Sigma_{2,f}^i)}{\partial T_{fuel}} \frac{\partial T_{fuel}}{\partial T_{RIH}} + \frac{\partial w_f}{\partial \alpha_v} \frac{\partial \alpha_v}{\partial T_{RIH}} (\gamma \Sigma_{1,f}^i + F_2 \Sigma_{2,f}^i) + w_f \frac{\partial (\gamma \Sigma_{1,f}^i + F_2 \Sigma_{2,f}^i)}{\partial \alpha_v} \frac{\partial \alpha_v}{\partial T_{RIH}} \end{aligned} \right] \quad (5.30)$$

**Table 5.5: Sensitivity of H Factor to RIH Temperature, via Thermodynamic Properties**

Parameter x	$\frac{\partial x}{\partial T_{RIH}}$	$w_f$	$\frac{\partial w_f}{\partial x}$	$\frac{\partial (\gamma \Sigma_{1,f}^i + F_2 \Sigma_{2,f}^i)}{\partial x}$	$\frac{\partial x}{\partial T_{RIH}} \frac{\partial (\gamma \Sigma_{1,f}^i + F_2 \Sigma_{2,f}^i)}{\partial x}$
Fuel Temperature	+0.8229	196.33	0	-2.26E-08	-1.86E-08
Coolant Temperature	+0.7018	196.33	0	-1.42E-07	-9.97E-08
Coolant Void	-0.9628	196.33	-4.42E-04	-8.98E-08	8.65E-08

## 5.2.8 Moderator Temperature

The moderator temperature will affect both the macroscopic fission cross section, as well as the amount of recoverable energy. The amount of recoverable energy is primarily influenced by the density of the moderator affecting the amount of gamma ray energy which can be captured. A Taylor series fit which has been used to calculate the moderator density as a function of temperature [39] is given below

$$\rho(T) = a + bT - cT^2 + dT^3 + eT^4 + fT^5 \quad (5.31)$$

Where,

$$a=1.1048, b=2.0374E-04, c=9.8367E-06, d=5.1097E-08, e=1.6844E-10, f=2.0429E-13$$

The effect of the variation in density is captured in the sensitivity of the components of the H factor.

$$\frac{\partial H}{\partial T_{mod}} = \left[ \frac{\partial w_f}{\partial \rho_{mod}} \frac{\partial \rho_{mod}}{\partial T_{mod}} (\gamma \Sigma_{1,f}^i + F_2 \Sigma_{2,f}^i) + w_f \frac{\partial (\gamma \Sigma_{1,f}^i + F_2 \Sigma_{2,f}^i)}{\partial \rho_{mod}} \frac{\partial \rho_{mod}}{\partial T_{mod}} \right] \quad (5.32)$$

Figure 5.12 shows the effect of changing the moderator density on the percentage of gamma ray energy that is recoverable in the lattice cell.

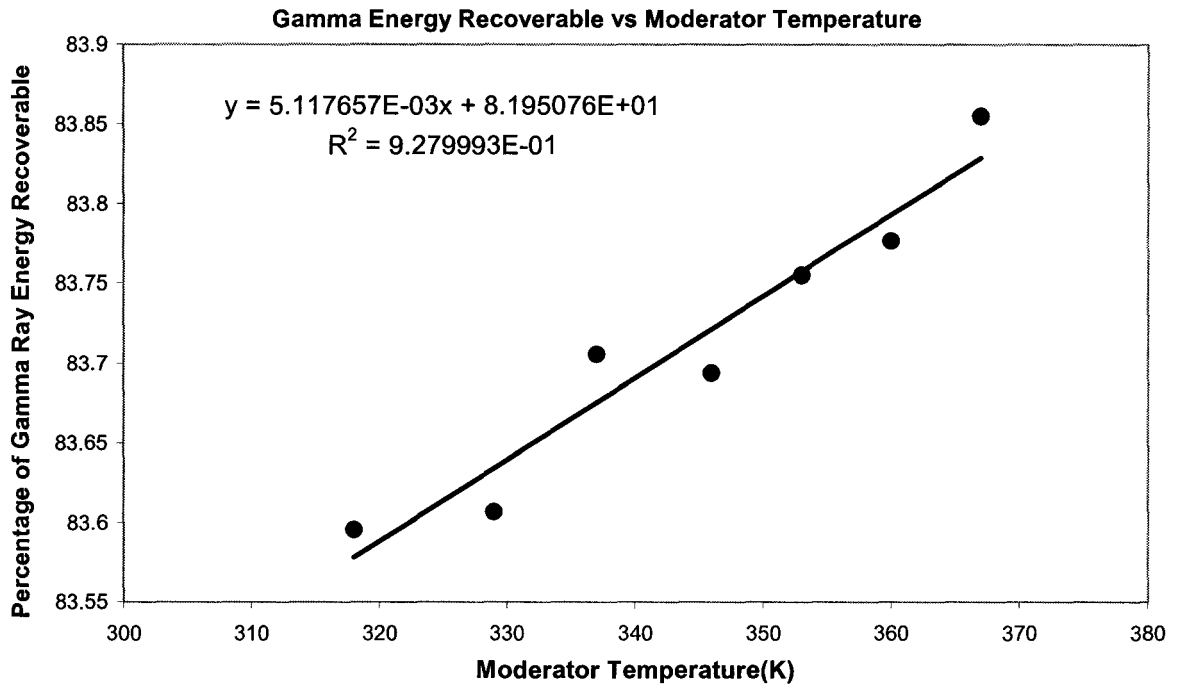


**Figure 5.12: Recoverable Energy vs the Change in The Moderator Density**

The graph shows that as the moderator density increases, the amount of recoverable energy in the lattice decreases. This result is expected since the probability of interaction with a substance is proportional to the density. Since the moderator has more interactions with the gamma rays, more energy is deposited, leaving a lower percentage for the heat transport system.

The effect of the moderator temperature on the fission cross section is displayed in Figure 5.13. As the moderator temperature increases the energy of the thermal neutrons will increase, which reduces the fission cross section of the fuel.

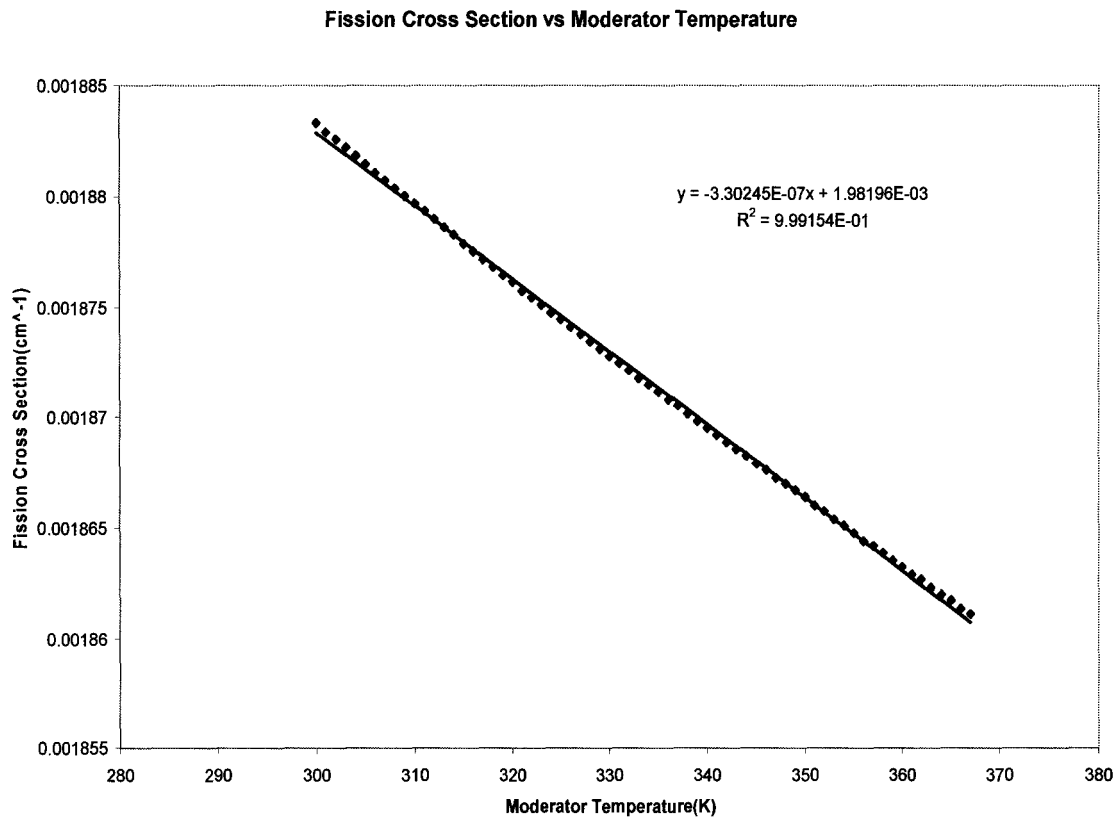


**Figure 5.13: Fission Cross Section vs Moderator Temperature**

### 5.2.9 Moderator Isotropic Purity

The moderator isotropic purity quantifies the amount of heavy water compared to the amount of light water in the moderator system

$$Purity\% = \frac{D_2O}{D_2O + H_2O} \quad (5.33)$$

As light water is introduced into the system the moderating ratio of the reactor will decrease, which influences the spectrum of the neutrons, as well as the amount of absorption which occurs in the lattice.

The moderator purity has no effect on the amount of gamma ray energy which is captured, since the number of electrons in a Hydrogen and Deuterium atom are the same. Thus only the variation in the fission cross section needs be examined. Figure 5.14 shows the variation in the adjusted fission cross section with moderator purity.

$$\frac{\partial H}{\partial Purity_{mod}} = \left[ \frac{\partial w_f}{\partial Purity_{mod}} (\gamma \Sigma_{1,f}^i + F_2 \Sigma_{2,f}^i) + w_f \frac{\partial (\gamma \Sigma_{1,f}^i + F_2 \Sigma_{2,f}^i)}{\partial Purity_{mod}} \right] \quad (5.34)$$

**Fission Cross Section vs Moderator Purity**

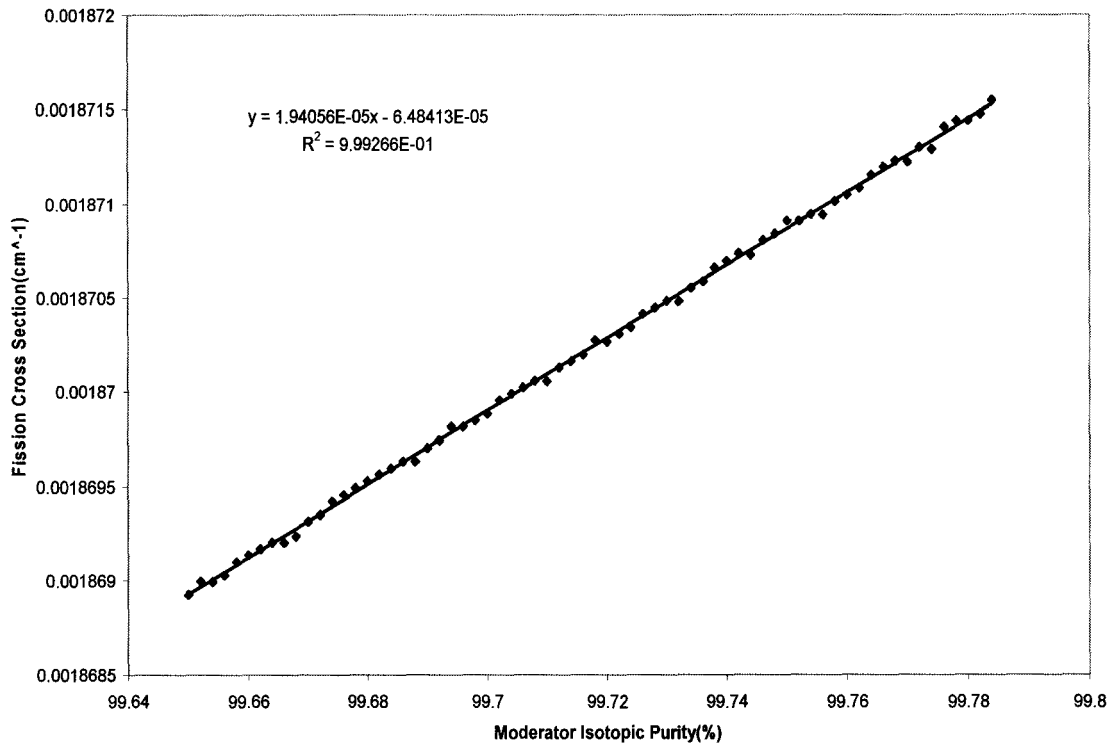


**Figure 5.14: Fission Cross Section vs Moderator Isotopic Purity**

### 5.2.10 Moderator Boron Content

The CANDU moderator has a variable boron content, which can give the reactor a days worth of reactivity holdup if, for some reason, the reactor cannot be fuelled.

The amount of boron in the moderator is specified in ppm of boron.

The H-factor sensitivity to Boron content is

$$\frac{\partial H}{\partial \text{Boron}} = \left[ \frac{\partial w_f}{\partial \text{Boron}} (\gamma \Sigma_{1,f}^i + F_2 \Sigma_{2,f}^i) + w_f \frac{\partial (\gamma \Sigma_{1,f}^i + F_2 \Sigma_{2,f}^i)}{\partial \text{Boron}} \right] \quad (5.35)$$

Fission Cross Section vs Boron Content

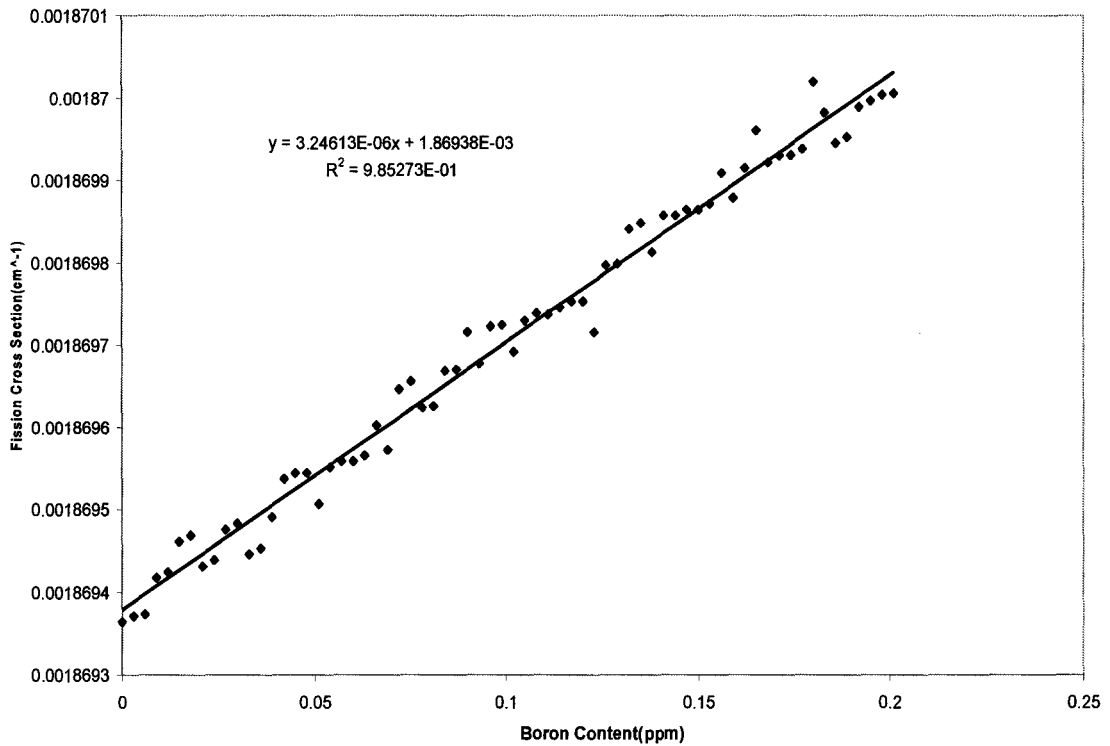


Figure 5.15: Fission Cross Section vs Moderator Boron Content

It is not intuitive that the adjusted fission cross section would increase as the Boron content in the lattice cell increases. To elucidate the influencing factors of Figure 5.15 the WIMS output for a Boron content of  $1.35e-7$ ppm and  $9.00e-8$ ppm is shown below,

For Boron content of  $1.35e-7$ ppm

PARTIAL GROUP	DIFFUSION		ABSORPTION	REMOVAL	NU-FISSION	FLUX-EFF	FLUX-INF	SLOWING DOWN	
	RADIAL	AXIAL						RADIAL	AXIAL
1	1.358	1.358	1.8000E-03	8.7628E-03	8.5050E-04	9.6013E+01	9.6013E+01	128.609	128.609
2	0.868	0.868	4.0182E-03	6.8773E-05	4.6273E-03	2.0586E+02	2.0586E+02	212.344	212.344

For Boron content of  $9.00e-8$ ppm

GROUP	DIFFUSION		ABSORPTION	REMOVAL	NU-FISSION	FLUX-EFF	FLUX-INF	SLOWING DOWN		PARTIAL
	RADIAL	AXIAL						RADIAL	AXIAL	
1	1.358	1.358	1.7999E-03	8.7628E-03	8.5048E-04	9.6013E+01	9.6013E+01	128.609	128.609	
2	0.868	0.868	4.0168E-03	6.8749E-05	4.6271E-03	2.0593E+02	2.0593E+02	212.420	212.420	

Observing the above WIMS output, as expected an increase in Boron content increases the thermal group thermal absorption. The nu-fission cross section represents the adjusted fission cross section, as the relative flux and F-factors are implicitly taken into account. Referring back to the definition of the adjusted fission cross section, the Boron content can increase the adjusted cross section by influences the actual fission cross sections, the F factors, or the ratio of fast to thermal flux. The increase Boron level in the moderator will have no effect on the actual fission cross sections. The primary effect of Boron is on the spatial flux profile. When Boron is added to the moderator, the flux in the moderator will decrease relative to the flux in the fuel, which by definition will increase the F-factor, particularly in the thermal group. The above statement illustrates how the reactivity of a lattice cell may decrease, while the H factor increases.

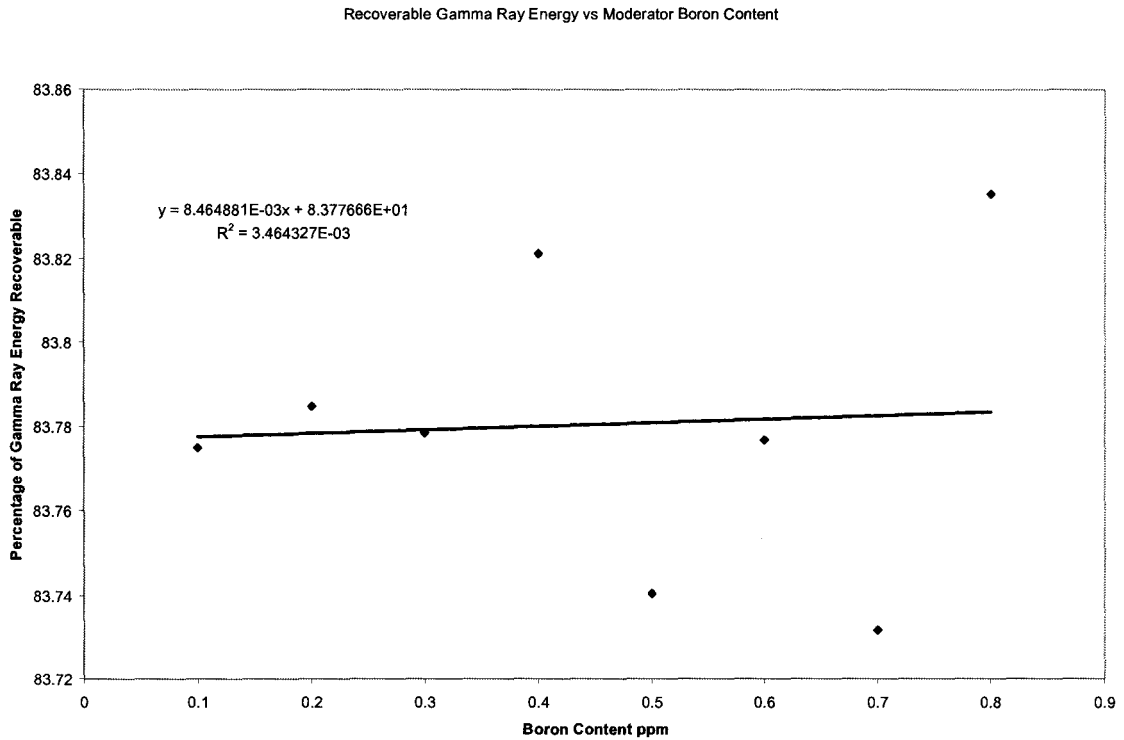


**Figure 5.16: Percentage of Gamma Ray Energy Recoverable With Changes in Boron Content**

Figure 5.16 shows the effect of adding boron to the moderator, on the amount of gamma ray energy absorbed in the moderator. As expected the amount gamma ray energy absorbed increases, with increasing boron, since boron has a higher Z than Deuterium. However the effect is negligible due to the small amount of boron added.

### 5.2.11 Survey Work Examining the Effects of Region Power on SORO Error

The power in the channel will have an effect on the temperature of the fuel. As seen previously in section 5.2.3. CANDU fuel temperature is a balance between the thermodynamic state and flow of the coolant, as well as the neutron flux within the fuel. The fuel temperature is not measured in the CANDU reactor so there is no direct of data on the channel averaged fuel temperature.

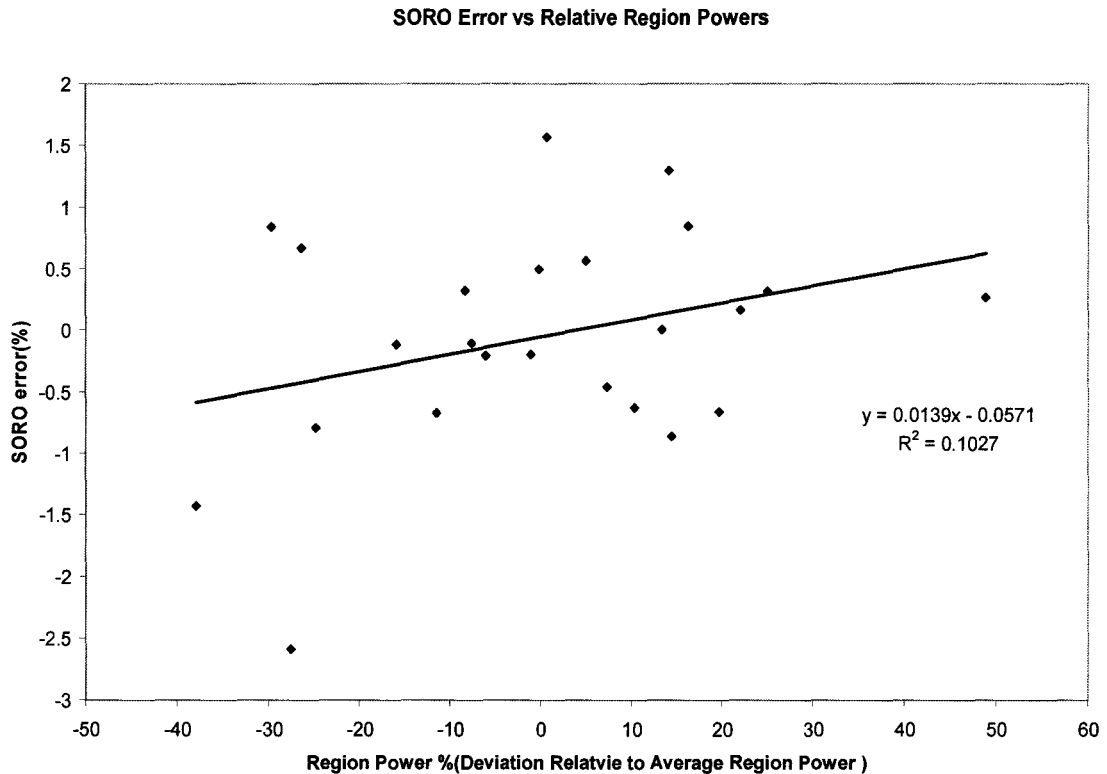
Since SORO assumes a constant H factor any perturbation in the H factor should lead to a discrepancy between the power in a particular region of the reactor, and the power calculated by SORO for that region. This statement assumes that the error in the flux is either negligible or not correlated to the factors affecting the H factor, which is unlikely to be completely true. Nevertheless the error between the measured and SORO calculated power can be checked for agreement with postulated theoretical trends. For instance if the channel power increases, thereby increasing the fuel temperature, the H factor should decrease, since Figure 5.8 shows the adjusted fission cross section decreases with fuel temperature. Thus for high fuel temperatures, the true H factor is lower than the average constant H factor. Since SORO uses the constant H factor, SORO would theoretically over predict the power in high powered regions. Similar logic says that SORO would under predict the power of low channels.

Table 5.5 predicts a comparison of measured region power vs the region power predicted by SORO[40]. The average region power is 101.36MW, so the deviation of the region power from the average region power is calculated and added to the Table. Now to

examine whether the hypothesis of the SORO error being correlated to the power in a region, Figure 5.17 plots the relative power of the region vs the difference between SORO and measured values of power.

**Table 5.6: Comparison of Measured Region Powers vs Calculated SORO Powers[40].**

Region	Measured	SORO Power	Difference	Deviation from Average
1	73.4	71.5	-2.588	-27.586
2	108.8	108.3	-0.459	7.337
3	117.9	118.9	0.848	16.315
4	102.1	103.7	1.567	0.727
5	62.9	62	-1.431	-37.945
6	115.7	117.2	1.296	14.144
7	106.4	107	0.564	4.969
8	114.9	114.9	0	13.355
9	111.8	111.1	-0.626	10.297
10	93.6	93.5	-0.107	-7.658
11	126.7	127.1	0.316	24.996
12	123.7	123.9	0.161	22.037
13	121.3	120.5	-0.659	19.669
14	89.7	89.1	-0.669	-11.505
15	116	115	-0.862	14.440
16	92.9	93.2	0.323	-8.348
17	76.2	75.6	-0.787	-24.824
18	74.6	75.1	0.670	-26.402
19	71.3	71.9	0.842	-29.658
20	101.2	101.7	0.494	-0.1603
21	85.2	85.1	-0.117	-15.945
22	100.3	100.1	-0.199	-1.048
23	150.9	151.3	0.265	48.871
24	95.2	95	-0.210	-6.079



**Figure 5.17: SORO Error vs Relative Region Powers**

Figure 5.17 is not very conclusive, although the linear regression exhibits a positive trend line, but a weak correlation coefficient. The effect of the fuel temperature on the difference between measured and SORO predicted power is minimal.

But how large an effect was expected? If the fuel temperature is to a first order approximation assumed to vary linearly with power, then the predicted effect on the H factor can be easily quantified. For example if it is assumed that the region power varies +/-30% of the average region power then the fuel temperature will vary +/-30%. If the average fuel temperature in the core is 1100C, then this will translate into a +/-330C. A difference of 660C between average fuel temperatures in two regions(a very large

variation), would translate into roughly a 1% variation in the SORO predicted power since,

$$RelativeH = \frac{(H^{AV} + \frac{dH}{dT^{fuel}} \Delta T^{fuel})}{H^{AV}} \approx 1\% \quad (5.36)$$

This variation is small enough that it could be lost within the other effects mentioned, as well as errors in the flux calculation. It would be worthy for authors with a more diverse SORO data set to explore this effect further, in future work as theory would predict that SORO is slightly overestimating the maximum channel and bundle powers.

### 5.3 Summary of Sensitivity Results

Table 5.7 summarizes the results from the graphs in the previous section. The table quantifies the variation of the recoverable energy released from fission with regards to the different influencing parameters, as well as the sensitivity of the adjusted fission cross section to the influencing parameters.

**Table 5.7: Summary of Effects on H factor**

Parameter	Sensitivity $\frac{\partial w_f}{\partial x}$	$\frac{\partial w_f}{\partial x} (\gamma \Sigma_{1,f}^i + F_2 \Sigma_{2,f}^i)$	Sensitivity $\frac{\partial (\gamma \Sigma_{1,f}^i + F_2 \Sigma_{2,f}^i)}{\partial x}$	$w_f \frac{\partial (\gamma \Sigma_{1,f}^i + F_2 \Sigma_{2,f}^i)}{\partial x}$
Burnup	3.49E-02	6.52E-05	-1.44E-06	-2.83E-04
Moderator Temperature	1.19E-03	2.22E-06	-3.30E-07	-6.48E-05
Boron Content	1.97E-03	3.73E-06	3.25E-06	6.38E-04
Moderator Purity	0	0	1.94E-05	3.81E-03
RIH Temperature	-4.30E-04	-8.03E-07	-3.18E-08	-6.24E-06
ROH Pressure	-4.42E-04	-8.26E-07	8.40E-08	1.65E-05

Note in Table 5.7 the values of  $w_f$  and  $\gamma\Sigma_{1,f}^i + F_2\Sigma_{2,f}^i$  are taken to be equal to the best estimate values.

$$(\gamma\Sigma_{1,f}^i + F_2\Sigma_{2,f}^i)_{BE} = 1.86937E-03 \text{ cm}^{-1}$$

$$(w_f)_{BE} = 196.33 \text{ MeV}$$

$$(Q_{\text{gamma}})_{BE} = 23.2 \text{ MeV}$$

Columns three and five in Table 5.7 are added to obtain the total sensitivity of the H factor to perturbations in the influencing parameters. As mentioned in section 2.3 each of the parameters will be ranked according to the product of their effect on the H factor and assumed range of variability of the parameter. This is shown in Table 5.8.

**Table 5.8: Ranking of Examined Phenomena**

Parameter	Sensitivity (dH/dx)	Range of Variability ( $\Delta x$ )	Ranking $\text{abs}[(dH/dx)(\Delta x)]$	Index	Rank
Moderator Temperature( $^{\circ}\text{C}$ )	-6.26E-05	4.4	2.75.E-04	100	High
Burnup (MWd/kg)	-2.18E-04	1.24	2.70E-04	98.2	High
Boron Content(ppm)	6.41E-04	0.058	3.72E-05	13.5	Med
Moderator Purity(%wt)	3.81E-03	0.009	3.43E-05	12.5	Med
RIH Temperature( $^{\circ}\text{C}$ )	7.04E-06	0.11	7.74E-07	0.3	Low
ROH Pressure(MPa)	1.56E-05	0.016	2.50E-07	0.1	Low

The factors which have a ranking of HIGH, are the fuel burnup and moderator temperature. These factors are sampled randomly about their respective probability distributions which are assumed to be normal. When combined with their sensitivity values, the effect on the relative H-factor can be evaluated.

$$\Delta H = \omega[0,1.24] \frac{dH}{d\omega} + T_{mod}[0,4.4] \frac{dH}{dT_{mod}} \tag{5.37}$$

The relative variation in the H factor is

$$relative\_variation = 1 + \frac{\Delta H}{H_{BE}} \quad (5.38)$$

This is used to illustrate the effect on the H factor in the histogram shown in Figure (5.18)

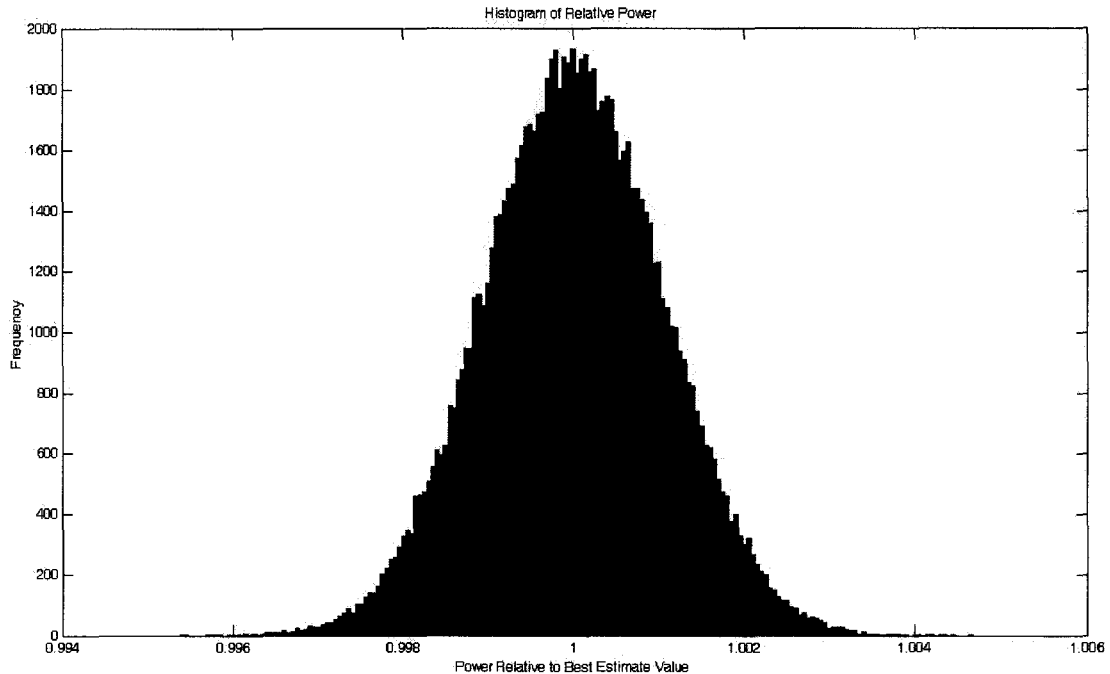


**Figure 5.18: Histogram of the combined effects of variability of Burnup and Moderator Temperature on the Conversion of Flux to Power.**

The overall impact of the parameters tested on the H factor using the models outlined is approximately 0.8%. That is the H factor varies between 99.6% and 100.4% of its best estimate value.

## 5.4 Uncertainty Analysis

As discussed previously the uncertainty in the fission power will result from an uncertainty in the H factor and an uncertainty in the flux profile. Looking at the result from the previous section the H factor will follow the probability distribution shown in

Figure 5.18. There is however an uncertainty in the probability distribution based upon the uncertainty in the components which were used to calculate the distribution. The uncertainty of the H factor,  $\xi_{Hfactor}$ , is given by

$$\xi_{Hfactor} = f(\xi_w, \xi_{adjustedFission}) \quad (5.39)$$

Where  $\xi_{Hfactor}$  is a function of the uncertainty in the recoverable energy from fission  $\xi_w$ , and the uncertainty of the adjusted fission cross section denoted by  $\xi_{adjustedFission}$ .

The amount of recoverable energy released can be further broken down into the constituent uncertainty components

$$\xi_w = g(\xi_{FP}, \xi_{Beta}, \xi_{Gamma}, \xi_{\psi}, \xi_n) \quad (5.40)$$

Where  $\xi_{FP}$  represents the amount of recoverable energy of the fission products,  $\xi_{Beta}$  from beta particles,  $\xi_{\psi}$  from gamma rays, and from neutrons  $\xi_n$ .

The adjusted fission cross section will be a combination of the approximations made in the WIMS model, combined with the uncertainty of the WIMS output.

$$\xi_{adjustedFission} = h(\xi_{WIMSCode}, \xi_{WIMSModel}) \quad (5.41)$$

Where  $\xi_{WIMSCode}$  represents the uncertainty of the WIMS code such as the uncertainty introduced through numerical methods, and  $\xi_{WIMSModel}$  represents the error in the physical modeling of the components, such as fuel element radii.

The uncertainty in the energy recoverable from gamma rays will stem from the uncertainty of the models in the code, and the inherent variability of the Monte Carlo method.

$$\xi_{\psi} = J(\xi_{MC}, \xi_{MCModel}) \quad (5.42)$$

Where  $\xi_{MC}$  is the statistical variation of the Monte Carlo method,  $\xi_{MCModel}$  represents the modeling uncertainty of the Monte Carlo Code.

Although the components can be broken down further, at this point a conservative estimate can be made for each of the above quantities, leading to an overall estimate of the uncertainty in the H factor probability distribution. Table 5.9 quantifies the estimates of the uncertainty in each of the components used to calculate the H factor.

**Table 5.9: Estimate of the magnitude of the constituent uncertainty components present in the H factor estimate.**

<b>Uncertainty Component</b>	<b>Contributing Phenomena</b>	<b>Estimate of Uncertainty Contribution</b>
$\xi_{FP}$	Fission fragment energy which may escape the heat transport system	0.1%
$\xi_{Beta}$	Beta particle energy which may escape the heat transport system	1.0%
$\xi_n$	Energy of Neutrons which may be deposited in the heat transport system	5.0%
$\xi_{MC}$	Statistical fluctuation of MCNP output	0.1%
$\xi_{MCModel}$	EPDL libraries[41]	3.0%
$\xi_{WIMSCode}$	Numerical modeling procedures	0.5%
$\xi_{WIMSMModel}$	Cross section libraries, Approximations of lattice geometry[42]	2.0%

An important point to note when estimating the uncertainty of sensitivity functions, the systematic uncertainty will have little effect on sensitivity estimates.

## Chapter SIX

### 6.0 Conclusion and Recommendations

The most important factors in the conversion of flux to power in a CANDU channel are the burnup of the fuel and the temperature of the moderator. The H factor was found to vary  $\pm 0.4\%$  of its best estimate under the assumptions of homogeneous channel burnup and a normally distributed moderator temperature. The location at which the energy is deposited in the reactor lattice cell was found to be largely invariant except in the case of gamma ray energy. The moderator temperature was seen to have a non-negligible effect on the amount of recoverable gamma ray energy. The effects of the moderator temperature on the percentage of recoverable gamma ray energy were found to be on the order of half a percent. The gamma ray energy deposition was studied using a Monte Carlo simulation of gamma ray transport in a CANDU lattice cell.

The work present here has some natural extensions

- 1) Application of the above methods to examine bundle to bundle variation of the H-factor. The variation of the H between bundles will likely be larger for lower burnup fuel than the channel averaged variation.
- 2) Examination of higher order effects. An example would be to observe how the moderator temperature effects which isotope undergoes fission, thereby influencing the energy released from fission.
- 3) Full analysis of the power profile. This would require a diffusion code such as RFSP. Analysis presented here could be furthered by observing the coupling between the

macroscopic and microscopic flux profiles. For example, does the systematic bias in the RFSP diffusion calculation compensate for the assumption of a constant H factor, or do the errors compound.

4) An examination of the variability of the H factor during a transient condition such as a LOCA. The question should be addressed if a variable H factor will have any impact on the key parameters such as fuel centerline temperature during accident conditions.

The extension to calculations of full core flux and power distributions using industry standard reactor physics codes was beyond the scope of this work. The primary focus has been on assessing the lattice cell properties to evaluate the effect on the channel averaged H factor.

Hopefully this work will aid others who wish to perform a detailed reactor core level BEAU analysis of the impact of conversion of flux to power, on channel and bundle powers, which are of primary importance in safety analysis.

## References

- [1] J.C. Luxat and R.G. Huget, "Overview of Best Estimate and Uncertainty Analysis Methodology," Ontario Power Generation, Ontario, Canada, Methodology Development Guideline MD-GD-01 Rev. 1, 2001.
- [2] B. Rouben, "Description of the Lattice Code POWDERPUFS-V," from an Internal Report by E.S.Y. Tin and P.C.Loken, October, 1995.
- [3] M.E.A. Abdelbaky et al, "Photon Electron Transport in CANDU Reactor Channels" in *Proceedings of the Fifteenth Annual Conference of the Canadian Nuclear Society*, June, 1994.
- [4] Judith F. Briesmeister, Ed., "MCNP A General Monte Carlo N particle Transport Code, Version 4B", Los Alamos national laboratory document LA-12625
- [5] J.C. Luxat, "Safety Analysis Technology: Evolution, Revolution and the Drive to Re-Establish Margins," in *Proceedings of the Twenty First Annual Conference of the Canadian Nuclear Society*, June 2000.
- [6] J.C. Luxat and R.G. Huget, "Guideline for Preparation of Phenomena and Key Parameter Identification and Ranking Tables," Ontario Power Generation, Ontario, Canada, Methodology Development Guideline MD-GD-03 Rev. 1, 2000.
- [7] J.C. Luxat, R.G. Huget and F. Tran, "Development and Application of Ontario Power Generations Best Estimate Nuclear Safety Methodology," in *Proceedings of ANS Topical Meeting on Best Estimate Methods*, November 2000.
- [8] J.C. Luxat and R.G. Huget, "Guideline for preparation of Physical Interdependency Functional Relationships & Functional Response Surfaces," Ontario Power Generation, Ontario, Canada, Methodology Development Guideline MD-GD-05 Rev. 1, 2001.
- [9] D.V. Altiparmakov, "WIMS-AECL Theory Manual," CANDU Owners Group, Toronto, Canada, COG 00-077, September 2001.
- [10] S.R. Douglas, "WIMS-AECL Release 2-5d Users Manual," Chalk River Laboratories, Chalk River, Canada, RC-1176 COG-94-52 Rev. 4 FFC-RRP-299, July 2000.

- [11] N. Hunt, "Best Estimate and Uncertainty Analysis of A Critical Large Break Loss of Coolant Accident at Darlington NGS," in *Sixth International Conference on Simulation Methods in Nuclear Engineering*, 2004, pp. 1-18.
- [12] Y. Orechwa, "Best-Estimate Analysis and Decision Making Under Uncertainty," in *International Meeting on Updates in Best Estimate Methods in Nuclear Installation Safety Analysis*, November 2004, pp. 1-8.
- [13] Atomic Archive, National Science Digital Library, "Nuclear Fission", <http://www.atomicarchive.com/Fission/Fission1.shtml>.
- [14] CANTEACH "CANTEACH Selected Images", Author: William Snook <http://canteach.candu.org/imagelib/00000-general.htm>
- [15] J.J. Whitlock, "Reduction of Coolant Void Reactivity Effect in a CANDU Lattice Cell," Ph.D. thesis, McMaster University, Hamilton, ON, Canada, 1995.
- [16] M.A. Lone, "Delayed Photo-Neutron Yields in D<sub>2</sub>O from Fission in <sup>235</sup>U, <sup>238</sup>U, <sup>239</sup>Pu, <sup>240</sup>Pu, and <sup>241</sup>Pu," in Proceedings of the Twenty Second Annual Conference of the Canadian Nuclear Society, June 2001.
- [17] J.J. Duderstadt and L.J. Hamilton, *Nuclear Reactor Analysis*. New York: John Wiley & Sons, 1976.
- [18] P. Sermer, C. G. Olive, and F.M. Hoppe, "A Methodology for Estimating Error in the Computed Maximum Fuel Bundle Power," in *Proceedings of the Twenty Second Annual Conference of the Canadian Nuclear Society*, June 2001.
- [19] G. F. Knoll, *Radiation Detection and Measurement*. New York: John Wiley & Sons, 2000.
- [20] N. Bohr, "Velocity-Range Relation for Fission Fragments," *Phys. Rev.*, vol. 59, pp. 270-275, February 1941.
- [21] S. Mukherji and B.K. Srivastava, "Universal range-velocity and stopping-power equations for fission fragments and partially stripped heavy ions in solid media," *Phys. Rev. B.*, vol. 9, pp. 3708-3719, May 1974.
- [22] James F. Ziegler, "The Stopping and Range of Ions in Matter", 2003, <http://www.srim.org/SRIM/SRIM2003.htm>.
- [23] H. Etherington, Ed., *Nuclear Engineering Handbook*. New York: McGraw-Hill, 1958.

- [24] CANTEACH, “Neutrons and Neutron Interactions”, July 2004,  
<http://canteach.candu.org/library/20040706.pdf>.
- [25] A. Luthi, “Development and validation of gamma-heating calculational methods for plutonium-burning fast reactors,” Ph.D thesis, Ecole Polytechnique Fédérale de Lausanne, Lausanne, Switzerland, 1998.
- [26] R.E. Donders, “Uncertainty in the Burnup to Lanthanum-Concentration Ratio for CANDU Fuel,” in Proceedings of the Twenty Second Annual Conference of the Canadian Nuclear Society, June 2001.
- [27] International Atomic Energy Agency, “Thermal Neutron Capture Gammas by Target”, February 1999, <http://www-nds.iaea.org/oldwallet/tnc/ngtblcontentbyn.shtml>.
- [28] Earth Atmospheric & Planetary Sciences Neutron Activation Analysis Laboratory, Massachusetts Institute of Technology, “Medical Geology/Geochemistry”, January 2006, <http://ocw.mit.edu/NR/rdonlyres/Earth--Atmospheric--and-Planetary-Sciences/12-091January--IAP--2006/EA1CA753-6257-4E66-8BA6-BDCD82AF98A0/0/session3.pdf>.
- [29] W.E. Burcham, *Nuclear Physics; An Introduction*. London: Longman, 1973.
- [30] F. Arqueros and G.D. Montesinos, “A simple algorithm for the transport of gamma rays in a medium,” *Am. J. Phys.*, vol. 71, pp. 38-45, January 2003.
- [31] CANTEACH, “Reactor Physics”, January 2003,  
<http://canteach.candu.org/library/20030101.pdf>.
- [32] M.J.F. Notley, A.M. Nicholson and V.C. Orpen, “CANDU Fuel Engineer’s Manual,” CANDU Owners Group, Toronto, Canada, COG 90-037-V8-R4, January 1998.
- [33] International Atomic Energy Agency, “Nuclear Data Services”, <http://www-nds.iaea.org/>.
- [34] International Atomic Energy Agency, “PREPRO 2004 Home Page”, June 2005,  
<http://www-nds.iaea.org/ndspub/ndf/prepro/>.
- [35] R.N. Blomquist and E.M. Gelbard, “An Assessment of Existing Klien-Nishina Monte Carlo Sampling Methods,” *Nuclear Science and Engineering*, vol. 83, pp. 380-384, 1983.

- [36] C.R. Boss, "Calculation of Gamma Fluxes in CANDU Lattices," in *Proceedings of Canadian Nuclear Society Annual Conference*, June 1980, pp. 23-33.
- [37] G.M. Frescurs and A.L. Wight, "CANDU-PHW Fuel Management- A Lecture Course," Ontario Power Generation, Ontario, Canada, Report No. 80023, May 1980
- [38] A. Durmayaz, "Approximate functions for the fast computation of the thermodynamic properties of heavy water," *Nuclear Engineering and Design*, vol. 178, pp. 309-329, 1997.
- [39] M.A. Mandour, H.E.S. Fath and M.A.I. Hussein, "Prediction of Moderator Temperature Distribution Inside CANDU Calandria and its Effect on Criticality and Safety," in *Proceedings of the Sixth Annual Conference of the Canadian Nuclear Society*, June 1985.
- [40] C.G. Olive, F.M. Hoppe and P. Sermer, "Sensitivity Studies for the Modeling of Core Reactivity Devices and Structures," in *Proceedings of the Twenty Second Annual Conference of the Canadian Nuclear Society*, June, 2001.
- [41] D.E. Cullen, "EPDL97: The Evaluated Photon Data Library", <http://www-nds.iaea.org/epdl97/document/epdl97.htm>
- [42] K.S. Kozier, "Comparison of MCNP4B and WIMS-AECL calculations of coolant-void-reactivity effects for uniform lattices of CANDU fuel.", Canadian Libraries.

Appendix A:

SAMPLE WIMS INPUT DECK

```
*$Id: verifl.wims,v 1.1 1996/03/15 13:45:41 laughton Exp$
* Test Typical CANDU lattice cell
* Heterogeneous cell
* ENDF/B-VI-based NDAS Library
* PERSEUS
* NEWRES
* B1
*
Prelude
Title "WIMS-AECL: CANDU lattice cell"
NDAS
Cell Cluster
Sequence 3
Scan
Preout
Initiate
*
ANNULUS 1 1.431 COOL
ANNULUS 2 2.182 COOL
ANNULUS 3 3.603 COOL
ANNULUS 4 4.98425 COOL
ANNULUS 5 5.1689 COOL
ANNULUS 6 5.6210 PT *PRESSURE TUBE
ANNULUS 7 6.4478 6 *AIR GAP
ANNULUS 8 6.6002 CT
NPIJAN #
POLYGON 9 4 4 14.2875

ARRAY 1 1 1 0 0
ARRAY 2 1 6 1.49 0
ARRAY 3 1 12 2.88 0.2618
ARRAY 4 1 18 4.33 0

RODSUB 1 1 0.61 FUEL1
RODSUB 1 2 0.654 CLAD
RODSUB 2 1 0.61 FUEL2
RODSUB 2 2 0.654 CLAD
RODSUB 3 1 0.61 FUEL3
RODSUB 3 2 0.654 CLAD
RODSUB 4 1 0.61 FUEL4
RODSUB 4 2 0.654 CLAD

Matlib matlib list
MATERIAL COOL 0.80406 563 3 O16 80.0427 DD2O 19.767 H1H2O 0.190227
*COOLANT D2O
MATERIAL Zr25Nb -1 563 MODER Zr90PT=0.0215075 Zr91PT=0.00469027 $
Zr92PT=0.00716917 Zr94PT=0.00726532 Zr96PT=0.00117048 $
Nb93=0.00108823 Fe54=0.192e-5 Fe56=3.01e-5 $
```

```

Fe57=0.696e-6 Fe58=9.2e-8 Cr50=0.27e-6 $
Cr52=5.11e-6 Cr53=0.58e-6 Cr54=0.14e-6 $
Ni58=1.59e-6 Ni60=6.1e-7 Ni61=2.7e-8 Ni62=8.5e-8 $
Ni64=0.2e-7 B10=9.5e-8
MATERIAL ZircII -1 377 MODER Zr90CT=0.0216725 Zr91CT=0.0047263 $
Zr92CT=0.0072242 Zr94CT=0.0073211 Zr96CT=0.0011795 $
Fe54=5.53e-6 Fe56=8.68e-5 Fe57=2.01e-6 $
Fe58=2.65e-7 Cr50=3.27e-6 Cr52=6.31e-5 $
Cr53=7.15e-6 Cr54=1.8e-6 Ni58=2.49e-5 $
Ni60=9.6e-6 Ni61=4.1e-7 Ni62=1.3e-6 Ni64=3.4e-7 $
B10=2.32e-7
MATERIAL FUEL1 10.358 1155 1 U235 0.62712 O16 11.865 U238 87.526 *Fuel
MATERIAL FUEL2 10.358 1155 1 U235 0.62712 O16 11.865 U238 87.526 *Fuel
MATERIAL FUEL3 10.358 1155 1 U235 0.62712 O16 11.865 U238 87.526 *Fuel
MATERIAL FUEL4 10.358 1155 1 U235 0.62712 O16 11.865 U238 87.526 *Fuel
MATERIAL Boron 1.08579 341 Moder b10=198.255 b11=889.889
MATERIAL WATER 1.078 341 4 O16 79.9368 DD2O 20.0059 H1H2O 0.057292 *D2O
Moderator
MIXTURE 4 WATER 1 Boron 1.42e-007 341 4
MATERIAL ZircIV -1 900 CLAD Zr90CL=0.0216391 Zr91CL=0.00471897 $
Zr92CL=0.00721304 Zr94CL=0.0073098 Zr96CL=0.00117764 $
Fe54=8.6e-6 Fe56=0.00013483 Fe57=3.1e-6 $
Fe58=4.1e-7 Cr50=3.3e-6 Cr52=6.3e-5 Cr53=7.1e-6 $
Cr54=1.8e-6 Ni58=3.2e-6 Ni60=1.2e-6 Ni61=5e-8 $
Ni62=1.7e-7 Ni64=4e-8 B10=2.34e-7
MATERIAL 6 0.11E-02 344.16 MO O16 100
MATERIAL PT=Zr25Nb
MATERIAL Clad=ZircIV
MATERAIL CT=ZircII
DENSITY Clad=0.9188
Mesh #
Newres
Tolerance 1.e-5
Power 1 34.26525 5 1 0.1e-02 1
SUPPRESS 1 1 1 1 1 1 1 1 1 1 1 1 1 1 -1 1 -1
Fewgroups 4 8 12 16 20 22 24 26 28 30 35 40 42 44 47 50 53 $
          56 59 62 65 67 69 71 73 75 77 79 81 83 85 87 89
*
Begin
Reaction ALL
Begin
Power 1 34.26525 2 2 0.1e-02 1
Begin
Begin

```

## Appendix B

**Table B.1: Photoelectric Effect Cross Sections**

Energy	Hydrogen	Boron	Oxygen	Zirconium	Uranium	Plutonium	Neptunium	Thorium
1E+01	0	3.38E+06	1.00E-13	3.29E+06	8.46E+06	2.42E+06	8.39E+06	1.25E+07
1E+02	5.20E+05	1.57E+06	5.39E+06	4.27E+06	9.53E+06	1.37E+07	1.11E+07	5.47E+06
1E+03	9.94E+02	2.21E+05	2.72E+05	2.17E+06	2.80E+06	2.76E+06	2.73E+06	2.89E+06
1E+04	5.34E-01	1.23E+03	7.59E+03	1.12E+05	3.95E+05	4.14E+05	4.04E+05	3.77E+05
1E+05	2.06E-04	8.68E-01	7.45E+00	2.04E+03	9.30E+03	9.66E+03	9.48E+03	8.96E+03
2E+05	5.58E-07	2.91E-03	2.88E-02	4.46E+01	8.54E+02	8.34E+02	8.44E+02	8.73E+02
3E+05	8.61E-08	4.64E-04	4.68E-03	8.57E+00	2.70E+02	2.93E+02	2.82E+02	2.49E+02
4E+05	2.88E-08	1.58E-04	1.61E-03	3.18E+00	1.13E+02	1.23E+02	1.18E+02	1.03E+02
5E+05	1.36E-08	7.52E-05	7.69E-04	1.59E+00	6.08E+01	6.65E+01	6.36E+01	5.54E+01
6E+05	7.82E-09	4.34E-05	4.45E-04	9.44E-01	3.80E+01	4.17E+01	3.98E+01	3.45E+01
7E+05	5.10E-09	2.83E-05	2.91E-04	6.26E-01	2.61E+01	2.87E+01	2.74E+01	2.37E+01
8E+05	3.63E-09	2.01E-05	2.07E-04	4.49E-01	1.91E+01	2.11E+01	2.01E+01	1.73E+01
9E+05	2.74E-09	1.52E-05	1.56E-04	3.41E-01	1.47E+01	1.62E+01	1.54E+01	1.33E+01
1E+06	2.13E-09	1.17E-05	1.20E-04	2.63E-01	1.14E+01	1.26E+01	1.20E+01	1.03E+01
2E+06	1.05E-09	5.37E-06	5.57E-05	1.22E-01	5.30E+00	5.85E+00	5.57E+00	4.79E+00
3E+06	4.63E-10	2.27E-06	2.35E-05	4.92E-02	2.09E+00	2.30E+00	2.19E+00	1.89E+00
4E+06	2.92E-10	1.42E-06	1.47E-05	2.95E-02	1.22E+00	1.35E+00	1.28E+00	1.11E+00
5E+06	2.13E-10	1.03E-06	1.06E-05	2.09E-02	8.47E-01	9.32E-01	8.89E-01	7.67E-01
6E+06	1.68E-10	8.08E-07	8.28E-06	1.60E-02	6.41E-01	7.05E-01	6.72E-01	5.81E-01
7E+06	1.38E-10	6.64E-07	6.79E-06	1.30E-02	5.13E-01	5.64E-01	5.38E-01	4.65E-01
8E+06	1.17E-10	5.63E-07	5.75E-06	1.09E-02	4.26E-01	4.69E-01	4.47E-01	3.86E-01

**Table B.2: Compton Scattering Cross Sections**

Energy	Hydrogen	Boron	Oxygen	Zirconium	Uranium	Plutonium	Neptunium	Thorium
1E+01	3.54E-06	1.26E-05	9.03E-06	6.69E-05	1.05E-04	1.04E-04	1.03E-04	1.08E-04
1E+02	3.54E-04	1.26E-03	9.02E-04	6.66E-03	1.04E-02	1.04E-02	1.03E-02	1.07E-02
1E+03	3.27E-02	1.14E-01	8.62E-02	5.24E-01	7.84E-01	7.75E-01	7.77E-01	8.09E-01
1E+04	4.72E-01	1.68E+00	2.25E+00	6.54E+00	1.06E+01	1.05E+01	1.06E+01	1.06E+01
1E+05	5.53E-01	2.64E+00	4.12E+00	1.73E+01	3.42E+01	3.48E+01	3.45E+01	3.36E+01
2E+05	4.45E-01	2.22E+00	3.53E+00	1.68E+01	3.64E+01	3.71E+01	3.67E+01	3.57E+01
3E+05	3.78E-01	1.89E+00	3.01E+00	1.47E+01	3.27E+01	3.33E+01	3.30E+01	3.20E+01
4E+05	3.34E-01	1.67E+00	2.67E+00	1.31E+01	2.95E+01	3.01E+01	2.98E+01	2.89E+01
5E+05	3.02E-01	1.51E+00	2.42E+00	1.20E+01	2.70E+01	2.76E+01	2.73E+01	2.64E+01
6E+05	2.78E-01	1.39E+00	2.22E+00	1.10E+01	2.50E+01	2.55E+01	2.53E+01	2.45E+01
7E+05	2.58E-01	1.29E+00	2.07E+00	1.03E+01	2.33E+01	2.38E+01	2.36E+01	2.28E+01
8E+05	2.42E-01	1.21E+00	1.94E+00	9.63E+00	2.19E+01	2.24E+01	2.22E+01	2.15E+01
9E+05	2.28E-01	1.14E+00	1.83E+00	9.09E+00	2.07E+01	2.12E+01	2.10E+01	2.03E+01
1E+06	2.15E-01	1.08E+00	1.72E+00	8.58E+00	1.96E+01	2.00E+01	1.98E+01	1.92E+01
2E+06	1.73E-01	8.65E-01	1.38E+00	6.91E+00	1.58E+01	1.62E+01	1.60E+01	1.55E+01
3E+06	1.29E-01	6.46E-01	1.03E+00	5.16E+00	1.19E+01	1.21E+01	1.20E+01	1.16E+01
4E+06	1.05E-01	5.24E-01	8.39E-01	4.19E+00	9.63E+00	9.84E+00	9.73E+00	9.42E+00
5E+06	8.90E-02	4.45E-01	7.13E-01	3.56E+00	8.18E+00	8.36E+00	8.27E+00	8.00E+00
6E+06	7.78E-02	3.89E-01	6.23E-01	3.11E+00	7.15E+00	7.31E+00	7.23E+00	6.99E+00
7E+06	6.94E-02	3.47E-01	5.55E-01	2.77E+00	6.38E+00	6.52E+00	6.45E+00	6.24E+00
8E+06	6.27E-02	3.14E-01	5.02E-01	2.51E+00	5.77E+00	5.89E+00	5.83E+00	5.64E+00

**Table B.3: Pair Production Cross Sections**

Energy	Hydrogen	Boron	Oxygen	Zirconium	Uranium	Plutonium	Neptunium	Thorium
1E+01	0	0	0	0	0	0	0	0
1E+02	0	0	0	0	0	0	0	0
1E+03	0	0	0	0	0	0	0	0
1E+04	0	0	0	0	0	0	0	0
1E+05	0	0	0	0	0	0	0	0
2E+05	0	0	0	0	0	0	0	0
3E+05	0	0	0	0	0	0	0	0
4E+05	0	0	0	0	0	0	0	0
5E+05	0	0	0	0	0	0	0	0
6E+05	0	0	0	0	0	0	0	0
7E+05	0	0	0	0	0	0	0	0
8E+05	0	0	0	0	0	0	0	0
9E+05	0	0	0	0	0	0	0	0
1E+06	0	0	0	0	0	0	0	0
2E+06	6.02E-05	1.51E-03	3.90E-03	1.16E-01	1.01E+00	1.07E+00	1.04E+00	9.53E-01
3E+06	3.38E-04	8.47E-03	2.18E-02	5.89E-01	3.99E+00	4.19E+00	4.09E+00	3.78E+00
4E+06	6.63E-04	1.66E-02	4.33E-02	1.10E+00	6.38E+00	6.67E+00	6.52E+00	6.10E+00
5E+06	9.62E-04	2.41E-02	6.35E-02	1.56E+00	8.31E+00	8.65E+00	8.47E+00	7.96E+00
6E+06	1.23E-03	3.07E-02	8.19E-02	1.95E+00	9.95E+00	1.03E+01	1.01E+01	9.56E+00
7E+06	1.47E-03	3.67E-02	9.86E-02	2.30E+00	1.14E+01	1.18E+01	1.16E+01	1.10E+01
8E+06	1.68E-03	4.20E-02	1.14E-01	2.62E+00	1.27E+01	1.31E+01	1.29E+01	1.22E+01